

Randomly Pinned Systems: Interfaces and Luttinger Liquids

Inaugural-Dissertation
zur
Erlangung des Doktorgrades
der Mathematisch-Naturwissenschaftlichen Fakultät
der Universität zu Köln

vorgelegt von
Friedmar Schütze
aus Leipzig

Köln, 2010

Berichterstatter: Prof. Dr. Thomas Nattermann
Prof. Dr. Joachim Krug

Tag der mündlichen Prüfung: 15. Oktober 2010

Contents

Introduction	1
1 AC-driven interfaces in random media	3
1.1 Introduction	3
1.2 The model	5
1.2.1 The equation of motion	5
1.2.2 The mean-field equation of motion	6
1.3 Mean field theory	7
1.3.1 The zero frequency limit	8
1.3.2 Finite Frequencies	18
1.4 Perturbation theory	25
1.4.1 The diagrammatic expansion	26
1.4.2 The failure of perturbation theory for $D \leq 4$	29
1.4.3 Interfaces subject to a constant driving force	31
1.5 Mean field perturbation theory	33
1.5.1 The diagrammatic expansion	33
1.5.2 Regularity of the perturbative series	35
1.5.3 Validity of perturbation theory	35
1.5.4 Perturbative harmonic expansion	36
1.6 Summary and Conclusions	40
2 The effect of electroelastic coupling on ferroelectric domain walls	41
2.1 Introduction	41
2.2 Electrostrictive coupling	42
2.2.1 The model	43
2.2.2 The effective Hamiltonian	44
2.2.3 The interface Hamiltonian	45
2.3 A simple model for KDP-type ferroelectrics	48
2.3.1 The model	48
2.3.2 The interface Hamiltonian in harmonic approximation	50
2.3.3 Domain wall roughness in the presence of random field disorder	52
2.3.4 Needle domains	53

3	Luttinger liquids with disorder	55
3.1	Introduction	55
3.2	The model	57
3.2.1	The disorder term	57
3.2.2	The replica action	60
3.3	Absence of the Mott Glass phase	62
3.3.1	Generalised rigidities	62
3.3.2	The ac conductivity	63
3.3.3	Fixed points and phases	64
3.3.4	The phase diagram	66
3.3.5	Concluding remarks	68
3.4	The replica instanton approach	68
3.4.1	The Euler-Lagrange equations	69
3.4.2	Solution of the Euler-Lagrange equations	70
3.4.3	A toy model	76
A	Appendices to chapter 1	83
A.1	Numerics	83
A.2	Generation of disorder forces with a cusped correlator	85
A.3	Derivation of the potential energy balance	86
A.4	The functional integral approach	87
A.5	The regularity of all perturbative orders in case $D > 4$	89
A.6	Analysis of the bush graphs	94
A.7	The width of ac-driven interfaces	96
A.8	Regularity of the mean-field perturbation expansion	98
B	Appendices to chapter 2	101
B.1	Interface Hamiltonian for the ϕ^4 model	101
B.2	The harmonic approximation	102
B.3	Derivation of H_{ee}	103
	Bibliography	105
	Danksagungen	113
	Abstract	115
	Zusammenfassung	117
	Erklärung	119
	Lebenslauf	121

Introduction

Over many decades, pioneering work in classical statistical mechanics has bred a canonical formalism to describe macroscopic systems in equilibrium, starting from microscopic models. The basic concept consists in averaging over microscopic degrees of freedom, that are irrelevant for macroscopic properties. These ideas have later been adopted to include also systems of many quantum particles. Their quantum nature becomes important at low temperatures. Nowadays, the application arena of statistical mechanics includes not only the evident fields of solid state physics, atomic physics, optics and chemistry but also covers the realms of cosmology as well as biology. Recent years have witnessed that the scope of statistical mechanics even successfully strives beyond the frontiers of pure natural sciences towards theoretical computer science, coding theory and quantitative finance.

The present challenges of statistical mechanics are mainly provided by systems out of equilibrium, noise induced behaviour and phenomena arising from the presence of disorder. In these areas, even classical physics is far from being exhaustively explained. The significance of an understanding of disordered systems can thereby hardly be overestimated. On the one hand, impurities and lattice defects are ubiquitous in everyday life materials, which suggests the technological quest for a quantitative description of possible deviations from results obtained using models for pure systems. On the other hand, the presence of disorder also has a major impact on the underlying physics. For instance, arbitrarily weak amounts of disorder increase the lower critical dimension of the Ising model [1] and drive non-interacting electronic systems from metallic to insulating behaviour in less than or equal to two dimensions [2]. Remarkably, some exciting phenomena, like the integer quantum Hall effect, even require the presence of disorder to appear.

A major difficulty with the study of random systems consists in the, frequently rather hidden, collapse of useful mathematical tools. A prominent illustrative example is the failure of dimensional reduction in connection with the random field Ising model [1], which has led to a long controversy about the lower critical dimension of this system. The idea of dimensional reduction is based on a conclusion from perturbation theory, that a d -dimensional random field system obeys the same critical behaviour like its pure counterpart in $d - 2$ dimensions [3]. It relies, however, on the incorrect assumption that perturbation theory is applicable. This will be discussed in more detail in chapter 1. It demonstrates, that for disordered systems, the art is to develop simple arguments which, fortunately, often turn out to be astonishingly robust. An example for such a stable but simple tool is the Imry-Ma argument [4].

In this thesis we treat two different kinds of systems exposed to disorder. In the first two chapters, we are dealing with elastic interfaces and in the last part, we take a look at

one-dimensional fermionic quantum systems, so called Luttinger liquids. It is important to distinguish between two types of disorder.

- (1) On the one hand, disorder may arise from isolated strong impurities, which serve as single pinning centres or scatterers.

For elastic interfaces, the pinning at single strong impurities sets a length scale, which is given by the typical distance l_{imp} between the impurities. This kind of pinning is of course only possible, if l_{imp} is large enough as compared to the thickness of the interface. In Luttinger liquids, the effect of an isolated strong impurity is relevant in case of repulsive interaction ($K < 1$, for the meaning of K cf. chapter 3) [5].

- (2) On the other hand, disorder can also be created by a finite density of weak impurities which act collectively. This is the so called Gaussian disorder.

Applied to elastic interfaces, where the disorder competes with the elasticity, the effect of many weak impurities has to accumulate to be able to oppose the elastic forces. Thus, in sufficiently low dimensions, the interplay of randomness and elasticity introduces a new length scale, called the Larkin length, above which disorder is strong enough to overcome elasticity. Whence beyond the Larkin length the static configuration of the system is mainly determined by the disorder and the interface is pinned at the fluctuations of the impurity density. In high dimensions, the elastic term dominates on all length scales and the interface is not pinned by weak disorder.

In Luttinger liquids the critical K below which the disorder is relevant is now shifted to $K_c = 3/2$ [6], whence also for weak attractive interaction disorder leads to localisation.

In this thesis, the focus is on quenched disorder of the second type, i.e. weak Gaussian disorder.

In the remainder of this introduction, we provide an outline of this thesis. Three different topics are considered, each of which is assigned an own chapter. All chapters should be self-contained to the greatest possible extent and can be read independently. Moreover, a comprehensive introduction to each topic is provided at the beginning of every chapter, so that in the following we describe only briefly the subjects and how this thesis is organised.

The topic of chapter 1 concerns interfaces in disordered systems, driven by an external force. Emphasis is put on the case of an ac-driving, for which we analyse the mean-field theory and study the perturbation expansion. In chapter 2, we consider a special case of elastic interfaces, namely domain walls in ferroelectric materials. The work in this part concentrates on the statics. We examine the effect of electroelastic coupling on the domain wall stiffness and use an Imry-Ma argument to predict the roughness in the presence of random-field disorder. In chapter 3, we leave the realm of purely classical physics and consider one-dimensional fermionic quantum liquids. First, we study the effect of randomness on the Mott state and dismiss the idea of a Mott glass phase, the existence of which has been hypothesised in recent publications. Then, we discuss the replica trick applied to the quantitative analysis of the conductivity in disordered one-dimensional electronic systems.

Chapter 1

AC-driven interfaces in random media

1.1 Introduction

The overdamped motion of an elastic manifold in a disordered environment, subject to an external driving force, is a key problem in the field of non-equilibrium statistical mechanics, that has attracted much attention for now more than two decades [7, 8]. Examples of physical systems that can be described by such models include interfaces, e.g. domain walls in disordered ferroic systems [9] or interfaces between immiscible fluids that are pushed through porous media [10, 11], as well as vortex lines in impure superconductors [12, 13, 14], dislocation lines in a solid [15] or driven charge density waves [16].

The importance of the effect of disorder on the motion of elastic systems arises in different contexts. In type-II superconductors, flux lines enclose normal conducting electrons in their core. The motion of a flux line thus ultimately causes energy dissipation. The presence of disorder leads to a pinning of the flux lines at attractive impurities and hence prevents their motion, so superconductivity is sustained. Other examples are the hardening of steel through pinning of dislocation lines by randomly distributed carbon atoms in the material, and the suppression of domain wall motion in ferroic memories.

Quite generally, elastic systems in random media exhibit a depinning threshold [17]. At zero temperature and below a certain critical driving force h_p , the system is pinned and remains at rest. Only if the force h exceeds h_p , the system moves with a finite velocity. Close to depinning, this velocity obeys a power-law dependence on the distance to the threshold, $v \sim (h - h_p)^\beta$. For finite temperatures, creep motion is present also below the critical force.

The depinning phenomenon at zero temperature shares many features with continuous phase transitions in equilibrium. In this analogy, v can be considered to play the role of an order parameter and one expects critical behaviour close to depinning. It is, however, highly non-trivial to obtain a quantitative understanding of this dynamic critical phenomenon. After a long controversy about the lower critical dimension d_l of the random field Ising model, which has been predicted to be $d_l = 3$ by dimensional reduction and $d_l = 2$ by Imry-Ma domain wall arguments [4], it has been pointed out by D.S. Fisher [1], that disordered elastic

systems have to be studied within a functional renormalization group (FRG) approach. The latter is necessary because the disorder force correlator develops a cusp singularity in the course of the FRG flow. Using FRG methods, the critical behaviour of finite dimensional interfaces [18, 19, 20, 21], charge density waves [22] and contact lines [23] has been worked out. These FRG studies have even been extended to take into account higher loop corrections [24, 25, 26]. The influence of finite temperatures has been studied as well, both, close to depinning [27, 28, 29, 30] and in the creep regime [28, 31, 32].

Beyond the problem of constant forces, the dynamics of ac-driven interfaces in random media recently became a subject of increasing prominence. Of special experimental interest is the ac susceptibility of ferroic systems [33, 34] which gets a considerable contribution from the domain wall motion [35, 36]. A phenomenological understanding of different regimes has been reported in Ref. [37], where the concept of waiting time distributions has been used. Moreover, an extension of the FRG flow equations from the problem with a constant driving force, combined with a scaling analysis has been used to work out the main characteristics of the velocity hysteresis loop [38]. In the limit of small frequencies, scaling behaviour has been found and the exponents of the remanent velocity at depinning as a function of frequency that have been determined for all dimensions $D < 4$ agree very well with numerical results. Further study of ac-driven elastic systems has been devoted to vortex lattices [39] and structural defects in liquid crystals [40].

Many questions related to ac-driven interfaces remain open. The mean-field equation of motion is not yet analysed, and a quantitative description of the velocity hysteresis has so far not been achieved. In this chapter, we are going to address some of the unsolved problems in the field. Our results are published in Refs. [41, 42]. A description of our work and how it embeds in the framework of previous study, is given at the beginning of each section. Here, we briefly describe how the present chapter is organised.

In the following section, we introduce the model equation of motion, discuss some important scales and derive the associated mean field theory.

In section 1.3, we study the mean field problem of driven interfaces in random media, where we distinguish between a smooth force correlator and a force correlator that has a cusp singularity at the origin. We start with an analysis of the problem with constant driving forces for which we discuss the motion close to depinning and derive the critical exponents. Then, we go over to consider ac-driven interfaces. Our main focus lies on the critical dynamics for small driving frequencies, which we study by analytical and numerical methods. We find power-law scaling for the velocity as well as the hysteresis loop area.

In section 1.4, we aim at going beyond mean-field theory and investigate the perturbative expansion of the equation of motion for ac-driven domain walls. After analysing the first non-vanishing order, we derive the diagrammatic expansion to account for higher orders. This can be used to argue, that perturbation theory works for $D > 4$. We will, however, see that in all physically interesting dimensionalities $D \leq 4$, perturbation theory is no longer useful. The failure of perturbation theory for $D \leq 4$ is analysed and explained. The well-known use of perturbation theory for estimates of the velocity of domain walls driven by a constant force, far in the sliding regime, does not contradict our statements for the ac-driving. We are going to take a look at this as well. The technically involved and more mathematical treatments are taken out of the main text and given in the appendices.

Formally corresponding to infinite dimensionality, mean-field theory admits a regular perturbation expansion. In section 1.5, we explore the perturbative series and numerically show, that it agrees very well with the solution to the full mean field equation. We prove, that the perturbative corrections are regular, i.e. they remain bounded in all orders. The bulk part of this inductive proof, the induction step, is outsourced to appendix A.8. Based on a numerical analysis, we conjecture a power-law scaling of the decay constants for the Fourier coefficients of the mean velocity with the strength of the driving force.

1.2 The model

1.2.1 The equation of motion

Our analysis models interfaces and domain walls that are thin such that they can be described by elastic D -dimensional manifolds, embedded in a $D + 1$ -dimensional space. The manifold

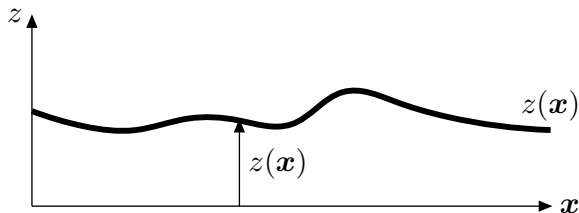


Fig. 1.1: Illustration of an elastic manifold, parametrised by a D -dimensional vector \mathbf{x} . Overhangs are not allowed.

itself is parametrised by a D -dimensional set \mathbf{x} of coordinates and its position in space is given by $z(\mathbf{x}, t)$. We confine ourselves to the study of the zero-temperature case, i.e. we do not take thermal noise into account. Moreover, our model assumes small gradients and does not allow for overhangs. We expose the interface to a periodic driving force

$$h(t) = h \cdot \cos \omega t. \quad (1.1)$$

Then, the overdamped dynamics of elastic interfaces can be described by the equation of motion

$$\gamma^{-1} \partial_t z(\mathbf{x}, t) = \Gamma \nabla_{\mathbf{x}}^2 z + h(t) + u \cdot g(\mathbf{x}, z), \quad (1.2)$$

which has already been introduced in earlier works [43, 44, 45]. In Eq. (1.2), Γ and γ are the stiffness and the inverse mobility of the domain wall. For simplicity, we set $\gamma = 1$ in the following. The function $g(\mathbf{x}, z)$ describes the quenched disorder, taken to be Gaussian with the correlators given by

$$\langle g(\mathbf{x}, z) \rangle = 0 \quad (1.3)$$

$$\langle g(\mathbf{x}, z) g(\mathbf{x}', z') \rangle = \delta^D(\mathbf{x} - \mathbf{x}') \Delta(z - z'), \quad (1.4)$$

where $\langle \dots \rangle$ denotes the average over disorder. The disorder correlator in z -direction is taken symmetric around 0 and decays exponentially on a length scale ℓ . Further, we demand $\Delta(0) =$

1, as the strength of the disorder shall be measured by u . To be definite, we choose

$$\Delta(z - z') = \exp \left[- \left(\frac{z - z'}{\ell} \right)^2 \right] \quad (1.5)$$

in case we need a precise formula. This choice corresponds to the case of an elastic interface exposed to random field disorder [20]. Throughout the whole chapter we assume weak disorder. This means, that pinning forces are weak and the interface is pinned at the fluctuations of the impurity concentration, and not at single pinning centres. A more precise definition can be found e.g. in Ref. [46]. For weak disorder, the random forces have to accumulate to overcome the elasticity. On small length scales, elastic forces dominate and the interface is essentially flat. By comparing the elastic and the disorder term in (1.2) one can estimate the length scale L_p , called the Larkin length, at which the two competing effects are of the same order. The result is

$$L_p = \left[\frac{\Gamma \ell}{u} \right]^{\frac{2}{4-D}}. \quad (1.6)$$

Thus, the elastic term dominates on all length scales for $D > 4$. Finally, we have to specify the initial configuration for the equation of motion (1.2), which we choose to be a flat wall $z(\mathbf{x}, t = 0) \equiv 0$.

1.2.2 The mean-field equation of motion

To obtain the mean field equation corresponding to our original equation of motion (1.2), we have to replace the elastic term by a uniform long-range coupling (cf. e.g. [47]). To do this, we formulate the model (1.2) on a lattice in \mathbf{x} -direction, i.e. the coordinates that parameterise the interface itself are discretised. The lattice Laplacian reads

$$\nabla_{\mathbf{x}}^2 z(\mathbf{x}_i) = \sum_{d=1}^D \frac{z(\mathbf{x}_i + a\mathbf{e}_d) + z(\mathbf{x}_i - a\mathbf{e}_d) - 2z(\mathbf{x}_i)}{a^2} = \sum_{d=1}^D \sum_{j_d=1}^N J_{ij_d} [z(\mathbf{x}_{j_d}) - z(\mathbf{x}_i)], \quad (1.7)$$

$$J_{ij_d} = \frac{1}{a^2} [\delta_{j_d+1,i} + \delta_{j_d-1,i}], \quad (1.8)$$

where a denotes the lattice constant. To get the mean field theory, J_{ij} is replaced by a uniform coupling but such that the sum over all couplings $\sum_j J_{ij}$ remains the same. Hence, we choose

$$J_{ij}^{\text{MF}} = \frac{1}{a^2 N}. \quad (1.9)$$

Now, the disorder has to be discretised as well, which is achieved if we replace the delta function in the correlator (1.4) by $\delta^D(\mathbf{x}_i - \mathbf{x}_j) \rightarrow \delta_{ij} a^{-D/2}$ (cf. Ref. [44]). The resulting equation of motion should be independent of \mathbf{x} , just the lattice constant a and the dimension enter because the disorder scales with a factor $a^{-D/2}$. Further, we replace the spatial average by the ensemble average with respect to the probability distribution of the disorder $P[g]$

$$\sum_i z(\mathbf{x}_i, t) = \int Dg(z) P[g(z)] z(t) \equiv \langle z(t) \rangle, \quad (1.10)$$

which is justified in the thermodynamic limit, where the spatial average does not fluctuate. Finally, for the mean-field equation of motion, we obtain

$$\partial_t z = c \cdot [\langle z \rangle - z] + h(t) + \eta \cdot g(z), \quad (1.11)$$

where $c = \Gamma/a^2$ and $\eta = u/a^{D/2}$. The disorder remains Gaussian with

$$\langle g(z) \rangle = 0 \quad (1.12)$$

$$\langle g(z)g(z') \rangle = \Delta(z - z'). \quad (1.13)$$

As before, $\Delta(z)$ is a function that decays to zero on a length scale ℓ and obeys $\Delta(0) = 1$. For the mean field equation of motion we are going to consider two different types of correlators. We distinguish between a correlator that is smooth and a correlator that shows a cusp singularity at the origin. As has been mentioned in the introduction, a cusp singularity in the correlator emerges as a fixed point solution of the functional renormalization group (FRG) flow in $4 - \epsilon$ dimensions and describes the effective randomness on scales larger than the Larkin length. This leads to the existence of a depinning threshold in all dimensions $d < 4$. Of course, in the framework of the mean field approximation an FRG study is senseless and a correlator with a cusp singularity has to be included manually.

The physical picture of the mean field equation of motion is that of a system of distinct particles, moving in certain realisations of the disorder. All of them are harmonically coupled to their common mean, i.e. the elastic coupling between neighbouring wall segments $\Gamma \nabla_{\mathbf{x}}^2 z$ is now replaced by a uniform coupling $c \cdot [\langle z \rangle - z]$ to the disorder averaged position $\langle z \rangle$, which in turn is determined self-consistently by the single realisations.

Apart from the correlation length ℓ of the disorder, there is another important length scale in the system. In the absence of any driving force (i.e. $h = 0$), we can easily determine the mean deviation of the coordinate z of a special realisation from the disorder averaged position $\langle z \rangle$. For $h = 0$ we have $\dot{z} = 0$ and (1.11) straightforwardly leads to

$$\langle (\langle z \rangle - z)^2 \rangle \simeq \frac{\eta^2}{c^2}. \quad (1.14)$$

So, η/c measures the order of the average distance from the common mean.

In what follows, the disorder averaged velocity $v = \langle \dot{z} \rangle$ will be denoted by the symbol v .

1.3 Mean field theory

A useful tool to achieve first insight in complicated physical problems is the mean field approximation. Before embarking on our mean-field treatment of driven domain walls, we briefly highlight the historical development of this field.

More than two decades ago, in a seminal work, D.S. Fisher has studied the depinning of charge density waves (CDW) from randomly distributed pinning centres [48, 47] by an external field h . He showed that the depinning transition is a dynamical critical phenomenon where the velocity close to the depinning threshold h_p plays the role of an order parameter exhibiting

a power law behaviour $v \sim (h - h_p)^\beta$. Within the mean-field approach, developed in [48, 47], the exponent β was found to be $\beta = 3/2$.

The mean field theory for driven interfaces in disordered systems has first been considered by Koplik and Levine [45] within the framework of perturbation theory. They found that the interface either follows a solution which moves with constant velocity or it remains pinned. They were, however, not able to extend their findings to the problem of spatially extended interfaces, because their perturbative approach lacks the necessary FRG analysis.

In a subsequent work, Leschhorn studied the mean field theory for domain walls in a model which treats the disorder in a simplified manner [49]. He considered a discretised lattice system and allowed the random force field to take values out of three possibilities only: -1 , 0 or $+1$. For his model, he also found pinned and sliding solutions and determined the velocity exponent as $\beta = 1$, which is the same as for CDWs when the disorder force has discontinuous jumps [22].

Vannimenus and Derrida [50] simplified the Leschhorn model even further and were able to derive an exact solution. The basic simplification of their model concerns the assumption of unit moves. This means, that per unit time step a segment of the interface either remains at rest, if the total force is smaller or equal to zero. Otherwise, it moves exactly one step forward, independent of the magnitude of the force. Though this assumption admits an exact solution, the restriction to unit moves entails a non-uniform periodic behaviour of the mean velocity close to the threshold. The time averaged velocity (over one period) has then a different exponent $\beta = 1/2$.

In the following, we present our work on the mean field theory for driven interfaces, modeled by Eq. (1.11). If not otherwise stated, throughout this section we measure z in units of ℓ and t in units of ℓ/η , such that $\ell = \eta = 1$.

1.3.1 The zero frequency limit

In this subsection, we consider a special case of the equation of motion (1.11), for which the driving force is constant in time. The equation of motion reads

$$\frac{\partial z}{\partial t} = c (\langle z \rangle - z) + h + g(z). \quad (1.15)$$

At sufficiently large driving force h , the average particle position $\langle z \rangle$ will move with constant velocity $v \geq 0$. In this case, Eq. (1.15) can be written as

$$\partial_t z = c(vt - z) + h + g(z) = g(z) - [c(z - vt) + h]. \quad (1.16)$$

In the following we will consider the case where the velocity is sufficiently small $v \ll h$. The positions where $\partial_t z = 0$ follow from the intersection of $g(z)$ with the straight line $c(z - vt) - h$ which moves to the right with velocity v (cf. Fig. 1.2). For sufficiently small c and smooth $g(z)$ there are in general $2n + 1$ intersections which we denote by $z_1 < z_2 < z_3 < \dots$. For $z < z_2$, z is driven towards z_1 , for $z_2 < z < z_4$ it is driven towards z_3 etc. If the particle starts with an arbitrary initial value, it will first develop towards the closest stable fixed point of (1.16), where the particle velocity is small. Let us assume this is z_1 . The force free point z_1 will then change according to $z_1(t) = vt + h/c + g(z_1)/c$. Eventually, the intersection point

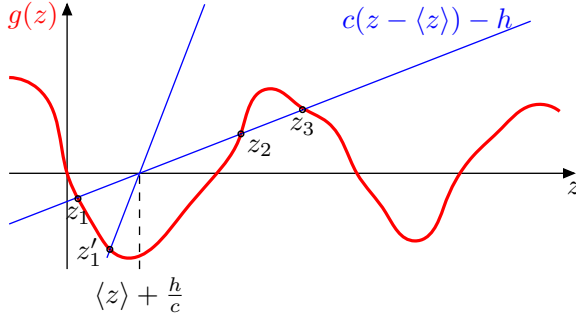


Fig. 1.2: Plot of the left and the right hand side of equation (1.20) for random forces with a smooth correlator. For small c there are several intersection points, for small values of c there is only one solution.

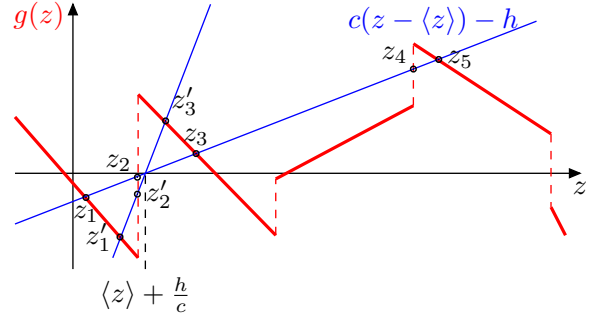


Fig. 1.3: Plot of the left and the right hand side of equation (1.20) for random forces associated to a scalloped potential, which shows a cusp singularity in the correlator. Random force realisations with a jump close to the origin yield more than one solution even for very small values of c .

$z_1(t)$ merges with $z_2(t)$ and then disappears. In this case $z(t)$ will grow sufficiently fast until it reaches $z_3(t)$ and the process repeats if we replace $z_n \rightarrow z_{n-2}$. Thus, the motion of the particle is jerky: periods of slow motion with velocity v are intermitted by fast periods where the particle is driven towards a new stable fixed point. Below, we will analyse this process in detail.

The general picture

A first overview results from considering some limiting cases.

(i) For large but finite c we can apply perturbation theory. Decomposing $z(t) = vt + \zeta(t)$, to lowest non-trivial order one obtains for the mean velocity (the derivation is analogous to the perturbation theory derived in Sec. 1.5)

$$v = h + \int_0^\infty dt e^{-ct} \Delta'(vt). \quad (1.17)$$

The depinning threshold $h_{p,\pm}$ for $h \leq 0$ follows from taking the limit $v \rightarrow \pm 0$, $h \rightarrow \pm h_p \pm 0$

$$h_{p,\pm} \equiv - \lim_{\varepsilon \rightarrow 0} c^{-1} \Delta'(\pm\varepsilon). \quad (1.18)$$

Thus, the force correlator has to have a cusp singularity to produce a finite threshold. If there is no cusp, perturbation theory in c^{-1} signals the absence of a depinning threshold. This argument applies however only to the region where perturbation theory is applicable, i.e. for $c \gg 1$. This perturbative result is in accordance with our numerical analysis, as is shown in Fig. 1.4.

As has been mentioned in the introduction, a cusp singularity in the correlator emerges as a fixed point solution of the functional renormalization group (FRG) flow in $4 - \epsilon$ dimensions and describes the effective randomness on scales larger than the Larkin length. This leads to the existence of a depinning threshold in all dimensions $D < 4$. Of course, in the framework of the

mean field approximation an FRG study is senseless and a correlator with a cusp singularity has to be included manually. Nevertheless, as we already see here, in many aspects the assumption of a correlator with a cusp gives different results compared to a smooth correlator.

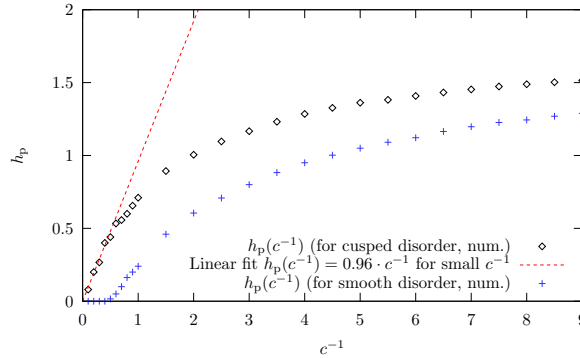


Fig. 1.4: Depinning threshold as a function of c^{-1} in the case of a dc-drive, $\omega = 0$. For the case of a cusp-correlator of the random forces (diamonds) the depinning threshold remains finite as long c^{-1} is finite. For a smooth correlator (crosses) the threshold vanishes for small c^{-1} as expected from perturbation theory.

(ii) Finally, we consider the case $c \ll 1$. For $c = 0$ the equation of motion (1.15) can be integrated

$$\int_0^z \frac{dz'}{h + g(z')} = t. \quad (1.19)$$

To calculate the integral we assume that $h > 0$ and $h + g(0) > 0$. Then for small z the lefthand side is positive and hence t as well, so the velocity is finite. However, since $g(z)$ is unbounded there is a value z_1 at which the denominator vanishes. The integral is then dominated by the integration in the vicinity of z_1 which gives $\text{const.} + a \ln(z_1 - z) = t$. Thus if z approaches z_1 the time scale diverges and the velocity vanishes, the particle is pinned at $z = z_1$. The same argument works for $h < 0$.

Static solution

One special class of solutions to the equation of motion (1.15) are the static solutions z_s with $\partial_t z_s \equiv 0$. Here, we are going to analyse under which circumstances such solutions can exist¹.

From the equation of motion Eq. (1.15) it is clear that

$$c(z_s - \langle z \rangle) - h = g(z_s) \quad (1.20)$$

must be obeyed, i.e. the system has to be located at force-free positions. Besides Eq. (1.20), one has to take into account that the self-consistency condition

$$h = -\langle g(z_s) \rangle, \quad (1.21)$$

¹Here and below we closely follow the arguments of D.S. Fisher [47] who considered the slightly different charge density wave problem.

which follows from averaging (1.20) holds. The maximal value on the righthand side of (1.21) is realised, if $z_s \equiv z_1$. Thus,

$$h_p = -\langle g(z_1) \rangle \quad (1.22)$$

is a critical field strength, above which no static solutions are possible. Conversely, we can conclude that close to depinning all particles are localised at the leftmost force free points.

Let us now apply this argument to the case $c \gg 1$. For a smooth potential as depicted in Fig. 1.2 there is typically only one solution z'_1 . For this single solution, $g(z'_1)$ can be positive or negative with equal probability. Thus, a pinned solution obeying $h = -\langle g(z'_1) \rangle$ does not exist apart from the case $h = 0$. Hence, in this case the interface is never pinned, in agreement with our result from perturbation theory. The situation is different in the case when the random force exhibits infinite slopes as is shown in Fig. 1.3. Then, due to the discontinuities there are in general several solutions z_i for any value of c from which the leftmost ones dominate the behavior in the neighborhood of the depinning threshold. Of course, the larger the value of c the smaller is the fraction of disorder realisations which allow for more than one force free solution. Thus, for large c , the depinning threshold is diminished but finite. The presence of infinite slopes is a special feature of disorder forces, the correlator of which has a cusp singularity at the origin. A detailed analysis of the cusped disorder, as is sketched in Fig. 1.3 is presented in App. A.2, where we discuss how such a class of disorder forces can be realised and derive the correlator explicitly.

To test these predictions, we have solved equation (1.15) numerically. The depinning threshold h_p is plotted in Fig. 1.4 as a function of c . It is clearly seen that the threshold increases with c^{-1} , it vanishes for $c > c_c$ for smooth random force correlations. For cusp correlations $c_c \rightarrow \infty$. These findings support the results from perturbation theory.

Scaling behaviour above depinning - general considerations

Now, we consider the behaviour slightly above the depinning threshold $h \gtrsim h_p$, when $\langle z \rangle = vt$ but $v \ll 1$. Our goal is to work out the scaling exponent β for the sliding velocity v , which we anticipate to vanish as a power law

$$v \sim (h - h_p)^\beta. \quad (1.23)$$

To this aim, we solve the equation of motion in an approximate manner. As the velocity of the interface is small, $v \ll 1$, we can also expect that $\partial_t z \ll 1$ for most of the time. Thus, $z(t)$ follows essentially from the vanishing of the righthand side of (1.16), which means that $z(t)$ stays close to the leftmost fixed point $z_1(t)$. Since the disorder averaged position $\langle z \rangle$ is in motion, we have to keep in mind, that the root of the straight line in Figs. 1.2 and 1.3 is now moving relative to $g(z)$. The intersection point $z_1(t)$ satisfies the relation

$$z_1(t) = vt + c^{-1}(h + g(z_1(t))). \quad (1.24)$$

Without loss of generality, we restrict ourselves to $v > 0$, so $z_1(t)$ moves now to the right. In this part of the motion, z_1 changes slowly (of order v). Eventually, z_1 merges with z_2 . Let us

assume that this happens at $t = 0$. For further reference we denote

$$z_0 \equiv z_1(-0) = z_2(-0). \quad (1.25)$$

For $t > 0$, these two solutions disappear and the intersection point $z_3(-0)$ becomes the new leftmost intersection point, i.e. $z_3(-0) \rightarrow z_1(+0)$, so effectively z_1 jumps instantaneously. Thus, at $t > 0$, the position $z(t)$ is not any more close to a force free position and therefore it moves faster to approach the new intersection point $z_1(t)$. The idea is now, that the mean velocity v is mainly determined by those disorder realisations, which move fast. In order to determine the scaling exponent β of v , it is thus our task to work out a quantitative description of the motion of a particle in a certain disorder realisation during a period of time between two collapses of force-free points. The temporal distance between two jumps of the leftmost force-free position is approximately given by

$$T = v^{-1}, \quad (1.26)$$

because this is the time needed to travel through a correlated region of the disorder (the length of which is of order $\mathcal{O}(1)$). We denote the distance to the new leftmost intersection point $z_1(t)$ by

$$\theta(t) = z(t) - z_1(t). \quad (1.27)$$

Note, that by definition $\theta(t)$ is negative. Now, Eq. (1.24) yields the identity

$$0 = \langle z(t) - vt \rangle = \frac{1}{T} \int_0^T dt \langle z_1(t) + \theta(t) - vt \rangle = \frac{1}{T} \int_0^T dt \langle c^{-1}h + c^{-1}g(z_1) + \theta(t) \rangle. \quad (1.28)$$

Using Eq. (1.22), we obtain from (1.28)

$$\frac{h - h_p}{c} = -\frac{1}{T} \int_0^T dt \langle \theta(t) \rangle. \quad (1.29)$$

The integral on the righthand side of (1.29) depends on the velocity. But, in order to use Eq. (1.29) to determine the scaling exponent, we have to describe the interface motion for $t > 0$, i.e. in the region of the fast motion between the previous and the new force free position. We are going to do this separately for the two types of disorder considered in this section.

Scaling theory for disorder with a smooth correlator

The motion of the interface position after the collapse of the two leftmost force-free points is best analysed in several steps. First of all, we note that at $t = 0$ when z_1 and z_2 merge, the relation

$$c = g'(z_0) \quad (1.30)$$

holds. For $t \gtrsim 0$, we can expect that $z(t)$ is still close to z_0 , so we can expand (1.16) around z_0 . Writing

$$\zeta(t) = z(t) - z_0 \quad (1.31)$$

and using (1.30), we obtain

$$\partial_t \zeta = cvt + \frac{g''(z_0)}{2} \zeta^2 + \mathcal{O}(\zeta^3), \quad \zeta(0) = 0. \quad (1.32)$$

For small ζ , we can neglect the second term on the righthand side and obtain

$$\zeta(t) \approx cvt^2/2. \quad (1.33)$$

On time scales $t \geq t_0 = 2[cvg''(z_0)]^{-\frac{1}{3}}$ the second term on the righthand side of (1.32) dominates the time evolution and we obtain

$$\zeta(t) \approx \frac{2}{g''(z_0)(t_d - t)}, \quad t_d = \frac{3}{2}t_0. \quad (1.34)$$

Clearly, this result can only be used until a time

$$t_1 \simeq t_d - \frac{2}{g''(z_0)}, \quad (1.35)$$

for which $\zeta(t_1) \lesssim 1$ since we made an expansion in ζ . It shows, however, that for $t_0 \lesssim t \lesssim t_1$ the coordinate z increases rapidly until it comes close to the new leftmost minimum $z_1(t)$. For $t > t_1$, $\theta(t)$ is already close to zero and therefore gives only higher order contributions to the righthand side of Eq. (1.29). The motion in between two jumps is sketched in Fig. 1.5

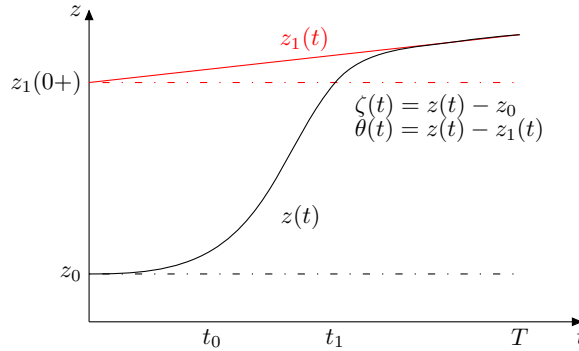


Fig. 1.5: Illustration of the motion $z(t)$ in between two jumps in the case of smooth disorder.

Now, we are going to evaluate the integral over $\theta(t)$ that occurs in Eq. (1.29). The equations (1.27) and (1.31) relate $\theta(t)$ and $\zeta(t)$

$$\theta(t) = \zeta(t) + z_0 - z_1(t). \quad (1.36)$$

The time dependence of $z_1(t)$ can be estimated from Eq. (1.24) as

$$\partial_t z_1(t) = v + c^{-1}g'(z_1(t))\partial_t z_1(t) \quad \Rightarrow \quad \partial_t z_1(t) = \frac{cv}{c - g'(z_1(t))} = \frac{cv}{\gamma} + \mathcal{O}(v^2), \quad (1.37)$$

where we have introduced $\gamma = [c - g'(z_1(0+))]$ for notational convenience. Since $z_1(0+)$ is a stable fixed point, we have $\gamma > 0$. Using

$$z_0 - z_1(t) \simeq \theta(0) - \frac{cv}{\gamma}t, \quad (1.38)$$

we obtain

$$\begin{aligned} \int_0^{t_0} dt \theta(t) &= \int_0^{t_0} dt \left[\zeta(t) + \theta(0) - \frac{cv}{\gamma}t \right] = \frac{cvt_0^3}{6} + t_0\theta(0) - \frac{cv}{\gamma} \frac{t_0^2}{2} \\ &= 2v^{-\frac{1}{3}}\theta(0)[cg''(z_0)]^{-\frac{1}{3}} + \mathcal{O}(1). \end{aligned} \quad (1.39)$$

Further, for $t_0 < t < t_1$, we have

$$\begin{aligned} \int_{t_0}^{t_1} dt \theta(t) &= \int_{t_0}^{t_1} dt \left[\zeta(t) + \theta(0) - \frac{cv}{\gamma}t \right] = \frac{2}{g''(z_0)} \ln \frac{t_d - t_1}{t_d - t_0} + \theta(0)(t_1 - t_0) - \frac{cv}{\gamma} \frac{t_1^2 - t_0^2}{2} \\ &= v^{-\frac{1}{3}}\theta(0)[cg''(z_0)]^{-\frac{1}{3}} + \mathcal{O}(\ln v). \end{aligned} \quad (1.40)$$

As we have already said, the integral over the remaining time $t_1 \dots T$ contributes to $\mathcal{O}(1)$ only. Thus, up to orders $\mathcal{O}(v \ln v)$, from (1.39) and (1.40) the expression on the righthand side of Eq. (1.29) follows as

$$\frac{1}{T} \int_0^T dt \langle \theta(t) \rangle \simeq -v^{\frac{2}{3}} 3 \left\langle |\theta(0)| [cg''(z_0)]^{-\frac{1}{3}} \right\rangle. \quad (1.41)$$

From (1.29) and (1.41), we obtain therefore

$$v \sim \frac{(h - h_p)^{3/2}}{c}, \quad (1.42)$$

i.e. $\beta = 3/2$.

Scaling theory for disorder with a cusped correlator

As we have mentioned before, if $\Delta(z)$ has a cusp singularity, the typical disorder force realisation exhibits discontinuous jumps, as is depicted in Fig. 1.3. A moment reflection shows, that a merging of two force free solutions z_1 and z_2 is only possible at such a discontinuity of the force field. The requirement, that z_1 is a stable fixed point entails that such a discontinuity is given by an upward jump in the force field. For the calculation we have to distinguish several cases.

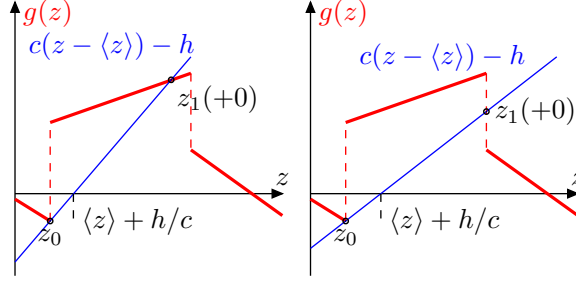


Fig. 1.6: Left: This picture corresponds to our assumption for case 1 that the new intersection point $z_1(+0)$ is left of the next discontinuity of the disorder force $g(z)$. It is obvious, that the inequality (1.43) has to be fulfilled. Right: A scenario contrary to case 1 is possible. However, the basic fact that the particle moves from the very beginning with a velocity $g(z) - [c(z - \langle z \rangle) - h] = \mathcal{O}(1)$ and therefore needs a time $t_0 = \mathcal{O}(1)$ to approach $z_1(+0)$, remains unchanged. So does the exponent β .

Case 1: In this case we assume, that the next stable intersection point occurs before the next discontinuity. Then, we have the inequality (cf. Fig. 1.6)

$$c > g'(z_0+). \quad (1.43)$$

It turns out that we have to solve the equation of motion in two time regimes. First, close to $t = 0$, $z(t)$ is in the vicinity of z_0 and we consider again the equation for

$$\zeta(t) = z(t) - z_0. \quad (1.44)$$

Now, since the merging of two fixed points occurs at the discontinuities of the potential, Eq. (1.30) is not meaningful, but instead z_0 fulfills the equation

$$cz_0 = g(z_0-) + h. \quad (1.45)$$

Using Eq. (1.45), it is easy to see that the equation of motion for $\zeta(t)$ takes the form

$$\partial_t \zeta(t) \approx c(vt - z_0) + g(z_0+) + (g'(z_0+) - c)\zeta + h = cvt - (c - g'(z_0+))\zeta(t) + \delta g. \quad (1.46)$$

Here, $\delta g = g(z_0+) - g(z_0-)$ denotes the jump of $g(z)$ which is of order one. Integration of (1.46) gives for short times $t \gtrsim 0$

$$\zeta(t) \approx \delta g t. \quad (1.47)$$

This result is approximately correct for $t < t_0$ with

$$t_0 = (c - g'(z_0+))^{-1}. \quad (1.48)$$

Note, that due to (1.43) the time t_0 is always finite and positive, in fact generically of order $\mathcal{O}(1)$. For $t > t_0$, also the term in Eq. (1.46) proportional to $\zeta(t)$ becomes relevant. Now, $z_0 + \zeta(t_0)$ has to be compared with $z_1(+0)$ which is the new leftmost intersection point for $t > 0$. From (1.24) we deduce that $z_1(+0)$ fulfills the equation

$$cz_1(+0) \approx h + g(z_0+) + g'(z_0+)(z_1(+0) - z_0), \quad (1.49)$$

from which we obtain

$$z_1(+0) \approx \frac{h + g(z_0+) - g'(z_0+)z_0}{c - g'(z_0+)} = \frac{[c - g'(z_0+)]z_0 + \delta g}{c - g'(z_0+)} = \zeta(t_0) + z_0 = z(t_0). \quad (1.50)$$

In the second step, we have replaced h using Eq. (1.45). Thus, after the time t_0 the particle has reached already the new intersection point z_1 .

To determine the exponent β , we want to employ equation (1.29) again. For $t \leq t_0$, the relevant function $\theta(t)$ as has been obtained so far reads

$$\theta(t) = z_0 - z_1(t) + \zeta(t) \approx z_0 - z_1(t) + \delta g t. \quad (1.51)$$

To approximate the time dependence of $z_1(t)$, we expand $z_1(t)$ around $z_1(+0)$ and get

$$z_1(t) \simeq z_1(+0) + \dot{z}_1(0)t. \quad (1.52)$$

Here, $\dot{z}_1(0)$ can be deduced from the defining equation (1.24), it follows as $\dot{z}_1(0) = cvt_1$ with

$$t_1 = (c - g'(z_1(0)))^{-1}. \quad (1.53)$$

Thus, in the regime where $\theta(t)$ changes fast, i.e. for $t \leq t_0$, we can write

$$\theta(t) \approx z_0 - z_1(t) + \zeta(t) \simeq \delta g(t - t_0) - cvt_1 t. \quad (1.54)$$

This shows, that for $t > t_0$, $\theta(t) = \mathcal{O}(v)$. However, the time scale t_0 is of the order $\mathcal{O}(1)$, and is thus small compared to T , $t_0 \ll T$. Therefore, it is important to carefully analyse the function $\theta(t)$ also for $t > t_0$. For $t > t_0$ we expand around $z_1(t)$ and the approximated equation of motion reads

$$\partial_t z \simeq c(vt - z) + g(z_1) + g'(z_1)(z - z_1) + h = -\frac{1}{t_1}\theta(t), \quad (1.55)$$

where t_1 is defined in (1.53). Then, using (1.24) and (1.27), we find

$$\partial_t \theta \simeq -\frac{1}{t_1}\theta(t) - cvt_1. \quad (1.56)$$

The solution to this equation, matching with equation (1.54) gives

$$\theta(t) \approx -cvt_1^2 + cvt_1(t_1 - t_0) e^{-(t-t_0)/t_1}. \quad (1.57)$$

The motion $z(t)$ in between two jumps is sketched in Fig. 1.7

Now, we can determine β using equation (1.29). In calculating

$$-\frac{1}{T} \int_0^T dt \langle \theta(t) \rangle \simeq v \left\langle \frac{\delta g t_0^2}{2} + ct_1^2 \right\rangle + \mathcal{O}(v^2), \quad (1.58)$$

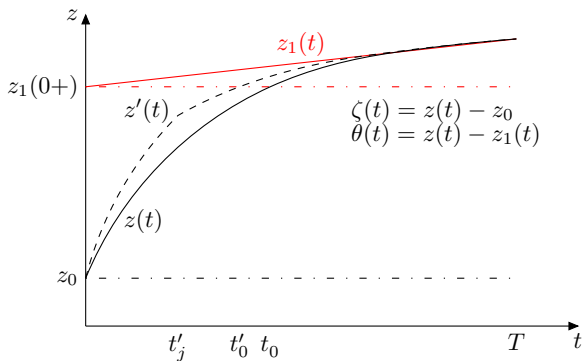


Fig. 1.7: Illustration of the motion $z(t)$ in between two jumps in the case of disorder with a cusped correlator. The difference between the absence (case 1, solid line) and the presence (case 2, dashed line) of a discontinuity of the force field $g(z)$ in between z_0 and $z_1(0+)$ is the appearance of a sharp kink in the curve $z'(t)$ at $t = t'_j$.

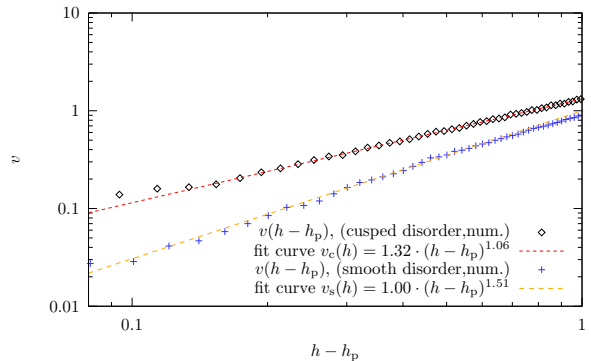


Fig. 1.8: The velocity as a function of $h - h_p$ for $c = 0.67$ in a double logarithmic plot. The numerically determined exponent for this measurement is $\beta = 1.06 \pm 0.08$ for cusp-like singularity of Δ (diamonds) and $\beta = 1.51 \pm 0.08$ for smooth force correlation (crosses).

we have decomposed the integral into the intervals $0 \dots t_0$ and $t_0 \dots T$, respectively. This gives

$$v \sim \frac{h - h_p}{c}, \quad (1.59)$$

from which we conclude, that in the case of cusped disorder the velocity exponent is $\beta = 1$.

Case 2: Now, we have to discuss what can change if there is a discontinuity of $g(z)$ in between z_0 and $z_1(0+)$. One possible scenario for this case is depicted in the right part of Fig. 1.6. We are going to discuss now, that our main result $\beta = 1$ remains unchanged. Indeed, as can be concluded from our previous calculation, the essential point that lead to the exponent $\beta = 1$ was the fact, that $z(t)$ approaches $z_1(+0)$ on a time scale t_0 which is of order $\mathcal{O}(1)$. Responsible for this is, that immediately after a collapse of the leftmost intersection point, the particle starts to move with a velocity of order $\delta g = \mathcal{O}(1)$. This remains unchanged. In Fig. 1.7 we have also sketched the motion when a discontinuity occurs in between z_0 and $z_1(0+)$. The respective quantities in Fig. 1.7 carry a prime. The only effect of the discontinuity that is crossed at a time t'_j is a singularity of the velocity $z'(t)$ at $t = t'_j$. The fundamental characteristics of the motion remain unchanged.

Thus, in case of k jumps of $g(z)$ the foregoing calculation remains basically unchanged, apart from the fact, that one should now decompose the motion in one more parts: $0 \dots t_{j_1}$; $t_{j_1} \dots t_{j_2}$; \dots ; $t_{j_k} \dots t_0$; $t_0 \dots T$. The first k pieces of the motion yield contributions to the integral (1.29) which are clearly all of the same type. Of course, this consideration changes the prefactor in Eq. (1.59), which is, however, anyway beyond our accuracy.

The two exponents $\beta = 3/2$ for smooth and $\beta = 1$ for cusped disorder are confirmed by our numerical solution as depicted in Fig. 1.8.

1.3.2 Finite Frequencies

In the finite frequency case, the disorder average over the solutions to the equation of motion (1.11) forms a hysteresis in the v - h -plane, as is illustrated in Fig. 1.9 for the two types of disorder considered here.

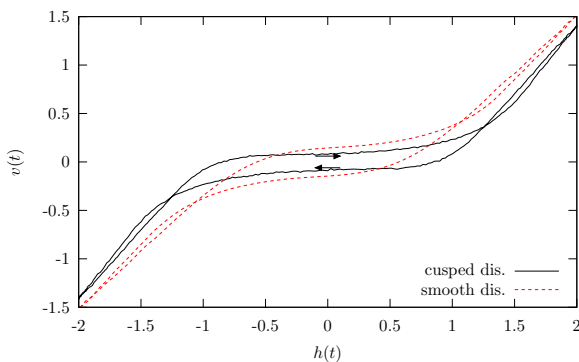


Fig. 1.9: In the presence of an ac driving field, a velocity hysteresis emerges. In this picture we illustrate these hystereses for the cusped and the smooth disorder for $c = 0.5$, $h = 2.0$ and $\omega = 0.1$. The inner hysteresis is traversed clockwise, the outer loops are passed through counter-clockwise

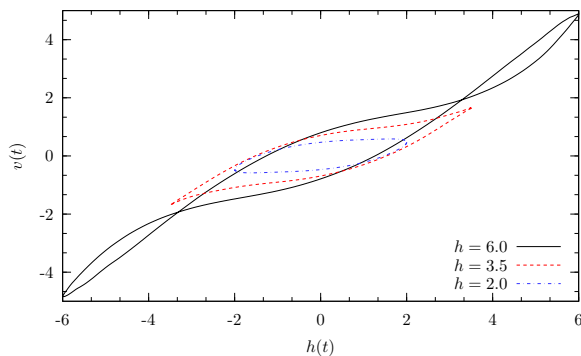


Fig. 1.10: The double hysteresis is only present for large enough driving field amplitudes. For small h , there is only a single hysteresis loop. This plot has been achieved for smooth disorder with the parameters $c = 1.0$ and $\eta = 2.5$, where t and z are measured in units such that $\omega = \ell = 1$.

The hystereses are invariant under the transformation $v \rightarrow -v$ and $h \rightarrow -h$. This can be explained directly using the equation of motion (1.11) and a statistical inversion symmetry. Taking the disorder average of (1.11) yields

$$\partial_t \langle z \rangle = v = h \cos \omega t + \langle g(z(t)) \rangle. \quad (1.60)$$

It is easy to see, that the aforementioned symmetry under $v \rightarrow -v$ and $h \rightarrow -h$ holds true if the probability density $P[g]$ (cf. Eq. (1.10)) obeys $P[g] = P[\hat{g}]$ where $\hat{g}(z) = -g(-z)$. This is obviously the case for our assumption of Gaussian disorder.

An interesting consequence of this symmetry is, that the even Fourier coefficients of the solution $v(t)$ (which is periodic with period $2\pi/\omega$) vanish. Once the steady state is reached, the symmetry requires $v(t) = -v(t + \pi/\omega)$. For the even Fourier modes this means

$$c_{2N} = \int_0^{\frac{2\pi}{\omega}} dt v(t) e^{i2N\omega t} = \int_0^{\frac{\pi}{\omega}} dt v(t) e^{i2N\omega t} + \int_0^{\frac{\pi}{\omega}} dt v\left(t + \frac{\pi}{\omega}\right) e^{i2N\omega t} = 0. \quad (1.61)$$

As the frequency is sent to zero $\omega \rightarrow 0$, the hysteretic trajectory approaches the depinning curve for an adiabatic change of the driving field that we have discussed in the previous subsection. This is shown in fig. 1.11. Moreover, the effect of large c is to reduce the effect of disorder. Clearly, for $c \rightarrow \infty$ we have $\langle z(t) \rangle = z(t)$ and hence after averaging over the disorder one finds $\langle z \rangle(t) = (h/\omega) \sin \omega t$ and $v(t) = h(t)$ as expected. Thus, for large c the hysteresis winds tightly around the diagonal.

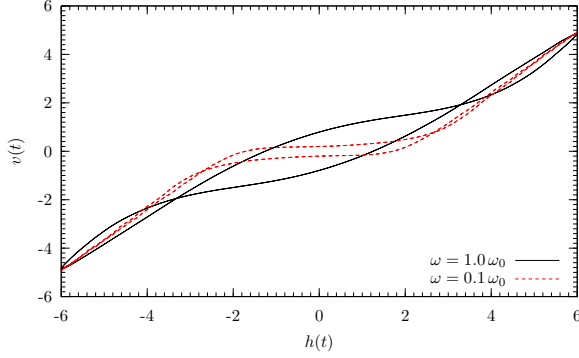


Fig. 1.11: Numerical solution of equation (1.11) for $h = 6.0$, $c = 1.0$ and $\eta = 2.5$ for different frequencies and smooth disorder, t and z being measured in units such that $\omega_0 = \ell = 1$.

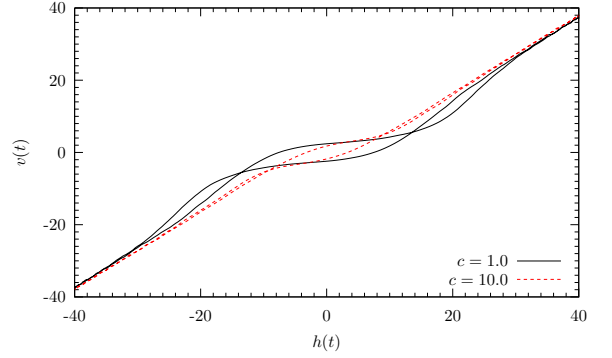


Fig. 1.12: Numerical solution of equation (1.11) for different elastic constants and $h = 40.0$, $\eta = 10.0$. The disorder is smooth and the units of t and z are chosen such that $\omega = \ell = 1$.

Qualitative discussion of the motion

To understand the shape of the hysteresis, we consider the motion of a particle for half of a period for the case $h \gg h_p$ and small frequency $\omega \ll c$. We start at a time $t = 0$, when $h(0) = -h_p$ and the field increases. Then, we can expect each particle to be located close to the rightmost force free point, i.e. the rightmost solution of

$$c(z_f(t) - \langle z \rangle(t)) - h(t) = g(z_f(t)). \quad (1.62)$$

In Fig. 1.13 it is illustrated, that due to the change of the driving field towards larger values,

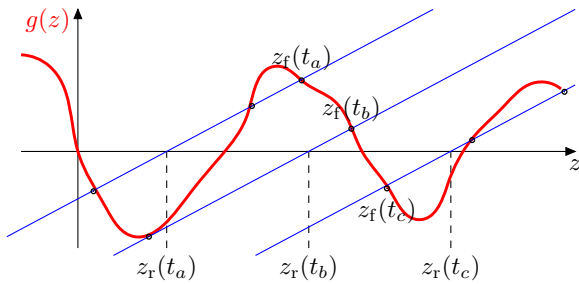


Fig. 1.13: At $h(t_a) \approx -h_p$, the particle is close to the rightmost force free point $z_f(t_a)$. This intersection point moves, due to the change of the zero $z_r(t) = \langle z \rangle(t) + h(t)/c$. The particle is following this point. At a later time t_c , when $h(t_c) \approx h_p$ this force free point has become the leftmost one.

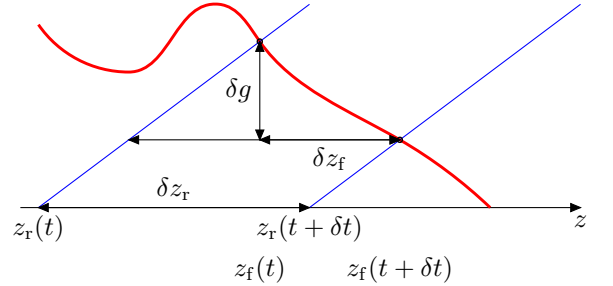


Fig. 1.14: Illustration for the velocity estimate. The motion of the root z_r of the straight line $c(z - \langle z \rangle) - h$ entails a change in z_f , that can be easily estimated in terms of simple trigonometry.

the root of the straight line, given by

$$z_r \equiv \langle z \rangle(t) + h(t)/c \quad (1.63)$$

moves with a velocity

$$\dot{z}_r = v(t) + \frac{\dot{h}(t)}{c}. \quad (1.64)$$

Since $\dot{h}(t) > 0$, this velocity is positive although the value of the field is still negative. Therefore, also the intersection point $z_f(t)$ to which the particle is connected, moves to the right. This fact is observed in the hysteresis loop, illustrated in Fig. 1.9. Actually, this understanding allows to estimate the velocity in simple geometrical terms. Using the notation explained in Fig. 1.14, we have $\delta g/\delta z_f \simeq g'(z_f)$ and thus

$$\delta z_r - \delta z_f = -\frac{\delta g}{c} = -\frac{g'(z_f)\delta z_f}{c}, \quad \Rightarrow \quad \delta z_r = \frac{c - g'(z_f)}{c}\delta z_f. \quad (1.65)$$

Now, Eq. (1.64) yields

$$\frac{\delta z_r}{\delta t} = \frac{c - g'(z_f)}{c} \frac{\delta z_f}{\delta t} \simeq \frac{\delta z_f}{\delta t} + \frac{\dot{h}(t)}{c}. \quad (1.66)$$

Solving the last approximate equality for $\delta z_f/\delta t$, we obtain

$$\dot{z}_f \simeq -\dot{h}/g'(z_f). \quad (1.67)$$

During the motion of $z_f(t)$, other intersection points to the left of $z_f(t)$ vanish, and new solutions to the right emerge. Finally, when $h(t_1) \approx h_p$, $z_f(t_1)$ has become the leftmost intersection point. From approximately this time on it happens, that occasionally in some disorder realisations $z_f(t)$ merges with an unstable fixed point and vanishes, so that the particle moves fast in order to catch up with the new leftmost force free point. This procedure has already been discussed earlier in Sec. 1.3.1. Since the velocity of a particle is given by the difference between $g(z)$ and the straight line $c(z - \langle z \rangle) - h$, it must fall back behind the leftmost intersection point to speed up. This can only happen due to the disappearance of force free points. Thus, the velocity grows slowly because after each jump the particle moves fast and thus approaches again the new intersection point. On the other hand, by virtue of Eq. (1.64), the larger $v(t)$ the faster $z_r(t)$ and thus also the faster the intersection points move. This leads to a positive feedback and entails a strong slope when the velocity is large enough such that the particle is no longer able to approach a force free point before the next jump sets in. Finally, far above h_p the particle is depinned. After the driving force has reached its maximum it decreases. Note that the root of the straight line z_r has now a velocity smaller than $v(t)$, because \dot{h} is negative. Therefore, the particle position $z(t)$ approaches $z_r(t)$ and slows down. Hence, \dot{h} is a measure also for the decrease of $v(t)$. On approaching h_p from above, all particles are still depinned and hence far enough behind the leftmost intersection point, so that the latter has only little influence on the motion of the particle and the velocity decays with the same slope all the time. Only when $v(t)$ has passed below \dot{h}/c , z_r moves in the negative direction and thus the intersection points as well. This means, that the leftmost intersection point approaches the particle *before* it is pinned. After the particle is a little to the right of the leftmost force free position, which happens about when $h(t) \approx h_p$, the velocity is negative. Now, the same procedure starts in the other direction.

As $\omega \rightarrow 0$, the hystereses approach the depinning curve that has been discussed in the previous chapter. In the following, we are going to take a closer look on the details of this limiting process.

Velocity exponents

First, we want to work out, how

$$v_{h_0} \equiv |v(h = 0)| \quad (1.68)$$

approaches zero as $\omega \rightarrow 0$. As we have explained in Sec. 1.3.2, the particle in each disorder realisation stays close to a force-free point, that we have agreed to label $z_f(t)$. The velocity $\partial_t z$ of the particle is now determined solely by the velocity of the force free position z_f that we are now going to calculate in a more accurate way than our estimate from Eq. (1.67). Let t_0 be the point in time, at which $h(t_0) = 0$. On time scales that are small compared to the period ω^{-1} , we can linearly expand the driving field around t_0

$$h(t) \simeq -h\omega(t - t_0). \quad (1.69)$$

Further, we want to expand (1.62) around $z_f(t_0)$. For small distances in time we can neglect possible changes in the velocity and write

$$z_f(t) \simeq z_f(t_0) + v_f(t - t_0), \quad (1.70)$$

where $v_f = \partial_t z_f$ is a shorthand notation. Using (1.69) as well as $\langle z \rangle(t) \simeq \langle z \rangle(t_0) - v_{h_0}(t - t_0)$, we have

$$\begin{aligned} 0 &= c[z_f(t_0) + v_f(t - t_0) - \langle z \rangle(t_0) + v_{h_0}(t - t_0)] + h\omega(t - t_0) - g(z_f(t_0)) - g'(z_f(t_0))v_f(t - t_0) \\ &= (t - t_0)[c(v_f + v_{h_0}) + h\omega - v_f g'(z_f(t_0))] \end{aligned} \quad (1.71)$$

Since this should hold for small but finite $|t - t_0|$, the expression in the rectangular brackets has to vanish. Solving (1.71) for v_f , taking the disorder average and using the self-consistency condition $\langle v_f \rangle = -v_{h_0}$ finally yields

$$v_{h_0} = -\frac{h\omega}{c - \langle [c - g'(z_f(t_0))]^{-1} \rangle^{-1}}. \quad (1.72)$$

Since $g'(z_f(t_0)) < 0$, which expresses the reasonable assumption that z_f is a stable force free position, v_{h_0} is indeed positive, which must be the case by its definition (1.68). Note, that our derivation so far does not make any assumption about the disorder correlator, whence it holds for cusped as well as for smooth disorder. In conclusion, for $\omega \rightarrow 0$ the width of the hysteresis at $h = 0$ behaves as $v_{h_0} \sim \omega^\kappa$ with $\kappa = 1$ for either kind of disorder. This exponent is verified by our numerical analysis, cf. figure 1.15.

Another interesting quantity to look at is

$$v_{h_p} \equiv |v(h = h_p)|, \quad (1.73)$$

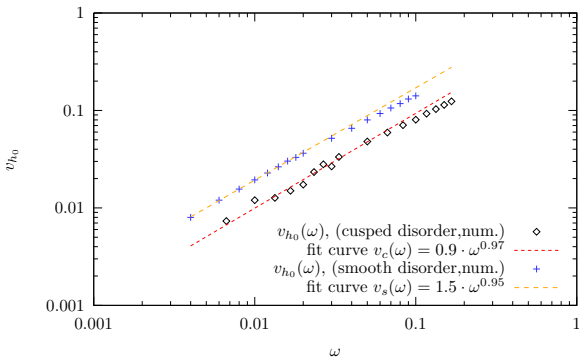


Fig. 1.15: The velocity v_{h_0} as a function of frequency. The plotted data correspond to numerical measurements at $c = 0.33$ for cusped and $c = 0.2$ for smooth disorder. For either type of disorder, the exponent is close to 1 ($\kappa_c = 0.97 \pm 0.07$ and $\kappa_s = 0.95 \pm 0.04$) in agreement with our analytical derivation given in the main text.

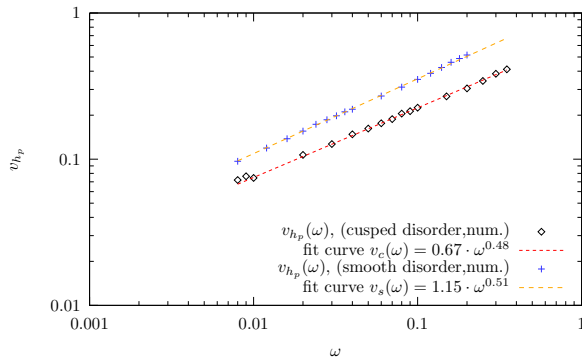


Fig. 1.16: The velocity v_{h_p} as a function of frequency. The plotted data correspond to numerical measurements at $c = 0.33$ for cusped and $c = 0.2$ for smooth disorder. For both types of disorder, the exponents are close to $1/2$ ($\mu_c = 0.48 \pm 0.02$ and $\mu_s = 0.51 \pm 0.01$).

of which we want to work out the limiting behaviour for $\omega \rightarrow 0$. As $h(t)$ increases further from 0 towards h_p , more and more of the force free points z_f , which the true positions in the disorder realisations are following, become the rightmost ones, so that occasionally jumps occur. On closely approaching $h(t) = h_p$ the dominant contribution originates from these jumps, which severely affects the exponent, so that $v_{h_p} \sim \omega^\mu$ with $\mu \simeq 1/2$, as can be inferred from our numerical analysis, shown in figure 1.16. This exponent is again independent of the shape of the disorder correlator at the origin (smooth or cusped). An analytical derivation of this exponent is much more complicated than it was the case for κ and in fact we did not find a rigorous prediction. For the finite dimensional case in $4 - \epsilon$ dimensions, the exponent μ has been found as $\mu = \beta/(\nu z)$, where ν denotes the correlation length exponent and z the dynamical exponent [38].

The area of the hysteresis loop

Next, we want to investigate the limiting behaviour of the hysteresis area. The physical meaning of the loop area can be concluded from the energy balance of an overdamped system. For the change of the disorder averaged potential energy in time, we find (cf. App. A.3)

$$\partial_t \langle E \rangle = h(t)v(t) - \langle (\partial_t z)^2 \rangle. \quad (1.74)$$

Here, $h(t)v(t)$ measures the energy gain through the work per unit time that is done by the external field and $\langle (\partial_t z)^2 \rangle$ measures the energy loss per unit time due to dissipation. The area of the hysteresis loop is determined via

$$A_{\text{hyst}}(\omega) = \oint v(t) dh = \int_0^T v(t) \dot{h}(t) dt. \quad (1.75)$$

This means, the loop area denotes the integrated change in work per unit time due to the change of the external field.

Note, that in the case of a double hysteresis (which occurs for large h , when the motion of the system over one period extends on average over more than one valley of the disorder potential), the area is given by the area of the inner hysteresis minus the area of the two outer hystereses (cf. Fig. 1.9). Formally, this is because the inner hysteresis is traversed clockwise, whereas the outer loops are passed through counter-clockwise. Physically, this can be understood as follows. Starting from $h = 0$ at the branch of increasing $h(t)$, the external field works against the potential gradient due to elastic energy and disorder. On going over into the regime of the outer loops, sliding behaviour sets in and thus the potential energy, stored so far in the system, adds to the work done by the external field. This fact is responsible for the steep slope at the beginning of the outer loop. In other words, during the period in the outer loops, the external field does not any more work against a potential gradient, but together with the potential energy the system is accelerated.

To work out the hysteresis loop area as $\omega \rightarrow 0$, we distinguish three cases.

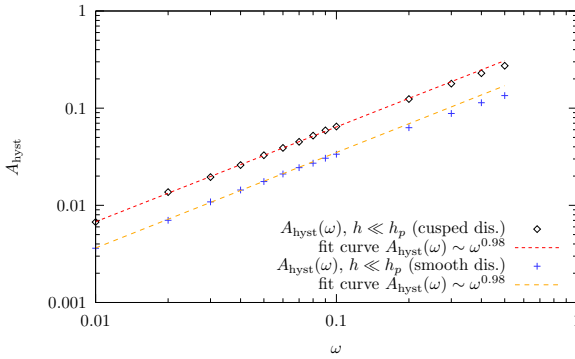


Fig. 1.17: The area of the hysteresis loop is plotted as a function of the driving frequency in case $h \ll h_p$. For small ω the area is diminished proportional to ω (exponent 0.98 ± 0.01), as expected.

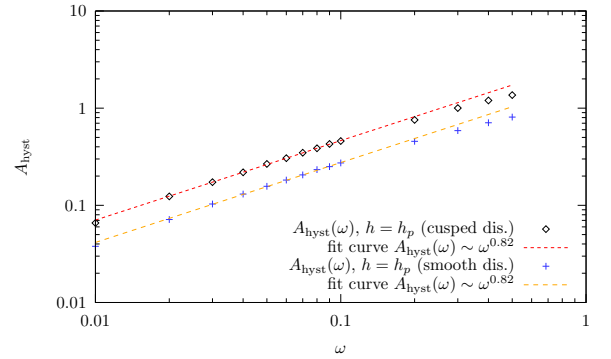


Fig. 1.18: The area of the hysteresis loop is plotted as a function of the driving frequency in case $h \simeq h_p$. For small ω the area vanishes with an exponent 0.82 ± 0.01 , independent of the type of disorder.

(a) $h \ll h_p$. In this situation, the hysteresis consists of a single loop. The outer loops, visible in Fig. 1.9, are absent. We expect the loop area to be given by $A_{\text{hyst}} \approx v_{h_0} h \sim \omega^\kappa$. Indeed, our numerical solution shows that the area of the hysteresis vanishes proportional to ω , independent of the type of disorder correlator, as shown in Fig. 1.17.

(b) $h = h_p$. For this case, the hysteresis loop is still single (no double hysteresis) and the hysteresis area decreases with the frequency as $A_{\text{hyst}} \sim \omega^{0.82}$ (cf. Fig. 1.18), still independent of the disorder correlator.

(c) $h \gg h_p$. Now, we face the situation of a double hysteresis and moreover, the behaviour of the hysteresis area as $\omega \rightarrow 0$ now depends on the shape of the disorder correlator. We find $A_{\text{hyst}} \sim \omega^\alpha$ with $\alpha \simeq 0.67 \approx 2/3$ for cusped and $\alpha \simeq 0.75 = 3/4$ for smooth disorder. This is shown in Fig. 1.19.

So far, our results suggest that the scaling exponents are insensitive to the nature of the

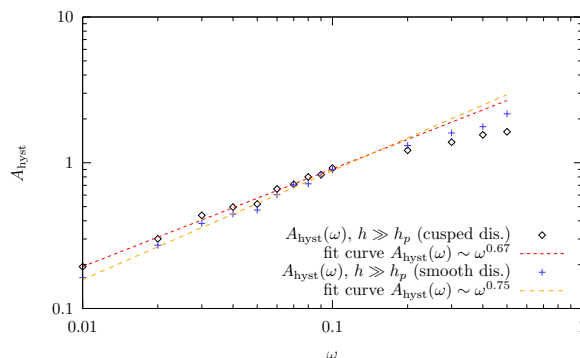


Fig. 1.19: The area of the hysteresis loop is plotted as a function of the driving frequency in case $h \gg h_p$. The diminution of the area with ω can be described as a power law with different exponents for cusped ($\alpha = 0.67 \pm 0.03$) and smooth disorder ($\alpha = 0.75 \pm 0.04$).

disorder correlator as long as the force amplitude does not exceed the threshold h_p . These findings seem to milden the non-universality conclusion by Fisher [47], who considered the response of a charge density wave system to an ac force in addition to dc driving. He distinguished different distributions of the random amplitude (pinning strength) of the disorder potential in addition to a random phase, and found a strong dependence of the behaviour on the type of disorder both above and below threshold.

For large frequencies, the area of the hysteresis loop vanishes as well. Above a certain crossover frequency, which depends on h , the motion of the particle is restricted to one minimum of the potential. Thus, for large enough frequencies we can approximate the potential by a harmonic one, such that the equation of motion for the disorder averaged position becomes

$$v(t) = h \cos \omega t - w z(t), \quad (1.76)$$

which has the solution

$$v(t) = \frac{w\omega h}{w^2 + \omega^2} \left[-\sin \omega t + \frac{\omega}{w} \cos \omega t \right]. \quad (1.77)$$

Thus, using Eq. (1.75) we find for the hysteresis loop area

$$A_{\text{hyst}}(\omega) = \int_0^T v(t) \dot{h}(t) dt = \frac{w\omega^2 h^2}{w^2 + \omega^2} \frac{\pi}{\omega} \sim \omega^{-1}, \quad (1.78)$$

where the last expression gives the asymptotics for large ω .

The decay of the hysteresis loop area for large and small frequencies of the driving force requires the existence of a maximum. This maximum is found to be proportional to the resonance frequency of the typical disorder potential wells $\omega_r = \gamma u_0 / \ell$, which equals 1 in our units. The proportionality factor is of order unity, and is found different for small driving fields (single hysteresis) and large drivings (double hysteresis).

1.4 Perturbation theory

In many cases, for a first quantitative analysis of complicated non-linear problems, like the equation of motion (1.2) considered in this section, one uses a perturbation expansion. However, perturbative approaches are sometimes hampered by mathematical subtleties, like non-analyticities or singular perturbation theory (cf. [51]), or by physical obstacles such as non-perturbative excitations or strong coupling. The difficulty with perturbation theory as a tool for the analysis of pinned elastic objects has its own interesting history.

Until the beginning of the eighties, the lower critical dimension d_l of the random field Ising model has been the subject of a long-lasting debate. Dimensional reduction predicted that the lower critical dimension equals $d_l = 3$, whereas domain-wall arguments [4] lead to the conclusion, that $d_l = 2$. Eventually, in 1984 a final decision could be made and dimensional reduction was proven to fail [52, 53]. The reason for the failure has been explained later [1, 54]. It is connected with the existence of many metastable states for the domain walls separating different regimes in a multidomain configuration. The plethora of metastable states arises from the dominance of the disorder over the domain wall elasticity on length scales above the so-called Larkin length L_p [55] for sample dimensions $d < 5$. A perturbative iteration to find the energy minimum will not necessarily yield the correct extremal state [56, 57]. Put in more mathematical terms, the formal perturbative treatment of the domain walls assumes an analytic disorder correlator. However, a functional renormalisation group (FRG) treatment shows [1], that any initially analytic disorder correlator develops a cusp-singularity at a finite length scale, which is the Larkin length L_p .

This insight has important consequences for the problem of an interface in a disordered environment exposed to a constant driving force h . The cusp singularity in the random force correlator provides for the existence of a sharp depinning transition at zero temperature, i.e. that the interface velocity is exactly zero in case $h < h_p$. Though the depinning threshold has already been estimated by Feigel'man [43] in 1983, his theory signals the absence of a sharp depinning if taken self-consistently. More generally, each perturbative expansion in the disorder, which has to assume an analytic force correlator, is bound to fail close to depinning. Thus, the depinning transition cannot be accounted for by perturbatively expanding the disorder.

On the other hand, for large driving fields, far in the sliding regime, the dynamic correlation length $\xi_v \sim v^{-\frac{1}{2}}$ is smaller than the Larkin length and thus the renormalisation flow stops before the cusp has emerged (for a detailed explanation, cf. Ref. [20]). In this case, the sliding velocity can well be estimated perturbatively.

Equipped with these insights we are going to analyse the perturbation theory for ac-driven domain walls. For the aforementioned reasons it is clear, that in the vicinity of the critical point $(h, \omega) = (h_p, 0)$ perturbation theory is expected to yield erroneous results, if not properly combined with an FRG treatment. Yet, FRG equations for the related problem of a constant driving force, have been obtained by the construction of a perturbative series and a subsequent ϵ -expansion. So, understanding the perturbation theory in the regime where it is expected to work, i.e. for large driving frequencies, is the first necessary starting point. For sufficiently large frequencies and driving field amplitudes, from the physical point of view there appears to be no contraindication against a perturbative procedure. However, as will become

clear in this section, for systems subject to periodic driving forces perturbation theory in the disorder strength gives non-regular contributions to the velocity corrections for an internal interface dimension $D \leq 4$. With the attribute non-regular we refer to expressions that grow unboundedly in time. Such unbounded contributions certainly do not reflect the true physical behaviour, but their origin deserves careful investigation. Far away from the critical point, this behaviour of perturbation theory cannot be related to the assumption of an analytic disorder correlator. Quite the contrary, working with a cusped disorder correlator brings additional difficulties due to the delta functions in its derivatives.

1.4.1 The diagrammatic expansion

There are little methods to tackle highly nonlinear differential equations, like our equation of motion (1.2). We present here an attempt via a perturbative expansion in the disorder strength u . We are going to derive the perturbation expansion directly for the equation of motion, since this appears simpler. There is, however, another approach via functional integrals which came in useful for the two loop functional renormalisation group calculations in the case of a constant driving force. The reader who is more familiar with this technique may find a brief treatment in appendix A.4 which reveals the connection to our methodology.

First order

The perturbation expansion of the equation of motion (1.2) is naturally performed around the solution for the problem without disorder², i.e. where $u = 0$. In this case, we have a flat wall following the driving field: $Z(t) = (h/\omega) \sin \omega t$. Thus, we decompose $z(\mathbf{x}, t)$ into the disorder-free solution and a correction, i.e. $z(\mathbf{x}, t) = Z(t) + \zeta(\mathbf{x}, t)$. The equation of motion for the disorder correction $\zeta(\mathbf{x}, t)$ is easily derived from Eq. (1.2)

$$(\partial_t - \Gamma \nabla_{\mathbf{x}}^2) \zeta(\mathbf{x}, t) = u \cdot g(\mathbf{x}, Z + \zeta). \quad (1.79)$$

The Green function for the differential operator on the left hand side is the well-known heat kernel

$$\begin{aligned} (\partial_t - \Gamma \nabla_{\mathbf{x}}^2) G(\mathbf{x}, t) &= \delta^D(\mathbf{x}) \delta(t) \\ G(\mathbf{x}, t) &= \Theta(t) \int \frac{d^D \mathbf{k}}{(2\pi)^D} e^{i\mathbf{k}\mathbf{x} - \Gamma k^2 t}. \end{aligned} \quad (1.80)$$

The \mathbf{k} -integral has to be cut off at some scale Λ , corresponding to the inverse smallest length scale in the system. To set up the perturbation series, we expand the correction in the disorder strength

$$\zeta(\mathbf{x}, t) = \sum_{n=1}^{\infty} u^n \zeta_n(\mathbf{x}, t) \quad (1.81)$$

²Another possibility is to expand around the disorder averaged solution $z(t) = \langle z(t) \rangle + \xi(t)$ with $\langle \xi(t) \rangle = 0$. This approach, however, complicates matters due to the lack of a definite expansion parameter but does not lead to a “better” expansion. We briefly glimpse this in App. A.7

and the disorder force around the non-disordered solution

$$g(\mathbf{x}, Z + \zeta) = \sum_{k=0}^{\infty} \partial_2^k g(\mathbf{x}, Z) \frac{\zeta^k}{k!}. \quad (1.82)$$

Thus, we obtain an equation for the first order correction:

$$\zeta_1(\mathbf{x}, t) = \int d^D \mathbf{x}' \int_0^{\infty} dt' G(\mathbf{x} - \mathbf{x}', t - t') g(\mathbf{x}', Z(t')). \quad (1.83)$$

Obviously, the disorder average vanishes. The disorder average for the second order contribution is given by

$$\langle \zeta_2 \rangle(t) = \int_0^t dt_1 \int_0^{t_1} dt_2 \Delta'[Z(t_1) - Z(t_2)] \int \frac{d^D \mathbf{k}}{(2\pi)^D} e^{-\Gamma k^2(t_1 - t_2)}. \quad (1.84)$$

The second order correction to the velocity follows straightforwardly

$$\langle v_2 \rangle(t) = \int_0^t dt' \Delta'[Z(t) - Z(t')] \int \frac{d^D \mathbf{k}}{(2\pi)^D} e^{-\Gamma k^2(t - t')}. \quad (1.85)$$

To get a first impression on how this expression behaves for large t , we split off the Fourier-0-mode:

$$\Delta'[Z(t) - Z(t')] = F_0(\omega t)/\ell + p(t, t') \quad (1.86)$$

$$F_0(\omega t) = \sum_{n=0}^{\infty} K_n \left(\frac{h}{\omega \ell} \right) \cdot \sin(2n + 1)\omega t. \quad (1.87)$$

Here, $p(t, t')$ is a well-behaved oscillation around 0 in t' . Since $p(t, t')$ yields a bounded contribution to $\langle v_2 \rangle(t)$, we consider only $F_0(t)$ to find out, how $\langle v_2 \rangle$ increases asymptotically in time. The Fourier coefficients K_n can be determined analytically. They are diminished when their argument increases or approaches zero and they remain bounded. Integration over t' yields

$$\langle v_2 \rangle(t) \sim \frac{F_0(\omega t)}{\ell} \frac{S_D}{(2\pi)^D} \int_0^{\Lambda} \frac{dk}{\Gamma} k^{D-3} [1 - e^{-k^2 \Gamma t}] = \frac{t^{\frac{2-D}{2}} F_0(\omega t)}{\ell \Gamma^{D/2}} \cdot a_D(t/\vartheta), \quad (1.88)$$

where $\vartheta = \Lambda^{-2}/\Gamma$ and

$$a_D(x) = \frac{S_D}{(2\pi)^D} \int_0^{\sqrt{x}} dp p^{D-3} [1 - e^{-p^2}]. \quad (1.89)$$

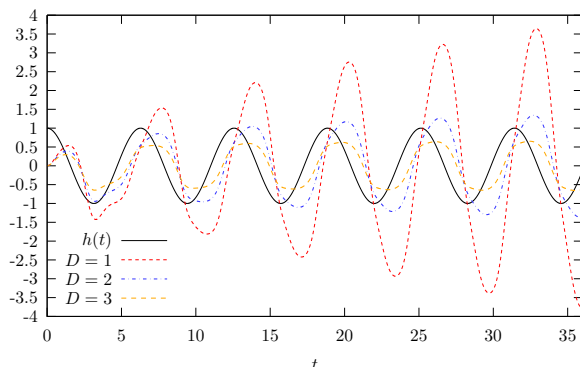


Fig. 1.20: Plot of the first non-vanishing perturbative correction $\langle v_2 \rangle(t)$ to the disorder average $\langle v(\mathbf{x}, t) \rangle$ for different interface dimensions. For the plot we used $h = 1$ and the units are chosen such that $\omega = \ell = 1$.

For $x \rightarrow \infty$ the integral a_D converges for $D < 2$ and diverges logarithmically for $D = 2$. Thus, the asymptotic behaviour of the first perturbative correction in time is given by

$$\langle v_2 \rangle(t) \sim c_D(t) \cdot \begin{cases} t^{\frac{2-D}{2}} & D < 2 \\ \ln t & D = 2 \\ \text{const} & D > 2 \end{cases} \quad (1.90)$$

where $c_D(t)$ is some bounded function. Figure 1.20 shows the plots of $\langle v_2 \rangle(t)$ for $D = 1, 2, 3$. Obviously, there is a problem of the perturbation expansion in low dimensions. In the following, we are going to see that perturbation theory does not work even for $D \leq 4$.

Higher order graphical expansion

Higher orders of the perturbation expansion are best expressed diagrammatically. To deduce the diagrammatic rules, all one has to do is plugging (1.81) into (1.82), rearranging the sum in powers of u and inserting this into (1.79). The diagrammatic rules that emerge are fairly simple: to express the perturbative correction of order n , we draw all rooted trees with n vertices and add a stem. Up to the fourth order, this tree graph expansion is given by

$$\zeta_1 = \text{---} \bullet \quad (1.91)$$

$$\zeta_2 = \text{---} \bullet \text{---} \bullet \quad (1.92)$$

$$\zeta_3 = \begin{array}{c} \bullet \\ \diagup \\ \text{---} \bullet \\ \diagdown \\ \bullet \end{array} + \text{---} \bullet \text{---} \bullet \text{---} \bullet \quad (1.93)$$

$$\zeta_4 = \begin{array}{c} \bullet \\ \diagup \\ \text{---} \bullet \\ \diagdown \\ \bullet \end{array} + \text{---} \bullet \text{---} \bullet \text{---} \bullet \text{---} \bullet + \begin{array}{c} \bullet \\ \diagup \\ \text{---} \bullet \\ \diagdown \\ \bullet \end{array} + 2 \cdot \begin{array}{c} \bullet \\ \diagup \\ \text{---} \bullet \\ \diagdown \\ \bullet \end{array} \quad (1.94)$$

Every vertex represents a disorder insertion $g^{(m)}(Z(t))/m!$, where m counts the number of outgoing branches (away from the root). Every line corresponds to an integral operator, the kernel being the propagator $G(\mathbf{x}, t)$. To get the graphical expansion for the velocities, just remove the first line. The disorder average can be carried out using Wick's theorem, since our disorder is assumed to be Gaussian. An immediate consequence is, that after averaging over disorder, only graphs with an even number of vertices survive. In the following, we are going to consider the perturbation expansion for the disorder averaged velocity $v(t)$. The pairing for the disorder average shall be denoted by a dashed line. An example graph from the 4th-order is


(1.95)

Using this graphical expansion, in appendix A.5 we take a look at the general behaviour of the diagrammatic contributions to all orders for $t \rightarrow \infty$ and argue that all graphs remain bounded in case $D > 4$.

1.4.2 The failure of perturbation theory for $D \leq 4$

For $D \leq 4$ the perturbation expansion is not as well-behaved as for $D > 4$. In this section, we show this and give an explanation why perturbation theory is ill-behaved in low dimensions.

Though the disorder averaged graphical structure can become complicated, one especially simple graph has the same structure in all orders: the one for which all vertices are connected directly to the root. In the equations (1.91-1.94), we have drawn those graphs at the very first place. Let us call them bushes. The general bush graph contribution to the velocity correction of order $2p$ thus corresponds to the following diagram


(1.96)

where the dotted line is a placeholder for other vertices that we have not drawn. Up to combinatorial factors, the general (disorder averaged) bush B_{2p} that occurs in the $2p$ -th order perturbative correction to the velocity v , reads

$$\langle B_{2p} \rangle (t) \propto \left[\int_0^t dt_1 dt_2 \Delta[Z(t_1) - Z(t_2)] \int \frac{d^D \mathbf{k}}{(2\pi)^D} e^{-\Gamma k^2(2t-t_1-t_2)} \right]^{p-1} \times$$

$$\int_0^t dt' \Delta^{(2p-1)}[Z(t) - Z(t')] \int \frac{d^D \mathbf{k}}{(2\pi)^D} e^{-\Gamma k^2(t-t')} \quad (1.97)$$

$$\equiv T_1^{p-1} \cdot T_2 \quad (1.98)$$

To work out the asymptotic envelope of $\langle B_{2p} \rangle (t)$ for large t we only need to take a look at the expression T_1 . Since Δ is an entirely positive function, and the \mathbf{k} -integral is certainly non-negative, we can replace Δ by its maximum $\Delta(0)$ to get an upper bound, and if we replace Δ

by the minimal value that is taken $\Delta[2h/(\omega\ell)]$, we get a lower bound for T_1 . In both cases, $\Delta[Z(t_1) - Z(t_2)]$ is replaced by a constant, so that the integration over t_1 and t_2 can be done easily. Consequently, up to a constant, the asymptotic envelope of T_1 is given by

$$T_1(t) \sim \int \frac{d^D \mathbf{k}}{(2\pi)^D} \frac{[1 - e^{-\Gamma k^2 t}]^2}{\Gamma^2 k^4} = \frac{\ell^2}{u^2} \left[\frac{t}{\tau} \right]^{\frac{4-D}{2}} A_D(t/\vartheta). \quad (1.99)$$

Here, the constants τ and ϑ are time scales, given by

$$\tau = \Gamma^{\frac{D}{4-D}} \left[\frac{\ell}{u} \right]^{\frac{4}{4-D}} = \left(\frac{\ell}{u} \right) L_p^{\frac{D}{2}} = L_p^2 / \Gamma, \quad (1.100)$$

$$\vartheta = \Lambda^{-2} / \Gamma, \quad (1.101)$$

and the function $A_D(x)$ has been introduced for notational convenience

$$A_D(x) = \frac{S_D}{(2\pi)^D} \int_0^{\sqrt{x}} dp p^{D-5} [1 - e^{-p^2}]^2. \quad (1.102)$$

The function $A_D(x)$ is increasing but bounded for $D < 4$ and grows logarithmically as $x \rightarrow \infty$ for $D = 4$. Thus T_1 grows monotonically in t for any $D \leq 4$.

Actually, our statement about the asymptotics in Eq. (1.99) is more robust than our simple argument suggests, and in fact does not rely on the positivity of Δ . A more detailed calculation, presented in appendix A.6 shows that

$$T_1 = \frac{\ell^2}{u^2} \left[\left(\frac{t}{\tau} \right)^{\frac{4-D}{2}} \kappa_D \left(\frac{t}{\vartheta} \right) + \left(\frac{t}{\tau} \right)^{\frac{4-D}{4}} \frac{u\Lambda^{\frac{D}{2}}}{\omega\ell} k_D \left(\frac{t}{\vartheta}, \omega t \right) + \frac{u^2\Lambda^D}{\omega^2\ell^2} P_D \left(\frac{t}{\vartheta}, \omega t \right) \right] \quad (1.103)$$

and

$$T_2 = \frac{\omega\ell}{u^2\ell^{2(p-1)}} \left[\frac{u\Lambda^{\frac{D}{2}}}{\omega\ell} \left(\frac{t}{\tau} \right)^{\frac{4-D}{4}} f_D \left(\frac{t}{\vartheta}, \omega t \right) + \frac{u^2\Lambda^D}{\omega^2\ell^2} p_D \left(\frac{t}{\vartheta}, \omega t \right) \right] \quad (1.104)$$

where all of the functions κ_D , k_D , P_D , f_D and p_D are bounded in t for $D < 4$. The first term of T_1 shows, that for $D \leq 4$ the whole expression grows for $t \rightarrow \infty$ without any bound. This is, because by definition (cf. equation (A.57)), $\kappa_D \propto A_D$, where A_D is given by (1.102). The other tree graphs that appear in the graphical representation of $\langle v_{2p} \rangle$ and that we have not analysed here, exhibit similar behaviour. Cancellations among diagrams do not occur. To have a little more evidence, that $D = 4$ really enters as an upper critical dimension, we have perturbatively investigated the interface's width in appendix A.7. In summary, perturbation theory is ill behaved for $D \leq 4$. The reason for this shall be discussed in the following.

The bushes $\langle B_{2p} \rangle$ that we have considered so far are part of an expansion of the disorder averaged velocity

$$v(t) = h \cdot \cos \omega t + v_{\text{dis}}(t) \quad (1.105)$$

in the disorder strength u . The dimensionless ratios, in which u occurs in that expansion are

$$\left(\frac{t}{\tau}\right)^{\frac{4-D}{4}} \quad \text{and} \quad \frac{u\Lambda^{\frac{D}{2}}}{\omega\ell}. \quad (1.106)$$

Since in the stationary state the interface is expected to follow the driving with frequency ω , its Fourier representation has to take on the form

$$v_{\text{dis}}(t) = \omega\ell \sum_n \left[e_n \left(\left(\frac{t}{\tau}\right)^{\frac{4-D}{4}}, \frac{u\Lambda^{\frac{D}{2}}}{\omega\ell}, \frac{t}{\vartheta} \right) \cos n\omega t + f_n \left(\left(\frac{t}{\tau}\right)^{\frac{4-D}{4}}, \frac{u\Lambda^{\frac{D}{2}}}{\omega\ell}, \frac{t}{\vartheta} \right) \sin n\omega t \right]. \quad (1.107)$$

Because of the ratio t/τ , an expansion in the disorder u brings powers of $t^{\frac{4-D}{4}}$ in every order, since τ depends on u (cf. equation (1.100)). The remaining question is the meaning of τ . Since τ appears as a time scale for the time dependence of the Fourier coefficients, which physically should approach a constant value in the stationary state $t \rightarrow \infty$, the most natural interpretation is the transience. Keeping in mind, that we start with a flat wall, we have to expect several kinds of transience effects. As we have seen, there are only two time scales in question: τ and ϑ . As can be concluded from their definitions (cf. equations (1.100) and (1.101)), they obey the same structure: an intrinsic length scale to the power 2 divided by Γ . The time scale τ involves the Larkin length L_p (cf. equation (1.6)), which measures the competition between disorder and elasticity: the interface is flat on length scales $L \lesssim L_p$. This indicates that, up to some dimensionless prefactor, τ describes the time during which correlated interface segments of extension L_p adopt to their local disorder environment, i.e. the roughening time of the interface. For $D > 4$, the interface is flat on all length scales, thus there is neither roughening nor a Larkin length, hence τ is meaningless and cannot occur. This agrees with our observation. For $D > 4$, there is no disorder-dependent time scale any more, which could bring powers of time in the perturbative corrections, therefore they remain finite as $t \rightarrow \infty$. However, also for $D > 4$ the disorder leads to a typical deviation of every point of the interface from the mean position. The built-up of this typical deviation towards its steady-state value happens on the time-scale ϑ , in agreement with the observation for mean-field theory (cf. section 1.5). Thus, both time scales can naturally be interpreted as the life times of two different transience effects.

1.4.3 Interfaces subject to a constant driving force

In the introduction, we already pointed out that perturbation theory in connection with interfaces driven by a constant force cannot properly account for the existence of the depinning transition and therefore gives misleading results for $D \leq 4$. But far above the depinning threshold, i.e. for $h \gg h_p$, the interface slides and its velocity can be estimated perturbatively. The dynamical correlation length $L_v = \Gamma\ell/v$ [20] is then small compared to the Larkin length L_p and thus working with an analytic disorder correlator and expanding the disorder in its moments works. Of course, also for constant driving forces one has to start with a definite initial condition, which is usually a flat wall. Thus, there will be transience effects for dc-driven interfaces as well [58, 59]. In this section we take a short glance to understand the

difference between ac and dc-driving. Our special interest is devoted to the time scales that determine the duration of transience effects.

The equation of motion for the elastic interface experiencing a constant driving force

$$\partial_t z(\mathbf{x}, t) = \Gamma \nabla_{\mathbf{x}}^2 z + h + u \cdot g(\mathbf{x}, z), \quad (1.108)$$

has the disorder-free solution ($u = 0$) $Z(t) = ht$. The perturbation expansion is essentially the same as in section 1.4.1, just the non-disordered solution around which we expand is different.

Actually, there is a problem with the decomposition $z = Z + \zeta$ here, since the sliding velocity v is different from h , hence $\zeta \sim (v - h)t$ is not a small quantity (compared to ℓ) for large t and the Taylor expansion (1.82) of the disorder is questionable. Since here we shall not be interested in large times $t > \ell/(h - v)$ but only want to determine the time scale of the transience (occurring at small $t \ll \ell/(h - v)$), this problem is safely ignored.

The first non-vanishing correction to the velocity is found to be (cf. eq. (1.85)) [60]

$$\begin{aligned} \langle v_2 \rangle(t) &= \int_0^t dt' \Delta' [Z(t) - Z(t')] \int \frac{d^D \mathbf{k}}{(2\pi)^D} e^{-\Gamma k^2(t-t')} \\ &= \frac{1}{h} \int \frac{d^D \mathbf{k}}{(2\pi)^D} \left[e^{-k^2 \Gamma t - \frac{h^2 t^2}{\ell^2}} - \varphi \left(\frac{\Gamma \ell k^2}{2h}, \frac{ht}{\ell} \right) \right] \\ &= \frac{\Lambda^D}{(t/\vartheta)^{\frac{D}{2}} h} \frac{S_D}{(2\pi)^D} \int_0^{\sqrt{t/\vartheta}} dp p^{D-1} \left[e^{-p^2 - \frac{h^2 t^2}{\ell^2}} - \varphi \left(\frac{p \ell}{2ht}, \frac{ht}{\ell} \right) \right] \end{aligned} \quad (1.109)$$

where we have introduced the function

$$\varphi(a, b) = 1 - \sqrt{\pi} a \cdot e^{a^2} \cdot [\operatorname{erf}(a + b) - \operatorname{erf}(a)] \quad (1.110)$$

for convenience. The time-scales on which transience effects disappear are obviously given by

$$\tau_{\text{dc}} = \frac{\ell}{h} = \frac{L_h^2}{\Gamma} \quad \text{and} \quad \vartheta = \frac{\Lambda^{-2}}{\Gamma} \quad (1.111)$$

and are manifestly disorder-independent. $L_h = \Gamma \ell / h$ denotes the correlation length of an interface moving with a velocity h . Of course, asymptotically the interface moves with a velocity $v < h$, but at the very beginning, when we start off with a flat wall, its velocity is indeed given by h (cf. (1.108)).

It is not surprising, that the time scale of the initial roughening is different for dc and ac driving. Either problem involves completely different physical processes to be responsible for transience. In the case of an ac-driving, the system undergoes a process of adaption of its configuration to the *local* disorder, such that a stable stationary oscillation is possible, and during which higher Fourier modes build up. For dc-driving, the system starts to move with a velocity of h , which then rapidly decreases, and roughens since segments of the interface are pinned and remain at rest until they are pulled forward by the neighbouring segments through the elastic coupling. The time for this process mainly depends on the velocity of the interface, not on the strength of the disorder.

1.5 Mean field perturbation theory

As we have seen in the previous section, perturbation theory fails to produce reasonable results in all physically interesting dimensions $D \leq 4$. In this section, we are going to take a look on the perturbation expansion for the mean-field theory. Formally corresponding to $D = \infty$, perturbation theory for the mean-field equation of motion works, at least sufficiently far away from depinning. Though this is true, the regularity of the mean-field diagrammatic expansion is not immediately obvious. The reader who has gone through App. A.5 may recall that there we came along diagrams that included zero-momentum lines. These diagrams are problematic in all dimensions, and in our mean-field analysis we encounter them again in a slightly different setup. Already Koplik and Levine [45] came along these non-regular diagrams on inspecting their expansion for interfaces driven by a constant force. They have verified up to sixth order, that the problematic diagrams compensate each other. We also prove that their singular parts mutually cancel. Our proof is valid for any kind of driving and extends to all perturbative orders.

Throughout the whole section, we have to assume a smooth disorder correlator. To be specific, for our analytical calculations, we take the disorder force correlator as is specified in Eq. (1.5).

1.5.1 The diagrammatic expansion

Since the mean-field equation of motion (1.11) cannot be solved exactly, we attempt an expansion in the disorder strength η . Therefore, as before, we decompose $z = Z + \zeta$, where $Z(t) = (h/\omega) \sin \omega t$ is the solution of the non-disordered problem ($\eta = 0$) around which we expand, and

$$\zeta = \sum_{k=1}^{\infty} \zeta_k \eta^k, \quad \langle \zeta \rangle = \sum_{k=1}^{\infty} \langle \zeta \rangle_k \eta^k. \quad (1.112)$$

is the perturbative correction. Still, we have the equations for ζ_k depending on $\langle \zeta \rangle_k$, which is also unknown. This eventually leads us to a set of two coupled equations

$$(\partial_t + c)\zeta = c \langle \zeta \rangle + \eta \cdot g(Z + \zeta) \quad (1.113)$$

$$\partial_t \langle \zeta \rangle = \eta \cdot \langle g(Z + \zeta) \rangle, \quad (1.114)$$

that we can solve iteratively for every order of the perturbation series, if we expand

$$g(Z + \zeta) = \sum_{n=0}^{\infty} \frac{g^{(n)}(Z)}{n!} \zeta^n. \quad (1.115)$$

If one is interested to keep small orders, this expansion of the disorder can only work if $\zeta \ll \ell$, because ℓ is the typical scale on which $g(z)$ changes. We will come back to that point later in section 1.5.3, when discussing the validity of perturbation theory. For the moment, we just do it.

The propagator corresponding to the left hand side of Eq. (1.113) reads

$$G(t) = \Theta(t) \cdot e^{-ct}. \quad (1.116)$$

Using this propagator, we can formally write down the solution and express it order by order in a power series in η . Up to the second order, the solutions are

$$\langle \zeta \rangle_1(t) = 0, \quad (1.117)$$

$$\zeta_1(t) = \int_0^t dt_1 e^{-c(t-t_1)} g(Z(t_1)), \quad (1.118)$$

$$\langle \zeta \rangle_2(t) = \int_0^t dt_1 \int_0^{t_1} dt_2 e^{-c(t_1-t_2)} \Delta'[Z(t_1) - Z(t_2)], \quad (1.119)$$

$$\zeta_2(t) = \int_0^t dt_1 e^{-c(t-t_1)} [c \langle \zeta \rangle_2(t_1) + g'(Z(t_1)) \cdot \zeta_1(t_1)]. \quad (1.120)$$

Since we assume Gaussian disorder, the disorder averaged corrections $\langle \zeta \rangle_n$ vanish for odd n . We use a diagrammatic representation to depict the nested perturbation expansion. For the interesting quantities $\langle \zeta \rangle_k$, the first two non-vanishing orders are given by:

$$\langle \zeta \rangle_2 = \text{diagram} \quad (1.121)$$

$$\begin{aligned} \langle \zeta \rangle_4 = & 3 \cdot \text{diagram} + \text{diagram} + 2 \cdot \text{diagram} + \\ & 2 \cdot \text{diagram} + 2 \cdot \text{diagram} + 2 \cdot \text{diagram} + \\ & \text{diagram} + \text{diagram} + \text{diagram}. \end{aligned} \quad (1.122)$$

The diagrammatic rules are fairly similar to those in section 1.4.1: we draw all rooted trees with k vertices, and add a stem. Each vertex corresponds to a factor $g^{(m)}(Z(t))/m!$, where m counts the number of outgoing lines (away from the root). The line between two vertices represents a propagator $G(t)$. Then Wick's theorem is applied to carry out the disorder average. Each two vertices, that are grouped together for the average, will be connected by a dashed line. Finally, there is one new feature, that we did not come along in section 1.4.1. Every straight line which, upon removing it, makes the whole graph falling apart into two subgraphs, has to be replaced by a curly line. A curly line symbolises the propagator of (1.114), which is just a Heaviside function $\Theta(t)$. Those graphs that contain an internal curly line are exactly the one-particle reducible (1PR) diagrams.

1.5.2 Regularity of the perturbative series

The perturbation expansion leaves some questions, that have to be addressed. It is not immediately obvious, that taking the disorder average of (1.120) gives the result in (1.119), i.e. $\langle \zeta \rangle_2(t) = \langle \zeta_2(t) \rangle$. However, a short calculation, using integration by parts reveals this relation to hold.

Another, much deeper problem is related to the diagrams involving a curly line in their interior. Due to the curly line, they grow linearly in time. Already in section 1.4.1 and appendix A.5, we have mentioned that there are trees that contain lines the assigned momentum of which equals 0. Here, for the mean-field problem these lines are found as the troublesome curly lines: they connect a subtree with internal Gaussian pairing. Koplik and Levine [45] explicitly checked for a time independent driving $h(t) = h$ up to sixth order, that the problematic terms of the 1PR diagrams mutually cancel. We give a very general version of this proof, that holds for any time-dependence of the driving field $h(t)$ and covers all perturbative orders. To illustrate, how this works, we present the calculation for the fourth order here. The somewhat technical induction step, which extends our argument to all orders is given in appendix A.8. For simplicity, we work with the velocity diagrams, that are obtained by just removing the curly line from the root.

$$\begin{aligned}
 2 \cdot \text{Diagram 1} &= \int_0^t dt_1 e^{-c(t-t_1)} \Delta''[Z(t) - Z(t_1)] \int_0^{t_1} dt_2 \int_0^{t_2} dt_3 e^{-c(t_2-t_3)} \Delta'[Z(t_2) - Z(t_3)] \\
 & \tag{1.123}
 \end{aligned}$$

$$\begin{aligned}
 \text{Diagram 2} &= \int_0^t dt_1 e^{-c(t-t_1)} (-\Delta''[Z(t) - Z(t_1)]) \int_0^{t_1} dt_2 \int_0^{t_2} dt_3 e^{-c(t_2-t_3)} \Delta'[Z(t_2) - Z(t_3)] \\
 & \tag{1.124}
 \end{aligned}$$

$$\begin{aligned}
 &= -2 \cdot \text{Diagram 1} + S \\
 & \tag{1.125}
 \end{aligned}$$

$$\begin{aligned}
 S &= \int_0^t dt_1 \int_0^{t_1} dt_2 e^{-c(t-t_2)} \Delta''[Z(t) - Z(t_2)] \int_0^{t_1} dt_3 e^{-c(t_1-t_3)} \Delta'[Z(t_1) - Z(t_3)] \\
 & \tag{1.126}
 \end{aligned}$$

The modification of the second diagram to express it as the sum of the first and S is merely integration by parts for the integral over t_1 . The term S now corresponds to the sum of the two diagrams. It is easy to see, that S remains bounded for large times. Every time integral carries an exponential damping term. Basically, we have thereby established, that the perturbation series exists and is well-behaved in the sense, that there are no terms that lead to an overall unbounded growth in time.

1.5.3 Validity of perturbation theory

Still, the question is open, whether one may assume ζ to be small compared to ℓ . This was a requirement for the Taylor expansion (1.115) to be valid. If c is large, any particle moving

in a particular realisation of a disorder potential is strongly bound to the disorder averaged position. This prevents it from exploring the own disorder environment and thus large c effectively scale down η . All realisations stay close to the disorder averaged position, the mean deviation being approximated by η/c . A problem now occurs, if the disorder averaged position deviates strongly from the $\eta = 0$ solution. For $h \gg \eta$ this can only happen during those periods, where $h(t)$ takes on small values. The time that has to elapse until every system has adopted to its own disorder realisation, and hence the time until the system can be pinned, is c^{-1} (see below). For perturbation theory to work, this time must be large compared to the length of the period during which $h \leq \eta$, which we roughly estimate as $\eta/(\omega h)$. This gives us a second condition for the applicability of perturbation theory: $h/\eta \gg c/\omega$.

In summary, the conditions for perturbation theory to hold are the following. The driving force amplitude h has to be large compared to η , $h/\eta \gg \max\{c/\omega, 1\}$ to make the series expansion work and to guarantee that the disorder averaged solution stays close to the $\eta = 0$ trajectory (around which we expand). Moreover, c must be large ($c \gg \eta/\ell$) to ensure proximity of each realisation to the disorder average.

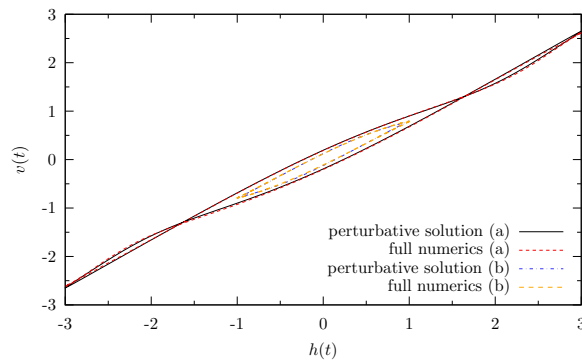


Fig. 1.21: Comparison of the full numerical solution of equation (1.11) with the result obtained from the first non-vanishing perturbative order eq. (1.127) for (a) $h = 3.0$, $c = 3.0$, $\eta = 1.5$ and (b) $h = 1.0$, $c = 1.0$, $\eta = 0.6$. The units of t and z are chosen such that $\omega = \ell = 1$.

The diagrammatic prescription yields

$$v(t) = h \cos \omega t + \eta^2 \int_0^t dt' e^{-c(t-t')} \Delta' [Z(t) - Z(t')] + \mathcal{O}(\eta^4). \quad (1.127)$$

A direct comparison of the numerical solution of (1.127) and the full equation of motion (1.11), shown in Fig. 1.21, confirms an excellent agreement.

1.5.4 Perturbative harmonic expansion

For an ac driving force, even the lowest perturbative order for the velocity, equation (1.127) is a very complicated expression. We know from the numerics that, in the steady state, the velocity is given by a periodic function with periodicity ω^{-1} . This recommends to aim a

harmonic expansion of the mean velocity v , i.e. to ask for the Fourier coefficients a_N and b_N in the ansatz

$$v(t) = \sum_{N=1}^{\infty} [a_N \cos N\omega t + b_N \sin N\omega t], \quad (1.128)$$

It is now an important question, whether the first-order perturbative correction can further be simplified to get an analytic description of interesting features of the trajectory. One idea could be, to take only the lowest Fourier modes. In this section, we want to investigate, under which circumstances this could be possible.

Starting from the first order result for v , given by eq. (1.127), we express the disorder correlator by its Fourier transform

$$\Delta'[Z(t) - Z(t')] = \int \frac{dq}{2\pi} (iq) \Delta(q) e^{iq \frac{h}{\omega} [\sin \omega t - \sin \omega t']} \quad (1.129)$$

and expand the exponential term in a double Fourier series in t and t' , respectively [60]:

$$\begin{aligned} e^{ia \sin \omega t} &= \sum_{n=-\infty}^{\infty} J_n(a) e^{in\omega t} \\ \int_0^t dt' e^{-c(t-t') - ia \sin \omega t'} &= \sum_{n=-\infty}^{\infty} J_n(-a) \frac{e^{in\omega t} - e^{-ct}}{c + in\omega}. \end{aligned}$$

Here, $J_n(a)$ are the Bessel functions of the first kind. As we are interested only in the behaviour for large enough times, we remove all terms that are damped out exponentially for $t \gg c^{-1}$ from the very beginning. Note, that c^{-1} is indeed the time scale for the transience, as has been claimed before.

For the mean velocity, we obtain

$$v(t) = h \cos \omega t + \eta^2 \sum_{m,n=-\infty}^{\infty} \int \frac{dq}{2\pi} (iq) \Delta(q) J_m\left(q \frac{h}{\omega}\right) J_n\left(-q \frac{h}{\omega}\right) \frac{e^{i(m+n)\omega t} (c - in\omega)}{c^2 + n^2 \omega^2}. \quad (1.130)$$

In principle, this is already a Fourier series representation, not very elegant, though. The argument $(m+n)\omega t$ of the expansion basis exponentials promises a rather complicated structure for the coefficients. A first observation, however, can already be made: Under the q integral we find an odd function $(iq)\Delta(q)$ and a product of two Bessel functions of order m and n , respectively. For the q -integral to result in a finite value, a function is required that is not odd in q . This necessitates the product of the two Bessel functions to be odd, or, equivalently, $m+n$ to be an odd number. Whence, we conclude, that to first perturbative order, our symmetry argument that we have established in Sec. 1.3.2 (the Fourier coefficients for even N must vanish) is fulfilled exactly.

It requires some tedious algebra to collect all contributions belonging to a certain harmonic order from the double series. Eventually, we obtain a series expansion

$$\frac{v(t)}{h} = \cos \omega t + \sum_{N=1}^{\infty} \left[A_N \left(\frac{\eta}{h}, \frac{\omega}{c}, \frac{h}{\omega \ell} \right) \cos N\omega t + B_N \left(\frac{\eta}{h}, \frac{\omega}{c}, \frac{h}{\omega \ell} \right) \sin N\omega t \right]. \quad (1.131)$$

Note, that taking $\omega \rightarrow 0$ is forbidden here, as we used $\omega \neq 0$ while deriving the coefficients and moreover perturbation theory breaks down (recall that $h/\eta \gg c/\omega$). The same holds for $\ell \rightarrow 0$. The remaining extreme limits $\omega \rightarrow \infty$ and $\ell \rightarrow \infty$ are not interesting, since in these limits the disorder is rendered unimportant. Therefore, in the following, we assume finite (positive) values for ℓ and ω and moreover set them equal to one $\omega = \ell = 1$, by appropriately choosing the units for z and t . This leaves us with three dimensionless parameters: h , c and η . The dependence of the first order perturbative Fourier coefficients on η is trivial. The connexion to c is also evident, as can be read off from (1.130). For larger c , the system is more tightly bound to the non-disordered solution, suppressing perturbative corrections.

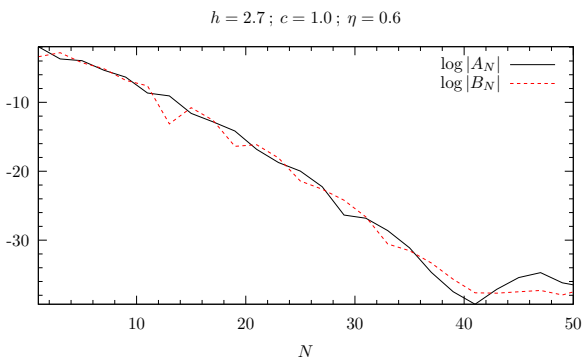


Fig. 1.22: Plotting the logarithms of $|A_N|$ and $|B_N|$ reveals the exponential decay with N . In the regime where numerical errors do not dominate the result, a linear regression seems appropriate.

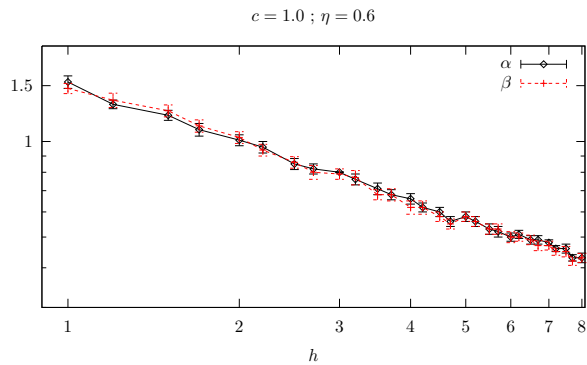


Fig. 1.23: Performing the linear regression for many h yields slopes α and β appearing to depend on h in a power-law fashion.

The most interesting but also the most difficult is the dependence of the Fourier coefficients on h . Actually, there are two competing effects. On the one hand, large driving strengths render the disorder unimportant in all cases accessible through perturbative methods. On the other hand, if one thinks of $g(Z(t))$ as a function of time, the more rapid $Z(t)$ changes the more g fluctuates on short time scales and thus brings higher frequency contributions to $v(t)$. The first remark is reflected in the overall weight of the Fourier coefficients as corrections to the non-disordered case, decreasing with h . The second idea is reflected in the decay of the Fourier coefficients with N . The larger h , the weaker we expect this decay to be.

The dependence of the higher harmonics on h is hidden in the Bessel functions in (1.130). The first extremum of the Bessel functions shifts to larger values as m and n increase, respectively. However, the complicated way in which these Bessel functions enter A_N and B_N hinders an analytic access to the decay law. A numerical determination of the Fourier coefficients for the perturbative result reveals an exponential decay, as shown in Fig. 1.22. The noisy behaviour for $N \geq 40$ is due to numerical fluctuations. Note, that these fluctuations are of the order 10^{-14} , which is quite reasonable. The plot in Fig. 1.22 is mere illustration of a more general phenomenon. This exponential decay has been found for many sets of parameters, thus one is led to the ansatz

$$|A_N| \sim \frac{\eta^2}{h^2} e^{-\alpha N} \quad ; \quad |B_N| \sim \frac{\eta^2}{h^2} e^{-\beta N}, \quad (1.132)$$

where α and β can be estimated through a linear regression up to a suitable N_{\max} . Of course, it is not expected, that α and β are distinct, nor that they depend on the parameters in different ways. Determining both just doubles the amount of available data.

c	η	C_α	C_β	ξ_α	ξ_β
1.0	0.6	1.52	1.52	0.61	0.61
51.5	0.6	1.56	1.56	0.58	0.59
2.0	0.6	1.56	1.59	0.58	0.60
2.5	0.6	1.63	1.62	0.61	0.61
3.0	1.0	1.66	1.66	0.63	0.63
3.5	1.0	1.71	1.68	0.62	0.62
4.0	1.0	1.69	1.65	0.61	0.60
4.5	1.0	1.72	1.68	0.62	0.62
5.0	2.0	1.71	1.67	0.61	0.60
5.5	2.0	1.73	1.73	0.61	0.62
6.0	2.0	1.77	1.72	0.62	0.62
6.5	3.0	1.76	1.77	0.62	0.62

Tab. 1.1: Results for the regression (1.133).

the functional dependence of α and β on c yields a complicated but rather weak dependence, which gives no further insight. The linear fit in Fig. 1.24 gives a fairly tiny slope, so the dependence of the decay constants on c may be assumed to be weak.

As our results are first-order perturbative, α and β must not depend on η . The main interest now focusses on the dependence of the decay constants on h . The results from a linear regression for a series of h -values, c and η kept fixed, suggest a power-law dependence

$$\alpha(h, c) = C_\alpha(c) \cdot h^{-\xi_\alpha}, \quad \beta(h, c) = C_\beta(c) \cdot h^{-\xi_\beta}. \quad (1.133)$$

Fig. 1.23 displays this relation for a particular example. Repeating this data collection and subsequent regression for different values for c and η yields the results summarised in Tab. 1.1.

While the exponent ξ appears constant $\xi \approx 0.6$, the prefactor seems to depend on c . An attempt to redo the same procedure, done for h , with the parameter c to gain information about

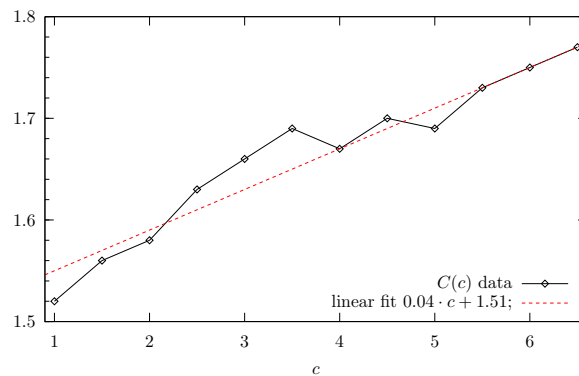


Fig. 1.24: Plot of the prefactor $C(c) = (C_\alpha + C_\beta)/2$ in (1.133). The linear fit yields a fairly tiny slope.

Certainly, it is desirable to ascertain the validity of this decay law beyond perturbation theory. In a few words, it ought to be explained, why we have not been able to do it. First of all, the logarithmic plots of the Fourier coefficients in Fig. 1.22 exhibit fluctuations around the linear decrease. This “noise” is authentic and not attributed to numerical inaccuracies. The exponential decay of the Fourier coefficients is superimposed on a true, complicated dependence. Hence, it requires a lot of data points to obtain reasonable data. Since the Fourier coefficients for even N vanish, in the example of Fig. 1.22 the regression can be

carried out over around 15-20 data points. This is a fair number. The quality relies heavily on the accuracy of the numerical determination of the Fourier coefficients. In Fourier analyses of the numerics for the full equation of motion (1.11), we did not manage to get a precision better than of the order of 10^{-3} . This means, the regression has to be stopped at N_{\max} , where $\ln A_{N_{\max}} \approx -7$. In the example of Fig. 1.22, this leaves us with less than 5 data points. In view of the natural fluctuations, a linear regression is not sensible any more.

In summary, we have numerically established the dependence of the decay constants for the Fourier coefficients on h : $\alpha, \beta(h) = C(c) \cdot h^{-\xi}$ with $\xi \simeq 0.6$.

1.6 Summary and Conclusions

We have investigated the problem of ac-driven elastic interfaces in random media within the mean field approximation as well as in perturbation theory.

As a starting point, we have worked out the scaling behaviour of the velocity as a function of a constant driving force in mean field theory close to depinning. We have thereby extended Fisher's [47] arguments for charge density waves. The scaling exponents are found to be different for disorder with smooth and cusped correlator. Our analytical results are supported by a numerical treatment.

Furthermore, in mean-field theory we have investigated the small-frequency behaviour of observables that characterise the velocity hysteresis in case the system is exposed to an ac-driving. We found that the frequency scaling exponents of the remanent velocity v_{h_0} and the velocity at the depinning field v_{h_p} do not depend on the presence or absence of a cusp-singularity at the origin of the disorder correlator. This also holds for the frequency exponents of the hysteresis loop area as long as the amplitude of the driving does not exceed the depinning force h_p . For force amplitudes above the depinning threshold, our numerical treatment yields different exponents for smooth and cusped correlators.

We have seen that the perturbation expansion for ac-driven elastic interfaces in random media fails for interface dimensions $D \leq 4$. We have resolved this puzzle, and the reason for the strange behaviour of perturbation theory has been found to be connected with the disorder-dependent time scale τ (cf. (1.100)) which measures the time for the initial roughening of interfaces in random environments. Due to its appearance within the disorder averaged velocity v as a transience relaxation time, attempts to determine v via a perturbation expansion in the strength of the disorder entail terms of unbounded growth in time. Although, most probably, the expansion yields the true solution if it could be summed up, it is useless, because the finite perturbative orders grow in powers of time. Hence, they fail to describe correctly the behaviour on large time scales. On the other hand, as we have signified, the perturbation expansion for $D > 4$ is regular.

The mean-field equation of motion formally corresponds to $D = \infty$ and admits a regular perturbative treatment that, where applicable, agrees very well with the numerics for the full equation of motion. It has been shown, that non-regular diagrammatic contributions cancel among each other, leaving a well-behaved perturbative expansion. The mean-field perturbation expansion helped to improve numerical results, which allowed us to establish the dependence of the decay constants of the Fourier modes on h as a power law.

Chapter 2

The effect of electroelastic coupling on ferroelectric domain walls

2.1 Introduction

Ferroelectric materials form an important field of research with various applications [61]. In modern technology, especially thin films of ferroelectric substances [62] represent promising candidates for new types of non-volatile memories [63, 64, 65], sensors [66, 67] and microwave applications [68]. Particularly for memory applications, multidomain configurations of ferroelectric materials are technologically relevant. Recent works on $\text{Pb}(\text{Zr}_x\text{Ti}_{1-x})\text{O}_3$ (PZT) [69, 70, 71] point out the renewed interest in an understanding of the statics of domain walls in ferroelectric systems, that separate regions of opposite polarisation. Apart from short-range elastic terms and disorder, the influence of long-range interactions, such as of dipolar type [72] turns out to be of immense importance [70]. In this chapter, we are going to examine the impact of a further source of long-range interaction, namely the coupling of the polarisation to the lattice displacement field, on the domain wall statics.

Actually, electroelastic coupling plays a dominant role for the properties of ferroelectric phase transitions, which are often classified as either of the displacement type or of the order-disorder type [73]. In order-disorder type ferroelectrics (like KH_2PO_4), electric dipole moments are present in each unit cell already in the paraelectric phase, which then order at low temperatures. On the other hand, materials that exhibit a displacive transition (for example BaTiO_3) obey a symmetric crystal structure in the paraphase, e.g. of cubic symmetry. Below the transition temperature, a spontaneous lattice strain entails a finite polarisation. Thus, for displacive ferroelectrics it is obvious, that the coupling of the polarisation to the lattice strain plays a prominent role. So, for instance, taking into account the elastic degrees of freedom Kwok and Miller [74] have developed a microscopic derivation for the parameters of the Landau-Ginzburg-Devonshire expansion for displacive ferroelectrics [75], which has later been improved by Vaks [76]. However, also for substances the transition of which is of the order-disorder type, the coupling of the polarisation to the lattice strain is important. The effect of piezoelectricity on the characteristics of the ferroelectric order-disorder transition in KH_2PO_4 (KDP), a typical order-disorder type ferroelectric material, has been investigated in

two seminal papers [77, 78] within the framework of the phenomenological Landau theory. It has been shown that the significance of the electroelastic coupling term expresses itself in the suppression of certain fluctuations of the order parameter close to the critical point.

The work presented in this chapter is organised in two parts.

In the following section, we derive an effective interface Hamiltonian for a bulk ferroelectric which is cubic in the paraphase and at the Curie-temperature T_c undergoes a second order phase transition to a tetragonal ferroelectric phase. To derive the interface Hamiltonian, we take into account the electrostrictive coupling of the polarisation to the lattice strain at high temperatures. It turns out, that the corrections due to the electrostrictive coupling, on length scales large compared to the domain wall thickness, just renormalise the interface tension coefficients.

In section 2.3 we develop an effective interface Hamiltonian for bulk samples of KDP-type ferroelectrics, which are piezoelectric in the paraphase. Due to the piezoelectricity above the Curie temperature, there is an important long-range contribution to the interface Hamiltonian. Assuming random field disorder we can then employ the Imry-Ma argument to calculate the roughness of domain walls in KDP. Moreover, we propose how the experimentally observed needle-like deformations of domain walls can be explained quantitatively.

2.2 Electrostrictive coupling

As has been said in the introduction, in this section we want to derive the interface Hamiltonian for materials that are cubic in the high-temperature phase and undergo a second order ferroelectric transition into a phase of tetragonal crystal symmetry. Actually, the assumption of a continuous transition is not vital for our considerations, with this restriction we just want to be specific as far as the choice of the phenomenological Ginzburg-Landau-functional is concerned.

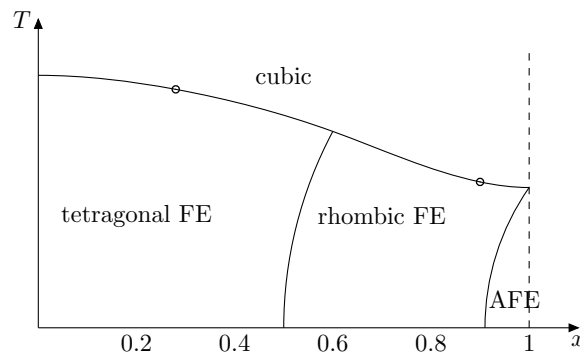


Fig. 2.1: Schematic phase diagram of lead zirconate titanate $\text{Pb}(\text{Zr}_x\text{Ti}_{1-x})\text{O}_3$ (PZT). The two dots mark the borders in between the ferroelectric transition is continuous.

Before we embark on the computational details, let us briefly introduce a material, which could serve as a potential candidate to be described by our model. Lead zirconate titanate $\text{Pb}(\text{Zr}_x\text{Ti}_{1-x})\text{O}_3$ (PZT) is a material with a rich phase diagram in the T - x -plane, that can be

explained by the phenomenological Landau-Ginzburg-Devonshire theory [79]. Depending on the fraction of zirconium x , the ferroelectric phase can be rhombic or tetragonal, and moreover the phase transition to ferroelectricity can be of first or second order [80, 81]. In the range $0.28 \lesssim x \lesssim 0.9$, we encounter a continuous transition [81]. The morphotropic phase boundary, separating the tetragonal from the rhombic ferroelectric phases occurs between $0.5 \lesssim x \lesssim 0.6$ depending on the temperature [82].

A sketch of the PZT phase diagram is shown in Fig. 2.1. The Hamiltonian that we are going to use models PZT with zirconium contents of $0.3 \lesssim x \lesssim 0.5$.

2.2.1 The model

We use the phenomenological Landau-Ginzburg-Devonshire theory to derive the effective Hamiltonian in the uniaxial ferroelectric phase. To fourth order in the polarisation \mathbf{P} the Landau-Ginzburg-Devonshire (LGD) functional for the high-temperature cubic phase reads

$$H = H_0 + H_{\text{es}} + H_{\text{el}}, \quad (2.1)$$

where the constituents are discussed in the following. First of all, we have

$$H_0 = \int_{\mathbf{k}} \left[\sum_i \frac{1}{2} (A + Dk^2 + f_i k_i^2) P_{i,\mathbf{k}} P_{i,-\mathbf{k}} + \frac{B_1}{4} \sum_i (P_i^2)_{\mathbf{k}} (P_i^2)_{-\mathbf{k}} + \frac{B_2}{4} \sum_{i \neq j} (P_i^2)_{\mathbf{k}} (P_j^2)_{-\mathbf{k}} \right]. \quad (2.2)$$

Here, the coefficient A is taken temperature dependent as usual, more precisely

$$A = A_0(T - T_c), \quad (2.3)$$

with T_c being the transition temperature and $A_0 > 0$. Additionally, we have the electrostrictive coupling to the components of the elastic tensor $\mathbf{u} = (u_{ij})$. The tensor \mathbf{u} is symmetric, and thus has 6 independent elements [83]. The electrostrictive cubic coupling reads

$$H_{\text{es}} = \int_{\mathbf{k}} \left[Q_{\parallel} \sum_i u_{ii,\mathbf{k}} (P_i^2)_{-\mathbf{k}} + Q_{\perp} \sum_i u_{ii,\mathbf{k}} \sum_{j \neq i} (P_j^2)_{-\mathbf{k}} + Q_s (u_{yz,\mathbf{k}} P_{2,\mathbf{k}} P_{3,\mathbf{k}} + u_{xz,\mathbf{k}} P_{1,\mathbf{k}} P_{3,\mathbf{k}} + u_{xy,\mathbf{k}} P_{1,\mathbf{k}} P_{2,\mathbf{k}}) \right]. \quad (2.4)$$

We concentrate on the case $B_1 > B_2$, when the system undergoes a transition from the paraelectric into the uniaxial ferroelectric phase, and choose the ferroelectric axis along the z -direction $\mathbf{P} = P \mathbf{e}_z$. Thus, our order parameter is given by $P = P_3$ and the Landau functional simplifies to

$$H_0 = \int_{\mathbf{k}} \left[\frac{1}{2} (A + Dk^2 + f_3 k_z^2) P_{\mathbf{k}} P_{-\mathbf{k}} + \frac{B_1}{4} (P^2)_{\mathbf{k}} (P^2)_{-\mathbf{k}} \right] \quad (2.5)$$

$$H_{\text{es}} = \int_{\mathbf{k}} \sum_i i k_i Q_i u_{i,\mathbf{k}} (P^2)_{-\mathbf{k}}. \quad (2.6)$$

Here, $Q_1 = Q_2 = Q_\perp$ and $Q_3 = Q_\parallel = Q_\perp + Q_\Delta$ and the vector \mathbf{u} denotes the elastic displacement field. Furthermore, we need to account for the cubic elastic energy [83]

$$H_{\text{el}} = \frac{1}{2} \int_{\mathbf{k}} \sum_{i,j} u_{i,\mathbf{k}} M_{ij}(\mathbf{k}) u_{j,-\mathbf{k}}. \quad (2.7)$$

The matrix M is given by

$$M_{ij}(\mathbf{k}) = (k^2 + dk_i^2) c_{44} \delta_{ij} + (c_{44} + c_{12}) k_i k_j, \quad (2.8)$$

where

$$d = \frac{c_{11} - c_{12} - 2c_{44}}{c_{44}} \quad (2.9)$$

measures the cubic anisotropy.

2.2.2 The effective Hamiltonian

To obtain an effective Hamiltonian, we integrate out the elastic degrees of freedom. The solution of the Euler equation without external stress is given by the displacement field

$$u_{i,\mathbf{k}}^0 = \sum_j ik_j Q_j (P^2)_{-\mathbf{k}} M_{ij}^{-1}(\mathbf{k}). \quad (2.10)$$

The effective Hamiltonian for P now gets the following contribution

$$H_{\text{eff}} = -\frac{1}{2} \int_{\mathbf{k}}' (P^2)_{\mathbf{k}} (P^2)_{-\mathbf{k}} \sum_{ij} Q_i Q_j k_i k_j M_{ij}^{-1}(\mathbf{k}) \equiv -\frac{1}{2} \int_{\mathbf{k}}' (P^2)_{\mathbf{k}} (P^2)_{-\mathbf{k}} R(\hat{\mathbf{k}}). \quad (2.11)$$

Here, we have introduced the notation $\hat{\mathbf{k}} = \mathbf{k}/k$. The prime at the integral denotes that the $\mathbf{k} = 0$ -mode has to be excluded from the integral. Working at finite system sizes, this means that the integral is cut off for small k , practically it tells us that we need not worry about the non-analyticity of $R(\hat{\mathbf{k}})$ for $\mathbf{k} = 0$. Actually, in the course of the determination of the critical properties of an Ising model on a cubic lattice, Bergman and Halperin [84] pointed out that the non-analyticity of $R(\hat{\mathbf{k}})$ at $\mathbf{k} = 0$ is difficult to deal with in the RG flow equations. Therefore, they have not eliminated the elastic degrees of freedom but have chosen to integrate out fast modes from P and \mathbf{u} . Though we are not going to consider RG flow equations, we should be aware of potential difficulties with the subtleties occurring for $\mathbf{k} \rightarrow 0$.

The function $R(\hat{\mathbf{k}})$ yields an effective long-range interaction, as has been noticed already by Wagner and Swift [85]. It requires a tedious computation to obtain the function $R(\hat{\mathbf{k}})$. We follow the calculation of Nambu and Sagala [86] but confine ourselves to the first order in an expansion in d . Then, when for convenience we agree to define

$$\kappa = \frac{c_{12} + c_{44}}{c_{12} + 2c_{44}}, \quad (2.12)$$

we find

$$\begin{aligned}
R(\hat{\mathbf{k}}) = & \frac{Q_{\Delta}^2}{c_{44}} \left\{ \hat{k}_z^2 - \kappa \hat{k}_z^4 + d \left[-\hat{k}_z^4 + 2\kappa \hat{k}_z^6 - \kappa^2 \hat{k}_z^8 \right] + \mathcal{O}(d^2) \right\} + \\
& \frac{Q_{\perp}^2}{c_{44}} \left\{ 1 - \kappa + d \left[- (1 - \kappa)^2 \sum_j \hat{k}_j^4 \right] + \mathcal{O}(d^2) \right\} + \\
& 2 \frac{Q_{\Delta} Q_{\perp}}{c_{44}} \left\{ (1 - \kappa) \hat{k}_z^2 + d \left[(2\kappa - 1) \hat{k}_z^4 + \kappa(2 - \kappa) \hat{k}_z^2 \sum_j \hat{k}_j^4 \right] + \mathcal{O}(d^2) \right\}. \quad (2.13)
\end{aligned}$$

In the case $d = 0$, i.e. where the elastic energy is isotropic, the total Hamiltonian can be written down explicitly.

$$\begin{aligned}
H[P] = & \frac{1}{2} \int_{\mathbf{k}} (A + Dk^2 + f_z k_z^2) P_{\mathbf{k}} P_{-\mathbf{k}} + \frac{1}{2} \int_{\mathbf{k}} \left(\frac{B_1}{2} - \frac{Q_{\perp}^2}{c_{12} + 2c_{44}} \right) (P^2)_{\mathbf{k}} (P^2)_{-\mathbf{k}} - \\
& \frac{1}{2} \int_{\mathbf{k}}' (P^2)_{\mathbf{k}} (P^2)_{-\mathbf{k}} \left(\alpha \hat{k}_z^2 - \beta \hat{k}_z^4 \right) + \mathcal{O}(d). \quad (2.14)
\end{aligned}$$

The two new parameters are given by

$$\alpha = \frac{Q_{\Delta}^2}{c_{44}} + 2 \frac{Q_{\Delta} Q_{\perp}}{c_{12} + 2c_{44}} \quad \text{and} \quad \beta = \frac{Q_{\Delta}^2}{c_{44}} \kappa. \quad (2.15)$$

For further use, we introduce

$$\tilde{B} = \frac{B_1}{2} - \frac{Q_{\perp}^2}{c_{12} + 2c_{44}}. \quad (2.16)$$

2.2.3 The interface Hamiltonian

In the following, we consider a domain wall between the two degenerate ground states $P = P_0 > 0$ and $P = -P_0 < 0$ in the system. It is well-known, that the interface profile of domain walls in the low-temperature phase of the pure P^4 problem, described by H_0 (cf. (2.2)) with negative A is given by

$$P = P_0 \cdot \tanh(x/b), \quad (2.17)$$

when the order parameter changes in the x -direction. The wall-thickness b can be worked out straightforwardly. For the pure ϕ^4 -model the respective analyses are sketched in appendix B.1. For our more extended model $H_0 + H_{\text{eff}}$, the shape of the wall profile is more complicated and it is much harder to determine the parameters describing it. However, in the case of ferroelectrics, domain walls are known to be thin and we are mainly interested in fluctuations of the domain wall on scales sufficiently large compared to the wall-thickness. Therefore, apart from a precise determination of the interface tension, the exact profile of domain walls in our system should be of little importance. So, we impose a domain wall profile which is convenient for computations

$$P(\mathbf{r}) = P_0 \cdot \text{sign}(x) \cdot \left[1 - \exp\left(-\frac{|x|}{b}\right) \right]. \quad (2.18)$$

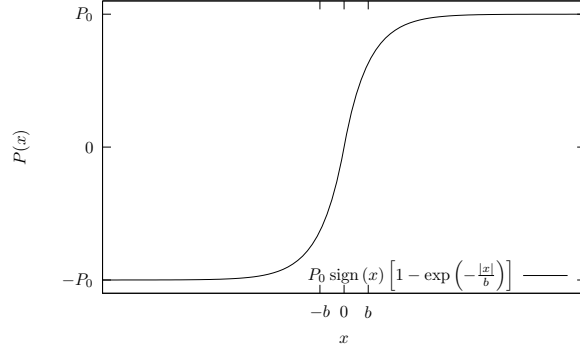


Fig. 2.2: Plot of the domain wall profile assumed in our calculation.

The shape of the profile is plotted in Fig. 2.2. Our first goal is to determine the two parameters in this domain wall ansatz, P_0 and b . To do this, we plug our profile (2.18) into (2.14), and obtain (up to terms of order $\mathcal{O}(L_x^{-1})$)

$$\frac{E(P_0, b)}{L_y L_z} = P_0^2 \left[\frac{D}{2b} + \frac{A}{2} (L_x - 3b) \right] + P_0^4 \frac{\tilde{B}}{2} \left[L_x - \frac{25}{6} b \right] + \mathcal{O}(L_x^{-1}). \quad (2.19)$$

If we want to minimise this expression for P_0 in the thermodynamic limit, we only need to take into account terms $\propto L_x$, so that we reproduce the result from the pure ϕ^4 theory

$$P_0 = \sqrt{-\frac{A}{4\tilde{B}}}. \quad (2.20)$$

The directional terms, proportional to α and β , do not contribute since $P(\mathbf{r})$ is constant in z -direction. There are however directional terms proportional to d , which include \hat{k}_x^4 (cf. eq. (2.13)). These turn out to be important for the determination of b . More precisely, we find

$$H_{\hat{k}_x} = \frac{d}{2} \frac{Q_{\perp}^2 c_{44}}{(c_{12} + 2c_{44})^2} \int_{\mathbf{k}} (P^2)_{\mathbf{k}} (P^2)_{-\mathbf{k}} \hat{k}_x^4 + \mathcal{O}(d^2). \quad (2.21)$$

This yields an additional contribution to the interface energy proportional to b :

$$\frac{E_{\hat{k}_x}(P_0, b)}{L_y L_z} = \frac{d}{2} \frac{Q_{\perp}^2 c_{44}}{(c_{12} + 2c_{44})^2} P_0^4 \frac{11}{6} b. \quad (2.22)$$

For the wall thickness b we thus find

$$b = \sqrt{\frac{D}{P_0^2} \left[\frac{11}{6} \tilde{B} + \frac{11}{6} \frac{dQ_{\perp}^2 c_{44}}{(c_{12} + 2c_{44})^2} + \mathcal{O}(d^2) \right]^{-1}} = \sqrt{-\frac{24D}{11A}} \left[1 - \frac{d}{2\tilde{B}} \frac{Q_{\perp}^2 c_{44}}{(c_{12} + 2c_{44})^2} + \mathcal{O}(d^2) \right] \quad (2.23)$$

Now, we consider deviations from the flat domain wall given in (2.18), by locally shifting the centre of the wall

$$P(\mathbf{r}) = P_0 \cdot \text{sign}(x - \xi(\mathbf{r}_{\perp})) \cdot \left[1 - \exp\left(-\frac{|x - \xi(\mathbf{r}_{\perp})|}{b}\right) \right]. \quad (2.24)$$

Here, $\xi(\mathbf{r}_\perp)$ describes the x -coordinate of the zero of the domain wall profile, $\mathbf{r}_\perp = (y, z)$. Then, in the harmonic approximation we can write (cf. App. B.2, Eq. (B.11))

$$P_{\mathbf{k}}P_{-\mathbf{k}} \simeq \frac{4P_0^2}{(1+b^2k_x^2)^2} \left[\xi_{\mathbf{k}_\perp} \xi_{-\mathbf{k}_\perp} - (2\pi)^2 \delta(\mathbf{k}_\perp) \int_{\mathbf{q}} \xi_{\mathbf{q}} \xi_{-\mathbf{q}} \right]. \quad (2.25)$$

A calculation similar to that in App. B.2 further yields

$$(P^2)_{\mathbf{k}} = P_0^2 \left[-\frac{12b}{4+5k_x^2b^2+k_x^4b^4} + 2\pi\delta(k_x) \right] \int d\mathbf{r}_\perp e^{ik_x\xi+i\mathbf{k}_\perp\mathbf{r}_\perp}, \quad (2.26)$$

and in the harmonic approximation we obtain

$$(P^2)_{\mathbf{k}}(P^2)_{-\mathbf{k}} \simeq \frac{144P_0^4b^2k_x^2}{(4+5k_x^2b^2+k_x^4b^4)^2} \left[\xi_{\mathbf{k}_\perp} \xi_{-\mathbf{k}_\perp} - (2\pi)^2 \delta(\mathbf{k}_\perp) \int_{\mathbf{q}} \xi_{\mathbf{q}} \xi_{-\mathbf{q}} \right]. \quad (2.27)$$

Equation (2.27) reveals, that it is important to work with a domain wall of finite width. In the limit $b \rightarrow 0$, all contributions to H (cf. (2.14)) which are of order P^4 vanish. Our next goal is to derive the interface Hamiltonian in the long-wavelength limit, i.e. we omit all terms of order $\mathcal{O}(k^3)$. Before we are going to do this, we shall discuss the contributions from higher orders in d . Generally, terms in $R(\hat{\mathbf{k}})$ that are proportional to $\hat{k}_y^{2i}\hat{k}_z^{2j}$ are of order $\mathcal{O}(b^3k^3)$ if $i+j > 1$. To order $\mathcal{O}(d)$ the only relevant terms in (2.13) are those corresponding to \hat{k}_z^2 , \hat{k}_x^4 and $\hat{k}_x^4\hat{k}_z^2$. For these, we find (with the prefactor from Eq. (2.27))

$$\int_{k_x} \frac{144b^2k_x^2}{(4+5k_x^2b^2+k_x^4b^4)^2} \hat{k}_z^2 = \frac{11}{6b} b^2 k_z^2 + \mathcal{O}(b^3k_\perp^3), \quad (2.28)$$

$$\int_{k_x} \frac{144b^2k_x^2}{(4+5k_x^2b^2+k_x^4b^4)^2} \hat{k}_x^4 = \frac{2}{3b} - \frac{11}{3b} b^2 k_\perp^2 + \mathcal{O}(b^3k_\perp^3), \quad (2.29)$$

$$\int_{k_x} \frac{144b^2k_x^2}{(4+5k_x^2b^2+k_x^4b^4)^2} \hat{k}_x^4 \hat{k}_z^2 = \frac{11}{6b} b^2 k_z^2 + \mathcal{O}(b^3k_\perp^3). \quad (2.30)$$

Now, plugging (2.25) and (2.27) into the effective Hamiltonian (2.14), we can integrate out k_x and obtain the interface Hamiltonian density. For completeness, we should also add the contribution resulting from the dipolar interaction, which to order $\mathcal{O}((kb)^0)$ has been derived in [72]. A more precise calculation, taking the finite width into account (cf. eq. (2.18)), we have to order $\mathcal{O}(kb)$

$$h_{\text{dip},\mathbf{k}}[\xi] = \frac{P_0^2}{2} \xi_{\mathbf{k}} \xi_{-\mathbf{k}} \delta k \cos^2 \vartheta \left(1 - \frac{3}{2} kb + \mathcal{O}(k^2b^2) \right), \quad (2.31)$$

where δ measures the dipolar coupling strength. Thus, the interface Hamiltonian density reads

$$h_{\mathbf{k}}[\xi] = \xi_{\mathbf{k}} \xi_{-\mathbf{k}} \frac{P_0^2}{2} \left[\sigma k^2 + \delta \frac{k_z^2}{k} + \sigma_z k_z^2 + \mathcal{O}(b^3k^3) \right] \quad (2.32)$$

$$\sigma = \left(\frac{D}{b} - P_0^2 b \frac{11}{3} \frac{dQ_\perp^2 c_{44}}{(c_{12} + 2c_{44})^2} \right) = \sqrt{-\frac{11}{24} DA} \left[1 - \frac{3}{2} \frac{d}{\bar{B}} \frac{Q_\perp^2 c_{44}}{(c_{12} + 2c_{44})^2} + \mathcal{O}(d^2) \right] \quad (2.33)$$

$$\sigma_z = \left[\frac{f_z}{b} - \frac{11}{6} P_0^2 b \left(\alpha + \frac{2Q_\perp Q_\Delta d}{c_{44}} \kappa(2 - \kappa) \right) - \frac{3}{2} \delta b \right]. \quad (2.34)$$

Recall, that our interface Hamiltonian is valid only on length scales sufficiently large compared to the wall thickness. Therefore, in (2.32) we have omitted all terms of order $\mathcal{O}(k^3 b^3)$.

In summary, electroelastic coupling does not lead to a long-range interaction term in the interface Hamiltonian, but just changes the interface tension coefficients in an anisotropic manner.

Finally, we want to discuss what changes if the ferroelectric transition is of first order. To account for a discontinuous transition we need to include terms of 6th order in the polarisation because the phenomenological Hamiltonian has to provide 3 local minima, namely $P = \pm P_0$ and $P = 0$. However, the electrostrictive coupling is not affected at all. Thus, the inclusion of higher order terms does not influence the interface Hamiltonian in any way. So, qualitatively our results remain unchanged.

2.3 A simple model for KDP-type ferroelectrics

One of the first materials that has been discovered to exhibit ferroelectric properties is potassium dihydrogen phosphate KH_2PO_4 (KDP), which has since been intensively studied and still remains a subject of ongoing research, both experimentally [87, 88] and theoretically [89]. Due to its optical properties, KDP has many applications in nonlinear optics and laser physics.

In the high temperature phase, KDP exhibits a piezoelectric tetragonal crystal structure, which becomes orthorhombic on passing below the transition temperature. Therefore, KDP is not only a ferroelectric, but due to its piezoeffect in the paraphase, it is at the same time ferroelastic. The piezo coupling above the Curie temperature has a pronounced effect on the ferroelectric phase transition, which has been investigated on a simple model in two seminal papers [77, 78] within the framework of the phenomenological Ginzburg-Landau theory. It has been shown that the significance of the electroelastic coupling term expresses itself in the suppression of certain fluctuations of the order parameter close to the critical point. A more general study of such structural phase transitions has been reported by Cowley [90].

Further, the ferroelasticity in the low-temperature phase has an impact on the multidomain configurations. The piezo term leads to an effective long range interaction, such that there are energetically favourable orientations for the domain walls, which become compelling in the infinite volume limit [91, 92]. The domain configurations of KDP have been studied in many early [93, 94, 95, 96, 97, 98, 99] as well as in more recent works [100, 98, 101].

In this section, we are going to derive the interface Hamiltonian for the ferroelectric domain walls in KDP-type ferroelectrics that are compatibly oriented. We use the simplified model that has already been considered in the works by Levanyuk & Sobyenin [77] and Villain [78]. We are going to see that due to a long range term, arising from the electroelastic coupling, the domain walls remain flat in the presence of random field disorder.

2.3.1 The model

We consider a model for order-disorder-type ferroelectric materials that are piezoelectric in the paraphase and undergo a continuous phase transition at $T = T_c$ to a ferroelectric and ferroelastic phase. We truncate the Ginzburg-Landau expansion after terms of fourth power

in the order parameter $P = P_z$, where we have chosen the ferroelectric axis to point along z . The Ginzburg-Landau-functional excluding the elastic degrees of freedom thus simply reads

$$H_0 = \int d^3\mathbf{r} D(\nabla P)^2 + AP^2 + BP^4. \quad (2.35)$$

Here, $A = A_0(T - T_c)$ with $A_0 > 0$ as usual. The piezoelectric coupling energy is taken to be

$$H_{\text{piezo}} = Q \int d^3\mathbf{r} P u_{xy}, \quad (2.36)$$

where x and y denote the coordinates along the crystal axes.

So far, our model is suitable to describe ferroelectric materials with a tetragonal symmetry above T_c , like for example KDP, in the continuum approximation. Now, the quadratic part of the elastic energy should also be taken according to a tetragonal symmetry. Since, however this leads to enormous technical complications, we decide to simplify our model such that the elastic energy be isotropic and the tetragonal anisotropy is taken into account solely within the piezoelectric coupling (2.36). Thus, we have

$$H_{\text{el}} = \frac{1}{2} \int_{\mathbf{k}} \sum_{i,j} u_{i,\mathbf{k}} M_{ij}(\mathbf{k}) u_{j,-\mathbf{k}}, \quad (2.37)$$

where the matrix M is given by

$$M_{ij}(\mathbf{k}) = \mu k^2 \delta_{ij} + (\lambda + \mu) k_i k_j. \quad (2.38)$$

The constants λ and μ denote the usual Lamé coefficients [83]. This model has been used already in earlier works [77, 78].

We consider the case of a non-clamped material, i.e. there is no uniform external stress. Solving the associated Euler equations (cf. [83]), we find

$$u_{\mathbf{k}}^x = -i \frac{QP_{\mathbf{k}}}{2} \left[M_{xx}^{-1}(\mathbf{k}) k_y + M_{xy}^{-1}(\mathbf{k}) k_x \right] \quad (2.39)$$

$$u_{\mathbf{k}}^y = -i \frac{QP_{\mathbf{k}}}{2} \left[M_{yy}^{-1}(\mathbf{k}) k_x + M_{xy}^{-1}(\mathbf{k}) k_y \right] \quad (2.40)$$

$$u_{\mathbf{k}}^z = 0, \quad (2.41)$$

and the inverse of M is given by

$$M_{ij}^{-1}(\mathbf{k}) = -\frac{\kappa}{\mu} \frac{k_i k_j}{k^4} + \frac{\delta_{ij}}{\mu k^2}, \quad \text{where} \quad \kappa = \frac{\lambda + \mu}{\lambda + 2\mu}. \quad (2.42)$$

Inserting the saddle point solution for \mathbf{u} into the piezo coupling (2.36), we obtain the following effective contribution to the Hamiltonian

$$H_{\text{eff}} = \frac{Q^2}{8\mu} \int_{\mathbf{k}} P_{\mathbf{k}} P_{-\mathbf{k}} \left[-1 + \frac{k_z^2}{k^2} + 4\kappa \frac{k_x^2 k_y^2}{k^4} \right]. \quad (2.43)$$

The prime at the integral means, that the $\mathbf{k} = 0$ -mode has to be excluded from the integral. Equation (2.43) agrees with the result in [77]. In a paper by Villain [78], the Hamiltonian (2.43) has also been derived but in a coordinate system that is rotated about an angle $\pi/4$ with respect to the crystal axes. The total effective Ginzburg-Landau functional for our model, which is now solely a functional of the polarisation, reads

$$H[P] = H_0[P] + H_{\text{eff}}[P]. \quad (2.44)$$

Below the transition temperature, i.e. for $A < 0$, we find a spontaneous polarisation. In the homogeneous single domain case without external stress, this polarisation takes on the value

$$P_0 = \sqrt{\frac{1}{2B} \left[\frac{Q^2}{8\mu} - A \right]}. \quad (2.45)$$

For the domain wall configuration, to a first approximation taken to be of zero width, we choose

$$P(\mathbf{r}) = P_0 \cdot \text{sign}(x - \xi) \quad (2.46)$$

where $\xi(\mathbf{r}_\perp)$ describes the x -coordinate of the domain wall position and $\mathbf{r}_\perp = (y, z)$. For the

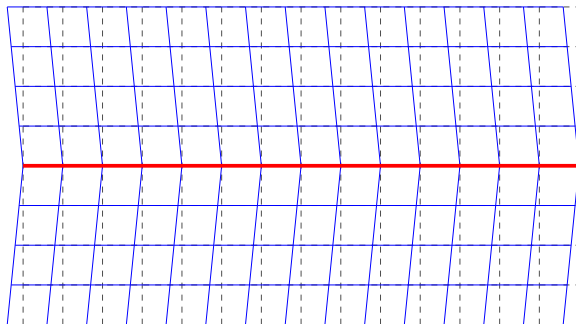


Fig. 2.3: A domain wall between two regions of opposite polarisation and lattice strain is shown. The dashed grey lines picture the x - y -plane of the tetragonal lattice structure in the paraphase. The blue lines symbolise the strained lattice in the ferroelectric-ferroelastic phase, determined from the equations (2.47). The thick red line is the domain wall, which is oriented along one of the crystal axes.

special choice $\xi(\mathbf{r}_\perp) \equiv 0$, the equations for the lattice strain (2.39) and (2.40) simplify to give

$$u^x = 0 \quad \text{and} \quad u^y = -\frac{QP_0}{2\mu} |x|. \quad (2.47)$$

These relations are visualised in Fig. 2.3.

2.3.2 The interface Hamiltonian in harmonic approximation

For ferroelastic ferroelectrics it is known that in infinite systems domain walls are allowed to be oriented along certain directions only, which can be determined using group theoretical

considerations [91, 92]. In our model, the mechanical compatibility constraint is only fulfilled for domain walls along the crystal axes [91]. If the mechanical compatibility is violated, elastic stress occurs in the domain wall region, which finally entails the creation of topological defects, i.e. dislocations, so that the overall energy grows with the domain wall area.

In this section, we consider the situation of a compatible domain wall, i.e. a wall which is oriented along one of the crystal axes. In order to illustrate, that domain walls in such systems are enormously stiff due to the effective long-range interaction, we are going to determine the roughness of the walls under the assumption of random field disorder in the sample. To calculate the interface tension, arising from the gradient term in H_0 , we cannot use a step-like domain wall profile. Instead, we should use a profile function $f(x)$, that changes smoothly from -1 to $+1$ over a finite width b . Thus, to compute the interface tension term, we use the following configuration for the polarisation field

$$P(\mathbf{r}) = P_0 \cdot f(x - \xi). \quad (2.48)$$

Then the interface tension term becomes

$$\int d^3\mathbf{r} D(\nabla P)^2 = \sigma P_0^2 \int dydz [1 + (\nabla_{\perp}\xi)^2], \quad (2.49)$$

where we have introduced the interface tension coefficient

$$\sigma = D \int dx [f'(x)]^2. \quad (2.50)$$

For all other contributions, we can safely neglect the finite width of the wall (which is generally of the order of the lattice spacing in ferroelectrics). We use the harmonic approximation for the polarisation (a derivation is provided in appendix B.2), which yields

$$P_{\mathbf{k}}P_{-\mathbf{k}} \simeq 4P_0^2 \left[\xi_{\mathbf{k}_{\perp}}\xi_{-\mathbf{k}_{\perp}} - \delta(\mathbf{k}_{\perp}) \int_{\mathbf{k}'} \xi_{\mathbf{k}'}\xi_{-\mathbf{k}'} \right]. \quad (2.51)$$

Plugging (2.51) into the effective Ginzburg-Landau functional (cf. (2.44)), we can do the integration over k_x . Now, that k_x is integrated out, we drop the index \perp , so that \mathbf{k} denotes \mathbf{k}_{\perp} for the remainder of this section. Including the Hamiltonian density $h_{\text{dip},\mathbf{k}}[\xi] = P_0^2 \delta \xi_{\mathbf{k}}\xi_{-\mathbf{k}} k_z^2/k$ that results from the dipolar interaction (see the discussion above in Sec. 2.2.3 and Ref. [72]), the total interface Hamiltonian reads

$$H[\xi] = \int_{\mathbf{k}}' \xi_{\mathbf{k}}\xi_{-\mathbf{k}} P_0^2 \left[\sigma k^2 + c_z \frac{k_z^2}{k} + ck \right], \quad (2.52)$$

$$c_z = \delta - \frac{Q^2\kappa}{2\mu} \left(1 - \frac{1}{2\kappa} \right) \quad \text{and} \quad c = \frac{Q^2\kappa}{2\mu}. \quad (2.53)$$

In the following, we assume $c_z > 0$ (which is not a restriction because otherwise only y and z exchange their role). Obviously, the piezoeffect in the paraphase has given rise to a new long-range interaction term $\propto ck$.

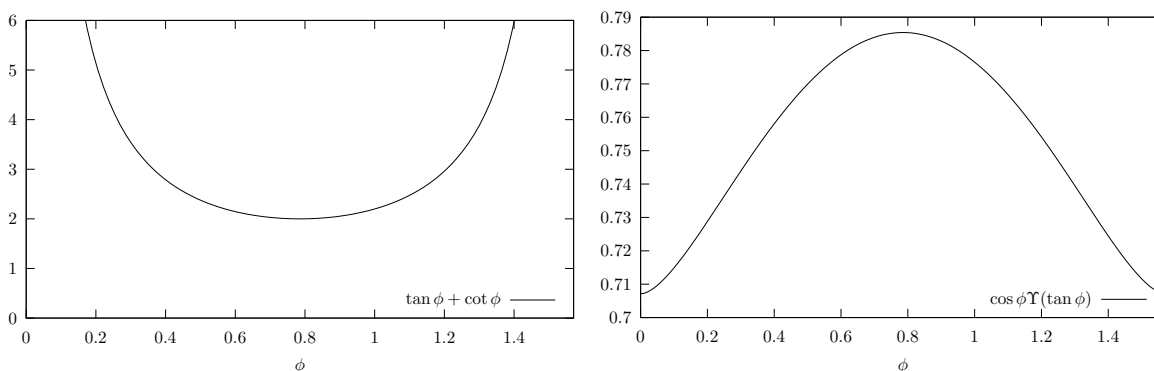


Fig. 2.4: Right: Plot of the function $\tan \phi + \cot \phi$, corresponding to the elastic bump energy. It is obvious, that this function takes a minimum for $\phi = \pi/4$ which means $L_y = L_z$. Left: Plot of the function $\cos \phi \Upsilon(\tan \phi)$, which describes the isotropic long-range term in (2.55) under the condition $L_y^2 + L_z^2 = 1$. The energy is found maximal at $\phi = \pi/4$.

2.3.3 Domain wall roughness in the presence of random field disorder

To calculate the domain wall roughness in the presence of random field disorder, we can employ the Imry-Ma argument [4]. The domain wall is imposed a bump configuration

$$\xi(y, z) = w \exp \left[-\pi \left(\frac{y^2}{L_y^2} + \frac{z^2}{L_z^2} \right) \right], \quad \xi_{\mathbf{k}} = w L_y L_z \exp \left[-\frac{k_y^2 L_y^2 + k_z^2 L_z^2}{4\pi} \right]. \quad (2.54)$$

The volume of the bump is exactly given by $w L_y L_z$, which will come in handy for the Imry-Ma argument. On inserting (2.54) into the interface Hamiltonian (2.52), we obtain the domain wall energy for the bump as a function of the parameters L_y and L_z , which is given by

$$\frac{E(L_y, L_z, w)}{w^2} = \frac{\pi\sigma}{2} \left[\frac{L_y}{L_z} + \frac{L_z}{L_y} \right] + c_z L_y \Xi \left(\frac{L_z}{L_y} \right) + c L_y \Upsilon \left(\frac{L_z}{L_y} \right). \quad (2.55)$$

Hereby we have introduced the two functions

$$\Xi(a) = \frac{2a^2}{\sqrt{\pi}} \int_0^\infty dx \sqrt{x} e^{-x(2a^2-1)} K_0(x) \sim \frac{\ln a + 2 \ln 2 - 1}{\sqrt{2}a} \quad (2.56)$$

$$\Upsilon(a) = \frac{1}{\sqrt{2}} E(1 - a^2) \sim \frac{1}{\sqrt{2}} \left[a + \frac{\ln a + \ln 2 - \frac{1}{4}}{a} \right]. \quad (2.57)$$

The function $K_0(x)$ in (2.56) is the modified Bessel function of the second kind and $E(x)$ in (2.57) designates the complete elliptic integral. The function $\Upsilon(a)$ originates from the isotropic long-range term in (2.52). The asymptotics provided in the equations (2.56) and (2.57) correspond to the expansion around $a = \infty$, i.e. writing $L_z = L \sin \phi$ and $L_y = L \cos \phi$ the asymptotics becomes exact for $\phi \rightarrow \pi/2$. Indeed, only the elastic short-range term in the bump energy (2.55) actually favours $L_z = L_y$, i.e. $\phi = \pi/4$ (cf. Fig. 2.4). The isotropic

long-range term (proportional to β) prefers either length scales to be as small as possible, independent of the other. Under the restriction $L_y^2 + L_z^2 = 1$ (cf. Fig. 2.4) this term supports a thin needle-like shape of the bump without preference for any direction. The directional long-range term (proportional to α) on the other hand, favours needles oriented along the z -direction, i.e. $L_z \gg L_y$. Since the long-range terms dominate on large length scales, the domain wall deformation exhibits a cigar-like shape along the z -direction. In this asymptotic expansion, ignoring logarithms, the energy reads

$$\frac{E(L_y, L_z, w)}{w^2} \simeq \frac{\pi\sigma}{2} \left[\frac{L_y}{L_z} + \frac{L_z}{L_y} \right] + \frac{2 \ln 2 - 1}{\sqrt{2}} c_z \frac{L_y^2}{L_z} + \frac{c}{\sqrt{2}} L_z. \quad (2.58)$$

Minimisation for a given length scale yields $L_y \propto L_z^{\frac{2}{3}}$. As expected, this agrees with the results that have been obtained for the pure dipolar case ($c = 0$) in [102]. To determine the roughness $w(L_y)$, we further have to include the random field term. This gives

$$E(L_y, w) = w^2 \left[\Sigma L_y^{\frac{1}{2}} + C_z L_y^{\frac{1}{2}} + C L_y^{\frac{3}{2}} \right] - \rho \sqrt{w L_y^{\frac{5}{2}}}, \quad (2.59)$$

where ρ measures the strength of the random field disorder and Σ , C , C_z are proportional to σ , c and c_z , respectively. Minimisation with respect to w provides us the desired relation

$$w^{\frac{3}{2}} = \frac{\rho L_y^{\frac{5}{4}}}{4 \left[C L_y^{\frac{3}{2}} + (\Sigma + C_z) L_y^{\frac{1}{2}} \right]} \Rightarrow w(L_y) \sim L_y^{-\frac{1}{6}}. \quad (2.60)$$

Thus, for $C \neq 0$ the wall is flat on large length scales. This agrees with a result in Ref. [26], which states that the critical dimension is given by $d_c = 2\alpha$ for an elastic energy $E_{\text{el}} \sim k^\alpha$. The case $C = 0$ corresponds to a system with only short-range elastic and dipolar interaction, for which the roughness has already been derived in Ref. [102] and reads $w(L_y) \propto L_y^{\frac{1}{2}}$.

2.3.4 Needle domains

Experimentally, interface deformations of a needle-like shape have been observed (cf. e.g. Refs. [94, 95]). They involve steep gradients and can thus not be accounted for in the harmonic approximation that we have used so far. We are going to work out, whether such types of domain wall deformations are explained by our model. In this section, we ignore the extension of the system in the direction along the ferroelectric axis (the z -direction). This amounts to the assumption that the polarisation is constant in z -direction, i.e. $P_{\mathbf{k}} \propto \delta(k_z)$, which is supported by experimental reports [94]. Then, the Hamiltonian reads (with $\mathbf{k} = (k_x, k_y)$)

$$H[P] = \int_{\mathbf{k}} [(Dk^2 + A)P_{\mathbf{k}}P_{-\mathbf{k}} + B(P^2)_{\mathbf{k}}(P^2)_{-\mathbf{k}}] + \frac{Q^2\kappa}{2\mu} \int_{\mathbf{k}}' P_{\mathbf{k}}P_{-\mathbf{k}} \frac{k_x^2 k_y^2}{k^4}. \quad (2.61)$$

Of special interest for us is now the contribution

$$H_{\text{ee}} = \frac{Q^2\kappa}{2\mu} \int_{\mathbf{k}}' P_{\mathbf{k}}P_{-\mathbf{k}} \frac{k_x^2 k_y^2}{k^4}. \quad (2.62)$$

To calculate the energy cost of a domain wall deformation beyond the harmonic approximation, we insert the general configuration (2.46). Now, we can integrate over k_x and transform (2.62) to a real space representation. One has to be careful because of the non-analyticity of the integrand at $\mathbf{k} = 0$. The calculation is presented in App. B.3. If, for convenience, we introduce

$$g = \frac{\xi(y_1) - \xi(y_2)}{y_1 - y_2}, \quad (2.63)$$

we find

$$H_{ee} = \frac{Q^2 P_0^2 \kappa}{2\pi\mu} \int dy_1 dy_2 \left[\frac{g^2}{1+g^2} - \frac{\ln(1+g^2)}{2} \right]. \quad (2.64)$$

To treat the full functional form without approximation, we have to insert a special configuration for ξ . A simple guess, which is able to interpolate between shallow and steep wall deformations is a triangular one, as shown in Fig. 2.5. We can now calculate the energy of

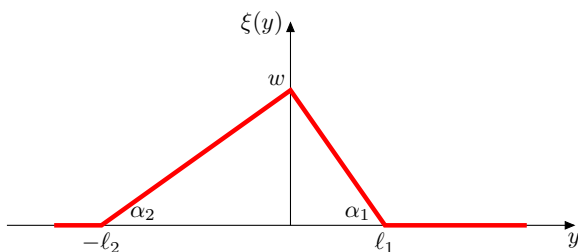


Fig. 2.5: Plot of the triangular domain wall deformation for which the energy is calculated.

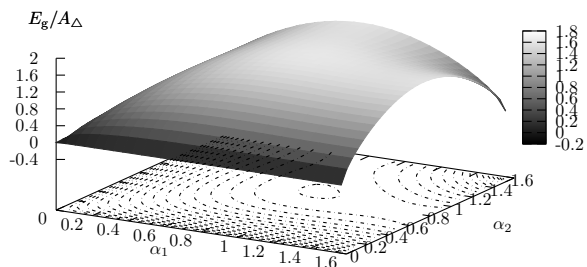


Fig. 2.6: The energy density E_{ee}/A_{Δ} as a function of the triangle parameters α_1 and α_2 .

this triangular configuration by integration over y_1 and y_2 . To shorten our notation, we use

$$A_{\Delta} = \frac{w(\ell_1 + \ell_2)}{2} \quad (2.65)$$

which denotes the area of the triangle enclosed by the domain wall and the deformation $\xi(y)$. The integrals over y_1 and y_2 are technically simple but tedious, their calculation requires a lot of partial fraction decomposition. Essentially, much of this task can be done by modern computer algebra systems, so we do not present the calculation here. The final results are most conveniently expressed in terms of the angles

$$\alpha_1 = \arctan \frac{w}{\ell_1} \quad \text{and} \quad \alpha_2 = \arctan \frac{w}{\ell_2}. \quad (2.66)$$

For the respective value of the energy area density, measured in units of $Q^2 P_0^2 \kappa / 2\pi\mu$, we find

$$\frac{E_{ee}}{A_{\Delta}} = \alpha_2 \sin^2 2\alpha_1 + \frac{\sin 4\alpha_1}{2} \ln \frac{\sin(\alpha_1 + \alpha_2)}{\sin \alpha_1} + \alpha_1 \sin^2 2\alpha_2 + \frac{\sin 4\alpha_2}{2} \ln \frac{\sin(\alpha_1 + \alpha_2)}{\sin \alpha_2} \quad (2.67)$$

This energy density is plotted against α_1 and α_2 in Fig. 2.6. Obviously, it is not only favourable to have both angles α_1 and α_2 close to zero, but also if the angles approach $\frac{\pi}{2}$, the energy of the wall deformation decreases. This can explain the needle-like domain pattern observed in the experiments.

Chapter 3

Luttinger liquids with disorder

3.1 Introduction

Meanwhile it is well known, that due to quantum mechanical interference, all states in non-interacting d -dimensional disordered fermionic systems are localised, if the disorder is strong enough [103]. In and below two dimensions ($d \leq 2$), the electronic states are completely localised even for arbitrarily weak disorder [104, 2]. Interactions among the electrons reduce the effect of disorder and may lead to metallic behaviour in $d = 2$ [105].

This chapter focusses on one-dimensional disordered fermionic systems with short range interactions. Renewed interest in one-dimensional systems arises from their realisation in quasi one-dimensional ultracold gases [106], as well as from the progress in manufacturing one-dimensional narrow quantum wires. Examples are carbon nanotubes [107, 108], polydiacetylen [109], quantum Hall edges [110], and semiconductor cleaved edge quantum wires [111]. Our main attention is devoted to the effect of disorder, which arises from a finite density of weak impurities. The problem of single strong impurities is not considered in this work. The one-dimensional case is particularly interesting because due to interactions even for clean systems the Fermi liquid theory breaks down and a Luttinger liquid is formed [112, 113]. In a Luttinger liquid, the excitations are collective and of bosonic nature. At zero temperature, if the interactions are repulsive or only weakly attractive ($K < 3/2$), disorder is relevant and drives the system into a localised phase, the so-called Anderson glass (or Anderson insulator), for which the linear conductivity vanishes. For weak external field f , the nonlinear conductivity is of quantum creep type $\sigma(f) \sim \exp(-c/\sqrt{f})$ [114, 115] with some constant c . Thermal fluctuations destroy the Anderson insulating state and one obtains the variable range hopping linear conductivity [115] $\sigma \sim \exp(-\tilde{c}/\sqrt{T})$ with some other constant \tilde{c} , but also at finite temperature disorder plays an important role on length scales below the thermal de Broglie wavelength of the bosonic excitations.

This chapter is organised as follows. In the following section 3.2, we introduce a model for one dimensional fermionic systems with short range interactions and disorder. We briefly describe the bosonisation procedure and derive the replica action. Slightly adopted versions of this model action are then used to study the following two problems.

In section 3.3 we investigate the effect of randomness on the Mott state. We study one-

dimensional disordered fermionic systems at commensurate fillings, where scattering processes that do not conserve momentum (Umklapp scattering) can lead to a site blockade among repulsively interacting electrons [116, 117]. Systems that are dominated by site blockade, which is a correlation effect, are called Mott insulators. A Mott insulator is characterised by a gap in the charge excitations and is therefore incompressible. Moreover, at $T = 0$ the linear ac-conductivity vanishes for frequencies which are smaller than twice the charge excitation gap. An Anderson glass, which on the other hand is realised for strong enough disorder, is compressible and has a finite ac-conductivity for arbitrarily small frequencies. Thus, depending on the relative strength of disorder and interaction, one expects the system to be described as either a Mott insulator for weak disorder, or an Anderson glass for strong disorder, respectively. But the question remains what happens if both, interactions and disorder, are relevant. Is there a single transition between the Mott insulator and the Anderson glass or is the scenario more complex due to the appearance of new phases? Early work by Ma [118] using the real space renormalisation group for the disordered 1d Hubbard model suggests a direct transition between the Anderson glass and the Mott insulator. This result contrasts with more recent work, where a new type of order was found [119, 120, 121, 122]. In particular, in Refs. [120, 121, 122], the existence of a new Mott glass phase was postulated which is supposed to be incompressible but has no gap in the optical conductivity. Analytical investigations are hampered by the strong coupling nature of the phases which does not allow an RG study. Alternative approaches like the variational method used in [120, 121] are difficult to control when applied to scalar fields as in the present case. Here, we follow a new approach via relating both, the compressibility and the ac conductivity to the energy connected with the topological excitations of the electronic displacement field. The results of our work are also published in Ref. [123].

The second problem, treated in section 3.4 concerns the applicability of the replica trick in order to determine the nonlinear conductivity of the Anderson insulating phase due to quantum tunneling and the linear conductivity at finite temperatures. Transport caused by quantum mechanical tunneling in the presence of dissipation, driven by an external field, corresponds to the decay of a metastable state. Within the framework of Euclidian field theory, this decay can be described in terms of instantons [124]. An instanton is associated to a solution of the Euler-Lagrange equations with finite action and describes the critical field configuration around which an unstable fluctuation mode exists that drives the system into a new metastable state of lower free energy. The decay rate of the metastable state can then be deduced from the contribution of the unstable fluctuation to the imaginary part of the free energy [125, 126, 127]. The instanton itself can be visualised as a critical nucleus of the new metastable state with lower free energy inside the old one. The unstable fluctuation mode then corresponds to the growth of this nucleus which finally fills the whole system. In recent works, the quantum creep at zero temperature as well as the linear hopping conductivity for systems at finite temperature has been calculated [115, 128]. However, it has not yet been possible to determine the prefactors in the exponent. We discuss, in how far the replica trick can be useful to reproduce the previous results and to fill this gap. For that purpose, approximate solutions to the Euler-Lagrange equations for the replica action are derived. It turns out, that the replica limit $n \rightarrow 0$ raises difficulties. We illustrate this in more detail at the example of a simple $0 + 1$ -dimensional toy model.

3.2 The model

We consider spinless fermions hopping on a one-dimensional lattice and describe them by the extended Hubbard model with a random on-site potential

$$H = H_0 + H_{\text{dis}} \quad (3.1)$$

$$H_0 = -t \sum_i (c_i^\dagger c_{i+1} + c_{i+1}^\dagger c_i) + \frac{V}{2} \sum_i (n_i - \bar{n})(n_{i+1} - \bar{n}) \quad (3.2)$$

$$H_{\text{dis}} = \sum_i U_i (n_i - \bar{n}). \quad (3.3)$$

Here, $n_i = c_i^\dagger c_i$ and \bar{n} denote the local and the average electron density, respectively.

In one dimension, the electrons cannot avoid each other which leads to the fact, that there are no single particle excitations. Rather, excitations are collective. The quanta of these collective excitations are of bosonic nature. The meanwhile standard bosonisation programme describes the system (3.1) in terms of these bosonic variables. Here, we are going to sketch the derivation briefly, for a more extensive review confere e.g. Refs. [129, 130, 6]. To obtain the low-energy physics it is sufficient to consider only excitations with wave-numbers close to the Fermi points at $\pm k_F$. This splits the particles under consideration into two families, corresponding to the different signs of the momentum. Particles with negative momentum are called left-movers, c_{iL}^\dagger and those that have positive momentum are known as the right-movers c_{iR}^\dagger . Going over to the continuum limit, we express the fermionic fields by slowly varying fields of left- $c_{iL}^\dagger \rightarrow \psi_L^\dagger(x)$ and right-movers $c_{iR}^\dagger \rightarrow \psi_R^\dagger(x)$.

The density now reads

$$\rho(x) = \psi_R^\dagger \psi_R + \psi_L^\dagger \psi_L + e^{-i2k_F x} \psi_R^\dagger \psi_L + e^{i2k_F x} \psi_L^\dagger \psi_R \quad (3.4)$$

$$= \rho_0 - \frac{1}{\pi} \nabla \varphi(x) + \frac{k_F}{\pi} \cos[2\varphi(x) - 2k_F x]. \quad (3.5)$$

We have hereby introduced $\rho_0 = k_F/\pi = \Lambda \bar{n}$, where Λ denotes the inverse lattice spacing, and the field $\varphi(x)$, taken to describe the long wavelength fluctuations of the density [131]. Its canonically conjugate field is denoted by Π . The Hamiltonian H_0 (cf. (3.2)) can be expressed in terms of the two conjugate fields φ and Π :

$$H_0 = \frac{1}{2} \int_0^L dx \left[\pi \frac{vK}{\hbar} (\Pi(x))^2 + \frac{\hbar v}{\pi K} (\nabla \varphi(x))^2 \right]. \quad (3.6)$$

In the non-interacting case ($V = 0$), we find $K = 1$ and $v = v_F$. The interactions $V \neq 0$ can be accounted for by adjusting the two, so called Luttinger liquid parameters v and K . Attractive interactions correspond to $K > 1$, whereas for repulsive interactions $K < 1$.

3.2.1 The disorder term

Also the disorder contribution to the Hamiltonian H_{dis} can be represented in terms of the bosonic field $\varphi(x)$. We assume the disorder to be generated by many weak impurities of small

constant strength U_0 . In the continuum limit, $U_i \rightarrow U(x)$ the disorder potential reads

$$U(x) = \sum_{i=1}^{N_{\text{imp}}} U_0 \cdot f(x - x_i). \quad (3.7)$$

Here, N_{imp} is the overall number of impurities in the system and x_i is the position of the i^{th} impurity. The x_i are uniformly distributed over the whole system. In our case, f is a normalised short-range function, which we take as a delta function for simplicity. Assuming a huge impurity density, the scale of variation of physical quantities is much larger than the typical distance among single impurities. Whence, we go over to a coarse-grained description. Therefor, we divide the system into cells of dimension $l \gg n_{\text{imp}}^{-1}$, where l is still small compared to the scale of variation of physical observables. The coarse-grained disorder potential then reads

$$V(x) = \frac{1}{l} \sum_{i=1}^{N_{\text{imp}}} U_0 \cdot \mathbb{1}_X(x_i) - U_0 n_{\text{imp}}. \quad (3.8)$$

Here, X is the name of the cell for which $x \in X$ and $\mathbb{1}_X$ is the indicator function of the set X , i.e. it obeys $\mathbb{1}_X(x) = 1$ for all $x \in X$ and vanishes elsewhere. We have subtracted the expectation value, since only the fluctuations of the impurity density are relevant, the expectation value is merely a shift of the overall energy. Since the impurity positions x_i are uniformly distributed, $\mathbb{1}_X(x_i)$ is a Bernoulli process. Whence, its sum (which is the number of impurities in the cell) satisfies a Poissonian distribution

$$P\left(\sum_{i=1}^{N_{\text{imp}}} \mathbb{1}_X(x_i) = k\right) = \frac{\lambda^k}{k!} e^{-\lambda}, \quad (3.9)$$

where $\lambda = l \cdot n_{\text{imp}}$ is the expectation value. If λ is large, which is the case for our model, we can approximate the Poissonian distribution by a Gaußian one.

$$P\left(\sum_{i=1}^{N_{\text{imp}}} \mathbb{1}_X(x_i) = k\right) \simeq \frac{1}{\sqrt{2\pi\lambda}} e^{-\frac{(k-\lambda)^2}{2\lambda}}. \quad (3.10)$$

From this we can conclude the probability density for the coarse-grained disorder potential at the point x :

$$\begin{aligned} P(V(x) = v) &= P\left(\sum_{i=1}^{N_{\text{imp}}} \mathbb{1}_X(x_i) = k\right) \cdot \frac{dk}{dv} = P\left(\sum_{i=1}^{N_{\text{imp}}} \mathbb{1}_X(x_i) = k\right) \cdot \frac{l}{U_0} \\ &= \frac{1}{\sqrt{2\pi\tilde{\sigma}}} e^{-\frac{v^2}{2\tilde{\sigma}}}. \end{aligned} \quad (3.11)$$

Here, $\tilde{\sigma} = U_0^2 n_{\text{imp}} / l$. Neglecting finite-size effects, the number of impurities in one cell does not depend on the number of impurities in adjacent cells. Therefore, we have

$$\langle V(x_i) V(x_j) \rangle = \tilde{\sigma} \cdot \delta_{ij} = \tilde{\sigma} \cdot l \cdot \delta(x_i - x_j) = U_0^2 n_{\text{imp}} \cdot \delta(x_i - x_j). \quad (3.12)$$

Now, we obtain the probability measure of the impurity potential:

$$P[V(x)] = \left(\sqrt{\frac{1}{2\pi\tilde{\sigma}}} \right)^{\frac{L}{l}} \exp \left[-\frac{1}{2} \int dx dx' V(x) D^{-1}(x-x') V(x') \right], \quad (3.13)$$

where L measures the size of the whole system and $D(x-x') = U_0^2 n_{\text{imp}} \delta(x-x')$ is the covariance function.

Taking only low-energy processes into account, we have to consider the Fourier components of the disorder potential close to $q \sim 0$ (forward scattering) and close to $q \sim 2k_F$ (backward scattering). This leaves us with

$$\mu(x) = \sum_{|q| \ll k_F} V_q e^{iqx} \quad (3.14)$$

$$\xi(x) = \sum_{|q| \ll k_F} V_{q+2k_F} e^{i(q+2k_F)x}; \quad \xi^*(x) = \sum_{|q| \ll k_F} V_{q-2k_F} e^{i(q-2k_F)x} \quad (3.15)$$

From the correlation function (3.12) which we have imposed on $V(x)$, it follows that a similar formula holds for its Fourier transform, namely:

$$\langle V_q V_{q'} \rangle = \frac{U_0^2 n_{\text{imp}}}{L} \cdot \delta_{q,-q'}. \quad (3.16)$$

This formula tells us, that forward and backward scattering parts are uncorrelated, as well as the backward expressions at different positions:

$$\langle \xi(x) \mu(x') \rangle = 0 \quad \text{and} \quad \langle \xi(x) \xi(x') \rangle = 0. \quad (3.17)$$

The forward scattering correlation obeys

$$\begin{aligned} \langle \mu(x) \mu(x') \rangle &= \sum_{|q|, |q'| \ll k_F} \langle V_q V_{q'} \rangle e^{i(qx+q'x')} = \frac{U_0^2 n_{\text{imp}}}{L} \sum_{|q| \ll k_F} e^{iq(x-x')} \\ &= \frac{U_0^2 n_{\text{imp}}}{2\pi} \cdot \frac{2}{(x-x')} \cdot \sin[\lambda(x-x')] \simeq U_0^2 n_{\text{imp}} \cdot \delta(x-x'). \end{aligned} \quad (3.18)$$

Here, λ is an upper cutoff for the wave-number summation, taken to be of the order of l^{-1} . A similar calculation yields

$$\langle \xi(x) \xi^*(x') \rangle = U_0^2 n_{\text{imp}} \cdot \delta(x-x'). \quad (3.19)$$

The disorder Hamiltonian H_{dis} can now be expressed in terms of the independent forward- and backward scattering potentials and the bosonic field φ . Writing $\xi(x) = |\xi(x)| e^{i(\alpha(x)+2k_F x)}$, we find

$$H_{\text{dis}} = \int_0^L dx U(x) (\rho(x) - \rho_0) = \frac{1}{\pi} \int_0^L dx [\mu(x) \cdot \nabla \varphi + k_F |\xi(x)| \cos(2\varphi - \alpha(x))] \quad (3.20)$$

3.2.2 The replica action

The central quantity for problems in equilibrium statistical physics is the partition function. Once the partition function is known, it is possible to derive all physical quantities of interest, as for example the free energy. The partition function can be represented in terms of the coherent state path integral (for a review see e.g. [132, 133])

$$Z = \int \mathcal{D}\varphi \mathcal{D}\Pi \exp \left[-\frac{1}{\hbar} \int_0^{\beta\hbar} d\tau \int_0^L dx (i\Pi \partial_\tau \varphi + \mathcal{H}[\Pi, \varphi]) \right] \quad (3.21)$$

$$\equiv \int \mathcal{D}\varphi \mathcal{D}\Pi \exp \left[-\frac{S[\varphi, \Pi]}{\hbar} \right], \quad (3.22)$$

where periodic boundary conditions in imaginary time ($\varphi(x, 0) = \varphi(x, \beta\hbar)$ and $\Pi(x, 0) = \Pi(x, \beta\hbar)$) are implicitly required. To get the action of our model with the Hamiltonian density

$$\mathcal{H}[\Pi, \varphi] = \frac{1}{2\pi} \left[\frac{vK}{\hbar} (\pi\Pi(x))^2 + \frac{\hbar v}{K} (\partial_x \varphi)^2 + 2\mu(x) \partial_x \varphi(x) + 2k_F |\xi(x)| \cos(2\varphi - \alpha(x)) \right], \quad (3.23)$$

we note that

$$i\Pi \partial_\tau \varphi + \mathcal{H} = \frac{\hbar}{2\pi} \left[\frac{1}{\hbar} (\pi\tilde{\Pi})^2 + \frac{1}{vK} (\partial_\tau \varphi)^2 + \frac{v}{K} (\partial_x \varphi)^2 + \frac{2}{\hbar} \mu(x) \partial_x \varphi + 2|\xi| \frac{k_F}{\hbar} \cos(2\varphi - \alpha) \right],$$

$$\pi\tilde{\Pi}(x) = \pi\Pi + \frac{i\hbar}{vK} \partial_\tau \varphi.$$

The action now simply follows as

$$S[\varphi, \Pi] = S[\varphi] + S[\tilde{\Pi}] \quad (3.24)$$

$$S[\varphi] = \frac{\hbar}{2\pi} \int_0^L dx \int_0^{\beta\hbar} d\tau \left[\frac{1}{vK} (\partial_\tau \varphi)^2 + \frac{v}{K} (\partial_x \varphi)^2 + \frac{2}{\hbar} \mu(x) \partial_x \varphi + 2|\xi(x)| \frac{k_F}{\hbar} \cos(2\varphi - \alpha(x)) \right]. \quad (3.25)$$

Note, that the contribution $S[\tilde{\Pi}]$ is quadratic and can thus be integrated out straightforwardly.

For random systems, the important physical quantities are the averages of observables with respect to the probability distribution of the disorder¹. In this sense, the partition function itself for a given realisation of the disorder is not useful, nor is the average of the partition function. To access the disorder averages of observables, different methods have been invented. Among them are dynamical equations and supersymmetric approaches, where the latter are by definition suited to strictly quadratic problems with a random covariance. We employ the beautiful replica trick to obtain the disorder averaged free energy. By definition, we have

$$F = -\frac{1}{\beta} \ln Z = -\frac{1}{\beta} \lim_{n \rightarrow 0} \frac{Z^n - 1}{n} \quad \Rightarrow \quad \langle F \rangle = -\frac{1}{\beta} \langle \ln Z \rangle = -\frac{1}{\beta} \lim_{n \rightarrow 0} \frac{\langle Z^n \rangle - 1}{n}. \quad (3.26)$$

¹Usually, one makes the implicit assumption that the observables are self-averaging, which means that small parts of a system under consideration behave as independent subsystems. For self-averaging observables, the disorder averages then describe the outcome of experiments. For a discussion see e.g. [134] or [6], chapter 9.

The replica trick interprets n as an integer number, so instead of a complicated average over a logarithm, we are left with the average over a power of Z . However, sophisticated subtleties come into play, when one tries to take the limit $n \rightarrow 0$ at the end of the calculation. For the moment, we shall not be bothered with this limit. Writing

$$\langle Z^n \rangle = \left[\prod_{p=1}^n \int \mathcal{D}\varphi_p \right] \left\langle \exp \left[-\frac{1}{\hbar} \sum_{p=1}^n S_p[\varphi_p] \right] \right\rangle \equiv \left[\prod_{p=1}^n \int \mathcal{D}\varphi_p \right] e^{-S_{\text{rep}}[\varphi]/\hbar}, \quad (3.27)$$

the *replica action* for n replica fields φ_p is defined as

$$\begin{aligned} \frac{S_{\text{rep}}[\varphi]}{\hbar} &= -\ln \left\langle \exp \left[-\frac{1}{\hbar} \sum_{p=1}^n S[\varphi_p] \right] \right\rangle \equiv -\ln \left\langle \exp \left[-\frac{\mathcal{S}}{\hbar} \right] \right\rangle \\ &= \frac{\langle \mathcal{S} \rangle}{\hbar} - \frac{1}{2\hbar^2} \left(\langle \mathcal{S}^2 \rangle - \langle \mathcal{S} \rangle^2 \right), \end{aligned} \quad (3.28)$$

where the last equality is the well known cumulant expansion. Since our disorder is Gaussian, it terminates after the second term. Using (3.24) as well as the fact that our disorder is centered around zero ($\langle \mu(x) \rangle = \langle \xi(x) \rangle = 0$), we obtain

$$\langle \mathcal{S} \rangle = \frac{\hbar}{2\pi} \sum_{p=1}^n \int_0^L dx \int_0^{\beta\hbar} d\tau \left[\frac{1}{vK} (\partial_\tau \varphi_p)^2 + \frac{v}{K} (\partial_x \varphi_p)^2 \right]. \quad (3.29)$$

For the second term, we additionally need the disorder correlators (3.17), (3.18) and (3.19)

$$\begin{aligned} \langle \mathcal{S}^2 \rangle - \langle \mathcal{S} \rangle^2 &= \frac{U_0^2 n_{\text{imp}}}{\pi^2} \sum_{p,q=1}^n \int_0^L dx \int_0^{\beta\hbar} d\tau d\tau' \\ &\quad \left[\partial_x \varphi_p(x, \tau) \partial_x \varphi_q(x, \tau') + \frac{k_{\text{F}}^2}{2} \cos [2\varphi_p(x, \tau) - 2\varphi_q(x, \tau')] \right]. \end{aligned} \quad (3.30)$$

Rescaling the coordinates to make them dimensionless $x \rightarrow \Lambda x$, $\tau \rightarrow y = \Lambda v \tau$, and adding an external field term, we finally obtain for the replica action

$$\begin{aligned} \frac{S_{\text{rep}}[\varphi]}{\hbar} &= \frac{1}{2\pi K} \sum_{p,q=1}^n \int_0^{\Lambda L} dx \int_0^{\Lambda \lambda_{\text{th}}} dy dy' \left\{ [(\partial_y \varphi_p)^2 + (\partial_x \varphi_p)^2 + 2f\varphi_p] \delta_{pq} \delta(y - y') - \right. \\ &\quad \left. \frac{\sigma}{2\pi K} \partial_x \varphi_p(x, y) \partial_x \varphi_q(x, y') + \frac{u}{2\pi K} \cos[2\varphi_p(x, y) - 2\varphi_q(x, y')] \right\}. \end{aligned} \quad (3.31)$$

The factor 2 in front of the strength of the external field f is mere convenience. Further, we have introduced the constants

$$\lambda_{\text{th}} = v\beta\hbar; \quad \kappa = \frac{K}{\pi\hbar v}; \quad \sigma = \frac{2\pi^2 U_0^2 n_{\text{imp}} \kappa^2}{\Lambda}; \quad u = \frac{\pi^2 k_{\text{F}}^2 U_0^2 n_{\text{imp}} \kappa^2}{\Lambda^3}. \quad (3.32)$$

The two dimensionless factors σ and u measure the strength of the forward and the backward scattering at the disorder, respectively, λ_{th} is the thermal de-Broglie wavelength and κ the compressibility [115, 128].

3.3 Absence of the Mott Glass phase

As mentioned in the introduction, in this section, we study the interplay between the Mott and the Anderson insulating state in a one-dimensional disordered fermionic system in order to draw a decision about the existence of an intermediate Mott glass phase, that has been proposed in Refs. [120, 121, 122]. We tackle this problem by relating both the compressibility and the ac conductivity to the kink energy of the bosonic displacement field $\varphi(x)$, describing electrons in one dimension. The approach has some similarities with the treatment of the flat phase of a surface undergoing a roughening transition [135] and may be useful for other strong coupling problems as well. Adding (removing) a charge at a site x corresponds to the insertion of a $\delta\varphi(x) = \pm\pi$ kink in the bosonic field. The compressibility of the systems is determined by adding kinks (or antikinks) to the classical ground state of the system. If the kink energy is finite, the system is incompressible. Similarly, the optical conductivity follows from transitions between the ground state and the first excited state which involves kink-antikink pairs. For vanishing kink energy, the level splitting between the ground state and the first excited state is exponentially small in the kink-antikink distance. A decreasing energy $\hbar\omega$ will then drive transitions between levels of pairs of ever increasing distance, and hence the ac conductivity remains finite for small ω . This is no longer the case when the kink energy is finite: the energy of the kink-antikink pair is the lower bound for the level splitting, and hence the optical conductivity shows a gap of this size. Thus, as long as there is no true long range interaction between charges, incompressibility and a gap in the optical conductivity require each other. Thus, we will finally conclude that there is no Mott glass phase for systems with short range interactions only.

To allow for Umklapp processes in our model (3.31), we have to include a commensurate periodic potential. This yields a new term in the replica action, so that the replica action that we are going to use in this section reads

$$\begin{aligned} \frac{S_{\text{rep}}[\varphi]}{\hbar} = & \frac{1}{2\pi K} \sum_{p,q=1}^n \int_0^{\Lambda L} dx \int_0^{\Lambda\lambda_{\text{th}}} dy dy' \left\{ [(\partial_y \varphi_p)^2 + (\partial_x \varphi_p)^2 - w \cos(2\varphi_p) + 2f\varphi_p] \delta_{pq} \delta(y - y') \right. \\ & \left. - \frac{\sigma}{2\pi K} \partial_x \varphi_p(x, y) \partial_x \varphi_q(x, y') + \frac{u}{2\pi K} \cos[2\varphi_p(x, y) - 2\varphi_q(x, y')] \right\}. \end{aligned} \quad (3.33)$$

Here, w measures the strength of the periodic commensurate potential. From this action, the ground state energy can be derived as

$$E_0 = \lim_{T \rightarrow 0} -\frac{1}{\beta} \ln \left[\prod_{p=1}^n \int \mathcal{D}\varphi_p \right] \exp \left[-\frac{S_{\text{rep}}[\varphi]}{\hbar} \right]. \quad (3.34)$$

3.3.1 Generalised rigidities

In this subsection, we discuss the rigidities, that are related to the (inverse) compressibility and the conductivity of the system. We will see that, if the rigidities diverge, the system is appropriately described by the kink energies $\Sigma_{x/y}$. We start with the consideration of a fixed strain ϑ by imposing the boundary conditions $\varphi(0, y) = 0$ and $\varphi(\Lambda L, y) = \pi\vartheta\Lambda L$. For

$\vartheta \ll 1$ and $L \rightarrow \infty$, the energy increase $\Delta E_0(\vartheta, 0) = E_0(\vartheta, 0) - E_0(0, 0)$ of the ground state energy $E_0(\vartheta, 0)$ in response to the boundary condition, is clearly an even but not necessarily an analytic function of ϑ . More precisely,

$$\lim_{L \rightarrow \infty} \frac{\Delta E_0(\vartheta, 0)}{L} \approx \begin{cases} \vartheta^2/(2\kappa) & \text{if } \Sigma_x = 0, \\ \Sigma_x |\vartheta| & \text{if } \kappa = 0. \end{cases} \quad (3.35)$$

The right-hand side of this relation is explained as follows: if $\Sigma_x = 0$ the stiffness κ^{-1} describes the response to the twisted boundary condition. The change in φ is spread over the whole sample. If, on the other hand, the system becomes incompressible, the kink energy Σ_x is nonzero. The change in φ then occurs in a narrow kink region of width $\xi \ll L$. The position of the kink is such that the energy becomes minimal. A nonzero kink energy resembles the step free energy of a surface below the roughening transition [135]. If, instead of the fixed boundary condition we apply an external stress, then Σ_x is a measure for the critical stress to generate the first kink.

Similarly, we can apply non-trivial boundary conditions in the y -direction by choosing $\varphi(x, 0) = 0$ and $\varphi(x, y) = \pi j y/e$. This amounts to imposing an external current $j = e \langle \partial_y \varphi \rangle / \pi$ at $x = 0$ and $x = L$:

$$\lim_{L \rightarrow \infty} \frac{\Delta E_0(0, j)}{L} \approx \begin{cases} j^2/(2D) & \text{if } \Sigma_y = 0, \\ \Sigma_y |j| & \text{if } D = 0. \end{cases} \quad (3.36)$$

The quantity $D = e^2 \kappa v^2$ is the charge stiffness, which determines the Drude peak of the conductivity [6, 136]

$$\sigma(\omega) = D \delta(\omega) + \sigma_{\text{reg}}(\omega). \quad (3.37)$$

In Lorentz invariant systems, such as the Mott insulator, the kink energies are related by $\Sigma_x = v \Sigma_y$ if both are finite. So far, we have assumed that Σ_x and Σ_y are self-averaging for $L \rightarrow \infty$. Equally, we may introduce local kink energies by applying twisted boundary conditions over a large but finite interval $[x, x + \Lambda L_x]$ with $\Lambda^{-1} \ll L_x \ll L$. Then, the kink energies in general depend on the size L_x of the chosen interval, and in the previous equations we have to replace $\Sigma_{x/y} \rightarrow \Sigma_{x/y}(L_x)$.

3.3.2 The ac conductivity

In this subsection we are going to reveal that the energy of the kink-antikink pair determines the gap in the optical conductivity. Using the relation between the compressibility and the kink energy that we have established in the previous subsection, this allows to conclude that a vanishing compressibility and a gap in the optical conductivity rely on each other.

In cases, where D vanishes, the frequency dependent conductivity $\sigma(\omega)$ may still be non-zero, provided ω is finite. For low kink energy Σ_x , spontaneous tunneling processes between metastable states and their instanton configurations occur, cf. Fig. 3.1. The metastable states are the classical ground states of the action (3.33). Distinct metastable states differ from each other through a shift of φ by an integer multiple of π . The instanton configuration connects

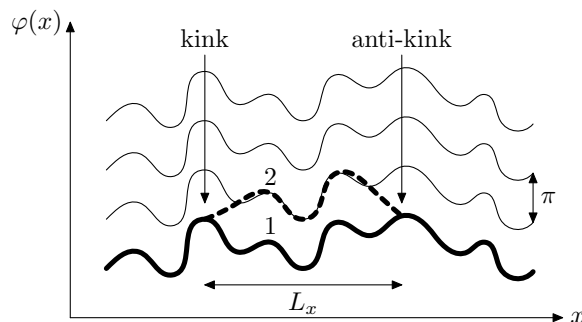


Fig. 3.1: Kink and antikink in the displacement profile $\varphi(x)$. The thin lines represent the minima of the potential in absence of the driving force. The boldface line (configuration 1) corresponds to one specific metastable state and the dashed line is the instanton configuration on top of it (labelled by 2). On applying a fixed strain to the system, only kinks (and/or antikinks) are enforced.

two neighbouring metastable states. The spontaneous tunneling leads to a level splitting of the two states which can be estimated to be of the order (see Ref. [137])

$$\delta E \approx \sqrt{4[\Sigma_x(L_x)]^2 + C \left(\frac{\hbar v}{\xi}\right)^2} e^{-2L_x \Sigma_y / \hbar}. \quad (3.38)$$

This has to match the energy $\hbar\omega$ of the external driving field. Here, \hbar/Σ_y plays the role of a tunneling length and $C > 0$ is a numerical factor. This mechanism was first considered for non-interacting electrons by Mott [138] and has later been extended to the interacting case [139, 140, 141]. Thus, to get a non-zero optical conductivity $\sigma(\omega)$ at arbitrarily low frequencies ω , we have to satisfy the relation $2\Sigma_x(L_x) < \hbar\omega \rightarrow 0$, which requires $\Sigma_x(L_x) \rightarrow 0$ for a finite density of kink positions. This implies a finite compressibility of the system, as we have seen in section 3.3.1.

3.3.3 Fixed points and phases

We are now going to discuss possible phases of our model action (3.33) by attributing them to their RG fixed points. The fixed points will be denoted by a superscript $*$ and the bare values carry a subscript $_0$. For small coupling constants w , σ and u , the lowest order RG equations read

$$\frac{dK}{dl} = -K(au + bw^2) \quad \frac{d\sigma}{dl} = \sigma(1 - 2bw^2) \quad (3.39)$$

$$\frac{dw}{dl} = w(2 - K - \pi\sigma) \quad \frac{du}{dl} = u(3 - 2K) + \frac{\sigma w^2}{2\pi} \quad (3.40)$$

$$\frac{d\kappa}{dl} = -\kappa(z - 1 + bw^2). \quad (3.41)$$

In these equations, l denotes the logarithm of the length scale. Moreover, a and b are positive non-universal constants. As far as there is overlap, our flow equations are in agreement with

those that are given in the references [142, 143]. The dynamical critical exponent has been chosen as $z = 1$ corresponding to the Luttinger liquid fixed point.

The *Luttinger liquid* (LL) phase is characterised by $u_L^* = w_L^* = 0$ and hence $\Sigma_x = \Sigma_y = 0$. Further, $K_L^* > 0$ and there is a finite compressibility $\kappa_L^* = K_L^*/(\hbar\pi v_L^*) > 0$. This fixed point is reached for sufficiently large values of K_0 . The long time and large scale behaviour of the system is that of a clean Luttinger liquid, characterised by both, a finite compressibility κ_L^* and a finite charge stiffness $D_L = e^2\kappa_L^*v_L^{*2}$. The dynamical conductivity is given by $\sigma_{\text{reg}} = iD_L/\omega$. Note, that the presence of the forward scattering term $\propto \mu(x)\partial_x\varphi$ does not change these results, because it can always be removed by the transformation

$$\varphi(x) \rightarrow \tilde{\varphi}(x) = \varphi(x) + \frac{K}{\hbar v} \int_0^x dx' \mu(x'). \quad (3.42)$$

For the *Mott insulator* (MI), we have $K_M^* = \kappa_M^* = u_M^* = \sigma_M^* = 0$ but $w_M^* \gg 1$. Clearly, this fixed point is beyond the range of applicability of our flow equations (3.39)-(3.41), but nevertheless some general properties of this phase can be concluded. The system is in the universality class of the two-dimensional classical sine-Gordon model which describes the Mott insulator to Luttinger liquid transition as well as the roughening transition of a two-dimensional classical crystalline surface [135]. In the Mott insulating phase, the compressibility κ and the Drude peak D of the conductivity vanish. So, the system is characterised by a finite kink energy $\Sigma_x = v\Sigma_y \sim (\kappa_0\xi_M)^{-1}$, where ξ_M denotes the correlation length of the Mott insulating phase [135]. According to Eq. (3.38), the ac-conductivity vanishes for small frequencies $\omega \lesssim 2\Sigma_x/\hbar$.

The *Anderson glass* (or *Anderson insulator*) (AG) corresponds to $w_A^* = K_A^* = 0$ but $u_A^* \gg 1$. The compressibility $\kappa_A^* \approx \kappa_0$ is finite, which results from the statistical tilt symmetry [144]: The boundary condition $\varphi(\Lambda L, y) = \pi\vartheta\Lambda L$ can be made periodic by the transformation $\varphi = \tilde{\varphi} + \pi\vartheta x$ and $\alpha = \tilde{\alpha} - \pi\vartheta x$ (recall that α is the random phase, see Eq. (3.20)). This transformation does not touch the statistical properties of α , i.e. α and $\tilde{\alpha}$ have the same statistical properties. The twist in the boundary conditions appears only in the elastic energy $(2\pi\kappa)^{-1} \langle (\partial_x\varphi - \pi\vartheta)^2 \rangle$. Hence, according to (3.35) we conclude $\Sigma_x = 0$.

Next, we look at the kink energy $\Sigma_x(L_x)$ at a finite length scale $\xi_A \ll L_x \ll L$, such that the parameters are close to their fixed point values. Here, ξ_A is the correlation length which diverges at the transition to the Luttinger liquid phase. To find the classical ground state of the system, we have to choose $2\varphi_i + \alpha_i = 2\pi n_i$ for integer n_i . Moreover, the elastic term has to be minimised with respect to the n_i . Here, the subscript i refers to the sites of the lattice with spacing ξ_A . The solution is [115, 128]

$$n_i = \sum_{j \leq i} \left\lfloor \frac{\alpha_j - \alpha_{j-1}}{2\pi} \right\rfloor, \quad (3.43)$$

where $\lfloor x \rfloor$ denotes the closest integer for any real number x . Thus, the ground state is uniquely determined by the α_j apart from those pairs of sites (of measure zero) at which $\alpha_j - \alpha_{j-1} = \pm\pi$

and where the ground state consequently bifurcates since two solutions are possible. For pairs at which $\alpha_j - \alpha_{j-1} = \pm\pi + \epsilon$ with $|\epsilon| \ll 1$, we can go over to an excited state by creating a kink which costs at most the energy $\Sigma_x \approx \epsilon/(\kappa_0 \xi_A)$. These almost bifurcating sites correspond to states close to the Fermi energy. The smallest energy ϵ found with a probability of order unity in a sample of length L_x is of the order $\epsilon \approx \xi_A/L_x$. Hence, $\Sigma_x \approx (L_x \kappa_0)^{-1}$. Thus, the kink energy vanishes for $L_x \rightarrow \infty$ and therefore the system is compressible. Twisted boundary conditions in the y -direction give $\Sigma_y \sim \hbar(K \xi_A)^{-1}$ [115, 128].

As we have already discussed, a vanishing of Σ_x is also crucial for the existence of the low frequency conductivity. For the Anderson glass phase this is of the form $\sigma(\omega) \sim (\omega \ln \omega)^2$ as has been discussed in detail in [139, 140, 141]. This result can be understood in terms of tunneling processes between rare positions at which the kink energies $\Sigma_x(x)$ are much smaller than $(\kappa_0 L_x)^{-1}$.

The *Mott glass* (MG) phase has been hypothesised in [120, 121] to occur for $K \leq 1$ as a phase that is characterised by a vanishing compressibility $\kappa_G^* = 0$ but a finite optical conductivity at low frequencies. Since this phase is considered to be glassy, the fixed point values for the disorder as well as for the commensurate potential, $u_G, w_G \gg 1$, respectively, are expected to be large. Application of the transformation (3.42) gives a second backward scattering term in (3.33). Then, similarly to the procedure for the Anderson glass phase, the ground state can be found by minimising first the two backward scattering terms and afterwards the elastic energy. Although the ground state is now more involved than for the MI and the AG phase in case $f = 0$, it is clearly periodic with period π . As before, kinks or antikinks with $\delta\varphi = \pm\pi$ allow the accommodation of twisted boundary conditions and the formation of instantons. A vanishing compressibility corresponds to a finite kink energy Σ_x , which, according to (3.38) leads to a gap in the ac conductivity. Therefore, in a system with nonzero $\sigma(\omega)$ for small ω , also the compressibility has to be finite, which contradicts the claims in [120, 121].

So far, we have assumed that all interactions are short range. In the case of an Anderson glass with additional long range Coulomb interaction $V(r) = e^2/(4\pi\epsilon_0\epsilon_s r)$, the bare compressibility is diminished by [6]

$$\kappa_0 \rightarrow \kappa_0 \left[1 + \frac{e^2}{2\pi\epsilon_0\epsilon_s} \ln(Lk_F) \right]^{-1}. \quad (3.44)$$

Thus, for $L \rightarrow \infty$ the Anderson glass becomes incompressible. The effect of Coulomb interaction on the optical conductivity $\sigma(\omega)$ is known for the special case $K = 1$ only, where [145]

$$\sigma(\omega) \propto \omega \ln \omega. \quad (3.45)$$

Hence, in the presence of long range interaction the Anderson glass is transformed into a Mott glass, but there are only two phases at small K_0 .

3.3.4 The phase diagram

Having discussed the possible phases and their properties, we go now over to the analysis of the phase diagram connected to our model (3.33). From (3.40) it follows that the random

backward scattering term is generated by forward scattering and the commensurate potential. Since $\sigma(l) \approx \sigma_0 e^l$, the strength of the forward scattering $\sigma(l)$ becomes large for not too small initial values σ_0 . So, for $K < 1$ the two Eigenvalues $\lambda_1 = 3 - 2K$ and $\lambda_2 = 4 - 2K - \sigma$ describing the RG-flow of u^2 and w^2 around the Luttinger liquid fixed point $u^* = w^* = 0$ have opposite sign: $u(l)$ increases whereas $w(l)$ decreases. Thus the hypothetical MG phase, if it existed, could clearly not reach up to the point $u = w = 0$, in contrast to the findings in Ref. [120]. From this we conclude, that for not too large values of w_0 the AG phase is stable, cf. Fig. 3.2.

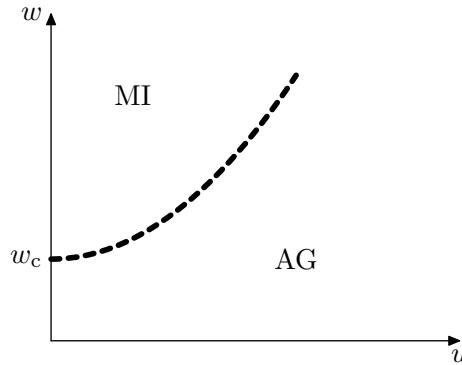


Fig. 3.2: Schematic phase diagram for $K < 3/2$. The MI-AG phase boundary $w_c \sim \sigma^2$ is obtained from the condition $\Sigma_x = 0$ (see text).

In order to find the phase boundary between the AG phase and the MI phase, we consider the stability of the MI phase with respect to the formation of a kink by the disorder. To lowest order in the disorder, we obtain for the kink energy in the Mott insulator phase

$$\Sigma_x \sim \frac{\sqrt{w_0}}{\kappa_0} \left[1 - \frac{1}{\pi} \frac{\sigma_0^{\frac{1}{2}}}{w_0^{\frac{1}{4}}} - \frac{2}{\pi^2} \frac{u_0}{w_0^{\frac{3}{4}}} \right]. \quad (3.46)$$

From the condition $\Sigma_x = 0$ we obtain the MI-AG phase boundary, as is shown in Fig. 3.2. A similar result follows from the self-consistent harmonic approximation.

So far, we have considered only typical disorder fluctuations. If rare events are taken into account for the Gaußian distributed functions $\mu(x)$ and $\xi(x)$ (cf. (3.20)), the result for Σ_x (3.46) remains valid if the replacements $\sigma_0 \rightarrow \sigma_0 \ln(L\Lambda)$ and $u_0^2 \rightarrow u_0^2 \ln(L\Lambda)$ are made [115, 128]. Thus, the size of the area in the parameter space associated to the MI phase is reduced but finite unless $L \rightarrow \infty$.

The phase diagram as depicted in Fig. 3.2 is also supported by the observation that the transformation (3.42) for sufficiently large length scales $L \gtrsim (\sigma_0 \Lambda)^{-1}$ leaves only a random backward scattering term of strength $u_0^2 + w_0^2 / (2\pi^4 \sigma_0)$ [146] in the replica action (3.33), if the bare disorder as well as the commensurate potential are sufficiently weak. Thus, for small K , w and u the Anderson glass phase is realised.

3.3.5 Concluding remarks

By tracing back the compressibility as well as the ac conductivity to a vanishing kink energy Σ_x of the electronic displacement field, we have shown that an incompressible system also has a vanishing optical conductivity. This excludes the existence of a Mott glass phase.

Finally, we briefly want to comment on the variational approach with replica symmetry breaking (RSB) that has been used in Refs. [120, 121]. In the variational approach, the full Hamiltonian is replaced by a harmonic one which leads to the decoupling of the Fourier components φ_q with different wave vector q . Without RSB, this approach recovers the results from perturbation theory which is valid only on length scales smaller than the Larkin length. The RSB mechanism gives then the possibility of a further reduction of the free energy. The results obtained in this way are exact only in cases when the coupling between different Fourier components is irrelevant and the physics is dominated by the largest length scale. Thus, RSB is not an intrinsic property of the true solution of the problem, but a property of the variational approach. An illustrative example is the related problem of the interface roughening transition in a random potential [147]. The variational approach with RSB gives three phases: a flat, a rough and a glassy phase [148], where the rough phase has Flory like exponents. The functional RG (which takes the coupling of different Fourier modes into account) gives, however, only two phases: the flat and the rough phase, but *at* the transition a logarithmically diverging interface width [147]. A similar situation may also exist in the present case.

3.4 The replica instanton approach to variable-range hopping and quantum creep

In this section, we present our attempt to determine the quantum creep and the finite temperature linear conductivity. To this aim, we use the quasi-classical instanton method, which is well known from field theory. For this method to be applicable, we have to employ renormalisation to scale the model into a regime, where quasiclassical methods are valid. In the following, we will not touch the details of the renormalisation group (RG) procedure. Essentially, the RG flow equations are already given for a related model (3.39)-(3.41). Note, however, that the flow equations (3.39)-(3.41) incorporate not only renormalisation but also rescaling. In that sense, they are not applicable here, because we need effective parameters, which are renormalised but unrescaled. In the following we silently agree that all parameters refer to the renormalised ones.

As we have already mentioned (cf. Eq. (3.42)), in the absence of a periodic potential, the forward scattering term can be gauged away from the Hamiltonian density (3.23) by a shift of the field variable

$$\partial_x \varphi(x) \rightarrow \partial_x \tilde{\varphi}(x) = \partial_x \varphi(x) + \frac{K}{\hbar v} \mu(x). \quad (3.47)$$

The backward scattering term just suffers a shift of the random phase which does not change the physics, and the remaining terms do not change at all. To calculate the conductivity we need a coupling to a dissipative bath. This is important for the system to relax after a

tunneling event. Thus the replica action for this section reads

$$\frac{S_{\text{rep}}[\varphi]}{\hbar} = \frac{1}{2\pi K} \sum_{p,q=1}^n \int_0^{\Lambda L} dx \int_0^{\Lambda \lambda_{\text{th}}} dy dy' \left\{ [(\partial_y \varphi_p)^2 + (\partial_x \varphi_p)^2 + 2f\varphi_p] \delta_{pq} \delta(y - y') - u \cos[2\varphi_p(x, y) - 2\varphi_q(x, y')] \right\} + \frac{S_{\text{diss}}[\varphi]}{\hbar}. \quad (3.48)$$

3.4.1 The Euler-Lagrange equations

As has been explained already, we need to find the critical droplet, called instanton, which is a solution of the Euler-Lagrange equations with finite action. Here, we give a derivation of the Euler-Lagrange equations for our model replica action. We start with a very general replica Lagrangian density

$$S_{\text{rep}}[\{\varphi_p\}] = \sum_{p,q=1}^n \int dx dx' L[\varphi_p(x), \nabla \varphi_p(x), \varphi_q(x'), \nabla \varphi_q(x')]. \quad (3.49)$$

To find the stationary point, we follow the standard route of variational calculus and consider the replacement

$$\varphi_p \rightarrow \varphi_p + \lambda_p \varepsilon_p, \quad (3.50)$$

where ε is, as usual, a variation which vanishes at the boundaries. The necessary condition for φ_p to be a stationary point is, that for all replica labels r the following holds true:

$$\begin{aligned} 0 = \partial_{\lambda_r} |_{\lambda=0} S_{\text{rep}}[\{\varphi_p\}] &= \partial_{\lambda_r} |_{\lambda=0} \sum_{p,q=1}^n \int dx dx' L[\varphi_p(x), \partial_x \varphi_p, \varphi_q(x'), \partial_{x'} \varphi_q] \\ &= \sum_{p,q=1}^n \int dx dx' \left[\delta_{r,p} (\partial_1 L \cdot \varepsilon_p + \partial_2 L \cdot \nabla \varepsilon_p(x)) + \delta_{r,q} (\partial_3 L \cdot \varepsilon_q + \partial_4 L \cdot \nabla \varepsilon_p(x')) \right] \\ &= \sum_{q=1}^n \int dx dx' \partial_1 L \cdot \varepsilon_r(x) + \sum_{q=1}^n \int dx' \left[\varepsilon_r(x) \partial_2 L \Big|_0^L - \int dx \partial_x \partial_2 L \cdot \varepsilon_r(x) \right] + \\ &\quad \sum_{p=1}^n \int dx dx' \partial_3 L \cdot \varepsilon_r(x') + \sum_{p=1}^n \int dx \left[\varepsilon_r(x') \partial_4 L \Big|_0^L - \int dx' \partial_{x'} \partial_4 L \cdot \varepsilon_r(x') \right] \\ &= \int dx \varepsilon_r(x) \left\{ \sum_{p=1}^n \int dx' \left[(\partial_1 - \partial_x \partial_2) L[\varphi_r(x), \partial_x \varphi_r, \varphi_p(x'), \partial_{x'} \varphi_p] + \right. \right. \\ &\quad \left. \left. (\partial_3 - \partial_x \partial_4) L[\varphi_p(x'), \partial_{x'} \varphi_p, \varphi_r(x), \partial_x \varphi_r] \right] \right\} \quad (3.51) \end{aligned}$$

The fundamental lemma of variational calculus now yields:

$$0 = \sum_{p=1}^n \int dx' \left[(\partial_1 - \partial_x \partial_2) L[\varphi_r(x), \partial_x \varphi_r, \varphi_p(x'), \partial_{x'} \varphi_p] + \right. \\ \left. (\partial_3 - \partial_x \partial_4) L[\varphi_p(x'), \partial_{x'} \varphi_p, \varphi_r(x), \partial_x \varphi_r] \right], \quad (3.52)$$

which has to hold true for all replica labels r and all positions x .

We apply (3.52) now to the replica action for our model (3.48) and obtain

$$0 = \partial_y^2 \varphi_p + \partial_x^2 \varphi_p + f - 2u \sum_{q=1}^n \int_0^{\Lambda \lambda_{\text{th}}} dy' \sin 2[\varphi_p(x, y) - \varphi_q(x, y')] \quad (3.53)$$

3.4.2 Solution of the Euler-Lagrange equations

The equations to be solved (3.53) form a non-linear system of coupled partial differential equations. Though these features lower the hope to solve them, with an intelligent guess it is possible to find non-trivial approximate solutions. The trivial solution is of course $\varphi_p \equiv 0$ for all p . Our intention is, to find critical-droplet solutions. Therefor we have to insert a guess for the shape of the instanton boundary. Actually, we were able to find approximate solutions to Eq. (3.53) for two instanton geometries. To get a sensible limit $n \rightarrow 0$ in the end, it will turn out to be necessary to have different solutions for different replicas. To keep calculations doable, we restrict ourselves to a one-step replica symmetry breaking. The translation in τ -direction, however, may be different for each non-trivial replica copy and it turns out essential to permit this. In x -direction on the other hand, we will fix the position of the instanton. Apart from saving the computations feasible, the pinning of the instanton walls by the impurities in the original model suggests that this assumption is reasonable. Thus, all following calculations do rely on the fact, that we take into account only one possible projection of the instanton shape onto the x -axis.

In previous works [115, 128], it has been found that instantons in disordered systems have a shape close to a rectangle. This is due to the fact, that the extension in x -direction is such that the surface tension of the boundary is minimal, which is the case in certain areas where the disorder potential provides optimal conditions for a wall. In our replicated model, the translation invariance in x -direction for a single replica solution is only broken by other replica configurations through the mutual coupling between replicas. Thus, from the point of view of the disorder, a rectangular shape is no longer compelling. On the other hand, also the presence of dissipation, which is necessary for tunneling to work, favours a rectangular instanton shape [149]. Thus it may indeed be true, that the rectangular instanton boundary is the more physical one. Nevertheless, we present our solution for circular instantons as well as for rectangular ones.

Circular instantons

We assume to have an instanton configuration described by a smooth convex boundary curve $x_c(y_c)$, which is symmetric with respect to both coordinate axes - at least after a suitable shift

of coordinates. More precisely, we restrict ourselves to circular boundary curves. We are going to employ a new additional coordinate system, that has been introduced by Hida and Eckern [149]. Instead of x and y we use a parameter r which measures the distance of a point in the

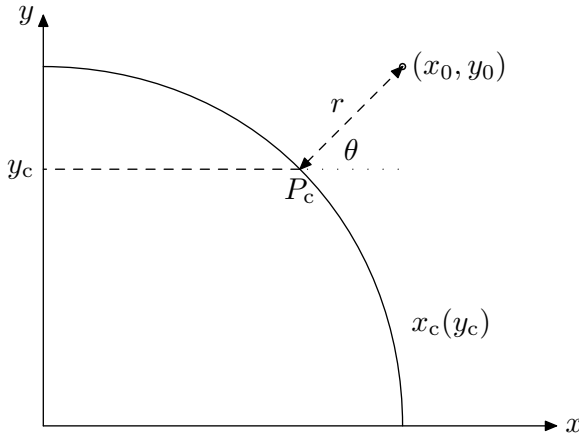


Fig. 3.3: The Hida-Eckern coordinate system $(x, y) \rightarrow (r, y_c)$. The x - y -plane is parametrised relative to the instanton boundary curve $x_c(y_c)$.

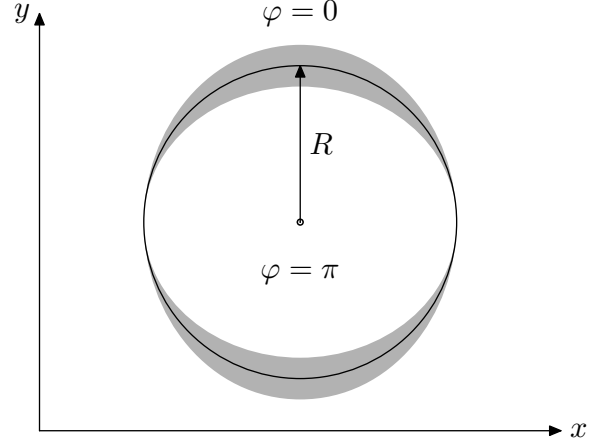


Fig. 3.4: Sketch of a circular instanton. The grey shaded area depicts the region, in which φ changes continuously from 0 to π . Its width depends on θ .

plane to the instanton boundary curve. Furthermore, we use a parameter y_c which specifies the base point P_c of the perpendicular from the point to the boundary curve $x_c(y_c)$ (cf. figure 3.3). The formulae that describe this change of coordinates are

$$x = x_c + r \cos \theta = x_c(y_c) + r \cdot \cos \arctan(-x_c'(y_c)) = x_c(y_c) + \frac{r}{\sqrt{1 + [x_c'(y_c)]^2}} \quad (3.54)$$

$$y = y_c + r \sin \theta = y_c + r \cdot \sin \arctan(-x_c'(y_c)) = y_c - \frac{r \cdot x_c'(y_c)}{\sqrt{1 + [x_c'(y_c)]^2}} \quad (3.55)$$

From (3.54) and (3.55) we can compute the partial derivatives

$$\frac{\partial x}{\partial r} = \frac{1}{\sqrt{1 + [x_c'(y_c)]^2}} \quad \frac{\partial y}{\partial r} = -\frac{x_c'(y_c)}{\sqrt{1 + [x_c'(y_c)]^2}} \quad (3.56)$$

$$\frac{\partial x}{\partial y_c} = x_c'(y_c) - \frac{r x_c'(y_c) x_c''(y_c)}{(1 + [x_c'(y_c)]^2)^{\frac{3}{2}}} \quad \frac{\partial y}{\partial y_c} = 1 - \frac{r x_c''(y_c)}{(1 + [x_c'(y_c)]^2)^{\frac{3}{2}}}, \quad (3.57)$$

which then in turn yield the Jacobian that will come in useful later for the transformation of the integrals

$$J = \det \begin{pmatrix} \frac{\partial x}{\partial r} & \frac{\partial x}{\partial y_c} \\ \frac{\partial y}{\partial r} & \frac{\partial y}{\partial y_c} \end{pmatrix} = \sqrt{1 + [x_c'(y_c)]^2} - \frac{r x_c''(y_c)}{1 + [x_c'(y_c)]^2}. \quad (3.58)$$

Now, we can rewrite the Euler-Lagrange equations partly in the new coordinates. We do not take the external field into consideration yet.

$$0 = \partial_r^2 \varphi_p(r, y_c) - 2u \sin 2\varphi_p(x, y) \sum_{q=1}^n \int_{-\Lambda\lambda_{\text{th}}/2}^{\Lambda\lambda_{\text{th}}/2} dy' \cos 2\varphi_q(x, y') \\ + 2u \cos 2\varphi_p(x, y) \sum_{q=1}^n \int_{-\Lambda\lambda_{\text{th}}/2}^{\Lambda\lambda_{\text{th}}/2} dy' \sin 2\varphi_q(x, y'). \quad (3.59)$$

Being guided by what we expect (a droplet solution) and some similarity of equation (3.59) with the sine-Gordon equation, we impose the following ansatz

$$\varphi_p(r, y_c) = \begin{cases} 2 \arctan \left[\exp \left(-\frac{r}{2d(\theta)} \right) \right] & p \in \{1, \dots, k\} \\ 0 & p \in \{k+1, \dots, n\} \end{cases} \quad (3.60)$$

The non-trivial part corresponds to a shifted Jacobian amplitude profile. In a first approximation, we assume that the integral over the sine vanishes for all $q \in \{1, \dots, n\}$:

$$\int_{-\Lambda\lambda_{\text{th}}/2}^{\Lambda\lambda_{\text{th}}/2} dy' \sin 2\varphi_q(x, y') = 0. \quad (3.61)$$

for all x . Since the integration is over y and not over r , this certainly is an approximation and becomes bad close to points with x -values for which $x_c'(y_c) \simeq 0$, because there the field never reaches π for any y . But such points turn out to be of little relevance, as will become clear immediately. Note, that the width of the instanton wall depends on θ ! Thus, we have

$$0 = \partial_r^2 \varphi_p(r, y_c) - 2u \sin 2\varphi_p(x, y) \sum_{q=1}^n \int_{-\Lambda\lambda_{\text{th}}/2}^{\Lambda\lambda_{\text{th}}/2} dy' \cos 2\varphi_q(x, y'). \quad (3.62)$$

The effective cross-section of the instanton wall parallel to the y -axis is $D = d(\theta)/\sin \theta$. This relation is exact for $\theta \approx \pi/2$, but gets bad for $\theta \rightarrow 0$, which is however not important as $d(\theta) \rightarrow 0$ for $\theta \rightarrow 0$ (see below). The integral over the cosine is then (we consider a full instanton, i.e. we integrate effectively over a kink and an anti-kink)

$$\sum_{q=1}^n \int_{-\Lambda\lambda_{\text{th}}/2}^{\Lambda\lambda_{\text{th}}/2} dy' \cos 2\varphi_q(x, y') = \left(n\Lambda\lambda_{\text{th}} - 16k \frac{d(\theta)}{\sin \theta} \right) \quad (3.63)$$

The Euler-Lagrange equation thus simplifies to the following form

$$0 = \partial_r^2 \varphi_p(r, y_c) - up \left(n\Lambda\lambda_{\text{th}} - 16k \frac{d(\theta)}{\sin \theta} \right) \sin 2\varphi_p(r, y_c), \quad (3.64)$$

and thus gives us the following self-consistency relation for the wall-width

$$d(\theta)^{-1} = 4\sqrt{u \left[n\Lambda\lambda_{\text{th}} - 16k \frac{d(\theta)}{\sin \theta} \right]} \quad (3.65)$$

We see from this that the wall width depends not only on the number of replicas k with instanton configuration, but also on the angle θ of the wall normal to the x -axis. If we solve the polynomial equation (3.65), we obtain

$$d(\theta)^{-1} \equiv 4\sqrt{a - \frac{b}{d(\theta)^{-1}}} \quad (3.66)$$

$$d(\theta)^{-1} = \frac{8a}{3^{\frac{1}{3}} \left(-9b + \sqrt{3}\sqrt{27b^2 - 64a^3} \right)^{\frac{1}{3}}} + \frac{2 \left(-9b + \sqrt{3}\sqrt{27b^2 - 64a^3} \right)^{\frac{1}{3}}}{3^{\frac{2}{3}}} \quad (3.67)$$

In the limit $b \gg a$, which will be achieved for $n \rightarrow 0$, this reduces to

$$d(\theta)^{-1} = - \left[\frac{2}{3} un\Lambda\lambda_{\text{th}} \left(\frac{2 \sin \theta}{uk} \right)^{\frac{1}{3}} + 8 \left(\frac{uk}{2 \sin \theta} \right)^{\frac{1}{3}} \right] \cdot \mathbf{1}_{k \geq 1} + 4\sqrt{un\Lambda\lambda_{\text{th}}} \cdot \mathbf{1}_{k=0}. \quad (3.68)$$

Here, we had to split off the replica symmetric $k = 0$ part. One easily verifies, that $d(\theta)$ vanishes as θ approaches 0. It should be mentioned, that the real solution (which we chose) becomes negative in the limit $n \rightarrow 0$.

To actually calculate the action for small n , we put our coordinate system such that the center of the instanton is its origin. Thus, for the integration we only consider the first quadrant (apart from the y -integrals that have to be done before). The non-disorder part can be transformed to the new coordinates (r, y_c) easily.

$$\begin{aligned} \frac{S_{\text{rep}}}{\hbar} = \frac{1}{2\pi K} & \left[\int_0^{y_c} dy_c \left(\frac{4k}{d(\theta) \cdot \cos \theta} - 8f\pi k x_c(y_c) \right) - \right. \\ & \left. \sum_{p=1}^n \int_{-\frac{\Lambda L}{2}}^{\frac{\Lambda L}{2}} dx \int_{-\Lambda\lambda_{\text{th}}/2}^{\Lambda\lambda_{\text{th}}/2} dy u \cos 2\varphi_p \sum_{q=1}^n \int_{-\Lambda\lambda_{\text{th}}/2}^{\Lambda\lambda_{\text{th}}/2} dy' \cos 2\varphi_q \right]. \quad (3.69) \end{aligned}$$

Using Eq. (3.63), we obtain

$$\frac{S_{\text{rep}}}{\hbar} = \frac{1}{2\pi K} \left[\int_0^{y_0} dy_c \left(\frac{4k}{d(\theta) \cdot \cos \theta} - 8f\pi k x_c(y_c) \right) - u \int_{-\frac{\Lambda L}{2}}^{\frac{\Lambda L}{2}} dx \left(n\Lambda\lambda_{\text{th}} - 16k \frac{d(\theta)}{\sin \theta} \right)^2 \right] \quad (3.70)$$

and the relation (3.65) further yields

$$\begin{aligned} \frac{S_{\text{rep}}}{\hbar} &= \frac{1}{2\pi K} \left[\int_0^{y_0} dy_c \left(\frac{4k}{d(\theta) \cdot \cos \theta} - 8f\pi k x_c(y_c) \right) - \int_{-\frac{\Lambda L}{2}}^{\frac{\Lambda L}{2}} dx \left(n\Lambda\lambda_{\text{th}} - 16k \frac{d(\theta)}{\sin \theta} \right) \frac{d(\theta)^{-2}}{16} \right] \\ &= \frac{1}{2\pi K} \left[\int_0^{y_0} dy_c \left(\frac{6k}{d(\theta) \cdot \cos \theta} - 8f\pi k x_c(y_c) \right) - \int_{-\frac{\Lambda L}{2}}^{\frac{\Lambda L}{2}} dx n\Lambda\lambda_{\text{th}} \frac{d(\theta)^{-2}}{16} \right]. \end{aligned} \quad (3.71)$$

In the last step, we used that the integral over x can be cast in an integral over y_c by $y_c = x \tan \theta$. Dropping the second term which is proportional to n and therefore irrelevant, we obtain

$$\frac{S_{\text{rep}}}{\hbar} = \frac{k}{\pi K} \int_0^{y_0} dy_c \left(\frac{3}{d(\theta) \cdot \cos \theta} - 4f\pi x_c(y_c) \right) \quad (3.72)$$

What we have to take care of, however, is the fact, that, as has been mentioned already, in the limit $n \rightarrow 0$, the wall width will become negative. Thus the instanton reverses its shape and is thus a fluctuation against the field! This can be taken into account by reversing the sign of the term, corresponding to the external field. We can do the integration over dy_c using $dy_c = R \cos \theta d\theta$ and obtain for $k \geq 1$

$$\begin{aligned} \frac{S_{\text{rep}}}{\hbar} &= -\frac{1}{2\pi K} \left[6kR \int_0^{\pi/2} d\theta \left\{ \frac{2un\Lambda\lambda_{\text{th}}}{3} \left(\frac{2 \sin \theta}{uk} \right)^{\frac{1}{3}} + 8 \left(\frac{uk}{2 \sin \theta} \right)^{\frac{1}{3}} \right\} - 2\pi^2 fkR^2 \right] \\ &= -\frac{1}{2\pi K} \left[6kR\sqrt{\pi} \left\{ un\Lambda\lambda_{\text{th}} \frac{\Gamma(2/3)}{\Gamma(1/6)} \left(\frac{2}{ku} \right)^{\frac{1}{3}} - 24 \frac{\Gamma(1/3)}{\Gamma(-1/6)} \left(\frac{ku}{2} \right)^{\frac{1}{3}} \right\} - 2\pi^2 fk \cdot R^2 \right] \\ &= -\frac{1}{2\pi K} \left[6kR\sqrt{\pi} \left[-24 \frac{\Gamma(1/3)}{\Gamma(-1/6)} \left(\frac{ku}{2} \right)^{\frac{1}{3}} \right] - 2\pi^2 fk \cdot R^2 \right] + \mathcal{O}(n) \end{aligned} \quad (3.73)$$

The critical radius for $n \rightarrow 0$ can be read off from the last equation and is given by

$$R_{\text{crit}} = -\frac{36\sqrt{\pi}\Gamma(1/3)}{\pi^2 f\Gamma(-1/6)} \left(\frac{ku}{2} \right)^{\frac{1}{3}}. \quad (3.74)$$

Note, that this result is positive, as it should be, since $\Gamma(-1/6) < 0$.

Rectangular Instantons

Guided by the calculation in the original model [128], we perform the replica calculation also for rectangular instantons. A schematic picture of such an instanton configuration is sketched in Fig. 3.5. We do not use the same coordinate system as in the preceding chapter but stay

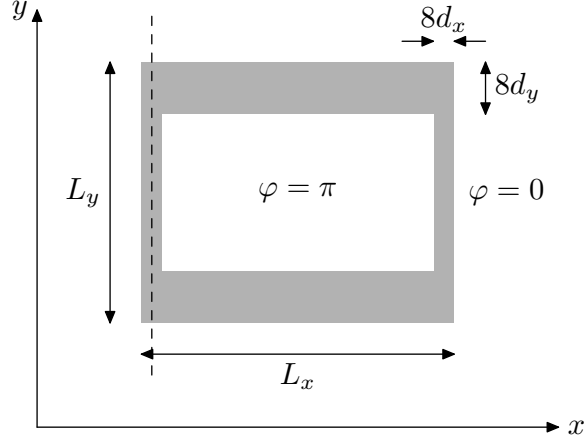


Fig. 3.5: Instanton configuration with an imposed rectangular boundary. The grey shaded area depicts the region in which the field φ changes between its metastable magnitudes 0 and π . The width of the wall is different for the horizontal and the vertical parts.

with the ordinary cartesian chart, which is most suitable to this problem. For the horizontal walls, we assume again a Jacobian wall profile such that

$$\int_{-\Lambda\lambda_{\text{th}}/2}^{\Lambda\lambda_{\text{th}}/2} dy' \sin 2\varphi_q(x, y') = 0 \quad \text{and} \quad \sum_{q=1}^n \int_{-\Lambda\lambda_{\text{th}}/2}^{\Lambda\lambda_{\text{th}}/2} dy' \cos 2\varphi_q(x, y') = (n\Lambda\lambda_{\text{th}} - 16kd_y). \quad (3.75)$$

and thus the Euler-Lagrange equation is

$$0 = \partial_y^2 \varphi_p - 2u(n\Lambda\lambda_{\text{th}} - 16kd_y) \sin 2\varphi_p. \quad (3.76)$$

Thus, the width of the boundary regime is determined by the following equation

$$d_y^{-1} = 4\sqrt{u[n\Lambda\lambda_{\text{th}} - 16kd_y]}. \quad (3.77)$$

The problem for the width of the vertical walls is a bit more subtle. Here, the kink solution described by a Jacobian amplitude function is only approximate. The integration over y is taken via a vertical line (e.g. the dashed line in Fig. 3.5), along which the field never reaches the value of π . Thus, its width is a local quantity depending on x . The Euler Lagrange equation furthermore reveals a second problem: The integral over the sine, i.e. the last term does not vanish any more. Thus, we also face a local phase shift term

$$\begin{aligned} 0 &= \partial_x^2 \varphi_p - 2u \sin 2\varphi_p \sum_{q=1}^n \int_{-\Lambda\lambda_{\text{th}}/2}^{\Lambda\lambda_{\text{th}}/2} dy' \cos 2\varphi_q + 2u \cos 2\varphi_p \sum_{q=1}^n \int_{-\Lambda\lambda_{\text{th}}/2}^{\Lambda\lambda_{\text{th}}/2} dy' \sin 2\varphi_q \\ &= \partial_x^2 \varphi_p - 2uk c(x) \sin[2\varphi_p + \psi(x)]. \end{aligned} \quad (3.78)$$

The functions $c(x)$ and $\psi(x)$ hinder a closed form for the profile of the horizontal walls. But we may assume that the wall has a width $d_x < d_y$, which follows from our considerations of the circular instantons. Now, we go over to calculate the action

$$\begin{aligned} \frac{S_{\text{rep}}}{\hbar} &= \frac{1}{2\pi K} \sum_{p=1}^n \int_{-\frac{\Lambda L}{2}}^{\frac{\Lambda L}{2}} dx \int_{-\frac{\Lambda \lambda_{\text{th}}}{2}}^{\frac{\Lambda \lambda_{\text{th}}}{2}} dy \left[(\partial_y \varphi_p)^2 + (\partial_x \varphi_p)^2 - 2f\varphi_p - u \sum_{q=1}^n \int_{-\frac{\Lambda \lambda_{\text{th}}}{2}}^{\frac{\Lambda \lambda_{\text{th}}}{2}} dy' \cos 2(\varphi_p - \varphi_q) \right] \\ &\simeq \frac{1}{2\pi K} \left[\frac{kL_x}{d_y} + \frac{kL_y}{d_x} - 2fkL_xL_y\pi - u(n^2\Lambda^2\lambda_{\text{th}}L - 32nk\Lambda\lambda_{\text{th}}L_xd_y + 16^2k^2d_y^2L_x) \right], \end{aligned} \quad (3.79)$$

where in the last step, we have neglected the contribution from the vertical walls in the integral over x . Using (3.77), we find

$$\frac{S_{\text{rep}}}{\hbar} \simeq \frac{1}{2\pi K} \left[\frac{2kL_x}{d_y} + \frac{kL_y}{d_x} - 2fkL_xL_y\pi \right] + \mathcal{O}(n). \quad (3.80)$$

3.4.3 A toy model

In the previous section, we have provided an approximate solution to the Euler Lagrange equations and have calculated the replica action. The main goal, however, is to determine the free energy from which we can extract information about the nonlinear conductivity of the system. Unfortunately, we did not manage to deal with the replica limit $n \rightarrow 0$. In this section, we present a simple toy model to point out the difficulties one faces in connection with the replica limit.

The model and the non-replica treatment

We consider the following action

$$S = \hbar M \cdot \int_0^{\lambda_{\text{th}}} d\tau \left[\frac{1}{2} (\partial_\tau \phi)^2 - u \cos(\phi) \right]. \quad (3.81)$$

Here, u shall be a random quantity which fluctuates from sample to sample. We assume it to be described by a Gaussian distribution, centered at zero with the covariance given by

$$\langle u^2 \rangle = \sigma. \quad (3.82)$$

The Euler-Lagrange equation for one specific realisation for u is given by

$$0 = \partial_\tau^2 \phi - u \sin(\phi). \quad (3.83)$$

This equation is solved by the Jacobian amplitude $\text{am}(x) = 4 \arctan[\exp(x)] - \pi$:

$$\phi(\tau) = \begin{cases} 2 \cdot \text{am}(\sqrt{u}\tau) + \pi & u \geq 0 \\ 2 \cdot \text{am}(\sqrt{-u}\tau) & u < 0 \end{cases} \quad (3.84)$$

The action for such a kink is given by

$$\Delta S = S_{\text{kink}} - S_0 = Mu\hbar\lambda_{\text{th}} - Mu\hbar\lambda_{\text{th}} + 8M\hbar\sqrt{u} = 8M\hbar\sqrt{u}. \quad (3.85)$$

Since we need to have solutions periodic in τ , we require an even number of kinks. We restrict ourselves to the simplest possible solution, which is called the one-instanton solution and consists of a kink and an anti-kink. The partition function thus takes into account only two possibilities: the trivial ground state and the one-instanton solution. Hence, we obtain

$$F = -\frac{1}{\beta} \ln Z = -\frac{1}{\beta} \ln \left[e^{Mu\lambda_{\text{th}}} + e^{-M(16\sqrt{u}-u\lambda_{\text{th}})} \right] = -\frac{1}{\beta} \ln \left[e^{Mu\lambda_{\text{th}}} \cdot \left(1 + e^{-16M\sqrt{u}} \right) \right] \quad (3.86)$$

What is neglected until now, but important, is the soft mode fluctuations, which describe the freedom of choice of placing the middle of an instanton. This gives an additional factor of $4\lambda_{\text{th}} \cdot u^{\frac{1}{4}}/\sqrt{2\pi}$. This, so far, is the free energy for a specific u . What we are interested in, however, is the averaged free energy

$$\begin{aligned} \langle F \rangle &= -\frac{1}{\beta} \left\langle \ln \left[e^{Mu\lambda_{\text{th}}} \cdot \left(1 + e^{-16M\sqrt{u}} \cdot 4\lambda_{\text{th}} \cdot \frac{u^{\frac{1}{2}}}{\sqrt{2\pi}} \right) \right] \right\rangle \\ &= -\frac{1}{\beta} M\lambda_{\text{th}} \langle u \rangle - \frac{1}{\beta} \left\langle \ln \left[1 + e^{-16M\sqrt{u}} \cdot 4\lambda_{\text{th}} \sqrt{\pi} \cdot \frac{u^{\frac{1}{2}}}{\sqrt{2\pi}} \right] \right\rangle \end{aligned} \quad (3.87)$$

This is still not the whole story, since, up to now, the free energy would vanish for $T \rightarrow 0$. What we have to do is to take into consideration also contributions coming from more instantons [124]. Thus, we get

$$\langle F \rangle = -\frac{1}{\beta} \left\langle e^{-16M\sqrt{u}} \cdot 4\lambda_{\text{th}} \cdot \frac{u^{\frac{1}{4}}}{\sqrt{2\pi}} \right\rangle. \quad (3.88)$$

There are plenty of other fluctuation modes that, in principle, ought to be considered as well. But to a first approximation, we neglect those contributions.

In principle it would have been nice to have a toy model, the free energy of which does not depend on the disorder at all. Such a model could have been realised by a random phase, following a Laplacian sample to sample distribution with density $p(\alpha) = (2\pi)^{-1}$. Such a model would also give the desired replica action in the first two cumulants

$$\langle \cos(\phi - \alpha) \rangle = \int_0^{2\pi} \frac{d\alpha}{2\pi} \cos(\phi - \alpha) = 0 \quad \text{and} \quad (3.89)$$

$$\langle \cos(\phi_1 - \alpha) \cos(\phi_2 - \alpha) \rangle = \int_0^{2\pi} \frac{d\alpha}{2\pi} \cos(\phi_1 - \alpha) \cos(\phi_2 - \alpha) = \frac{1}{2} \cos(\phi_1 - \phi_2). \quad (3.90)$$

However, now also higher cumulants exist and are important. Thus, unfortunately, this kind of model is not helpful.

The replica calculation

This calculation should provide some idea, which enormous technical complication one faces in connection with the replica limit $n \rightarrow 0$. The first thing one has to note, is, that all calculations in the replica framework have to be carried out at finite temperature. This is due to the fact that there are terms containing the thermal de-Broglie wavelength, which thus diverge for $T \rightarrow 0$. These divergencies vanish in the limit $n \rightarrow 0$. Thus, the calculations also hold for the $T = 0$ case, if one pays attention to take the limit $n \rightarrow 0$ *before* doing the $T \rightarrow 0$ limit. For the free energy we have

$$\langle F \rangle = -\frac{1}{\beta} \langle \ln Z \rangle = -\frac{1}{\beta} \lim_{n \rightarrow 0} \frac{\langle Z^n \rangle - 1}{n} \quad (3.91)$$

The replica action is defined by

$$\langle Z^n \rangle = \prod_{\gamma=1}^n \left[\int \mathcal{D}\phi_\gamma \right] e^{-S_{\text{rep}}/\hbar}, \quad (3.92)$$

and thus determined to be

$$\begin{aligned} S_{\text{rep}}[\{\phi_\gamma\}] &= -\hbar \ln \left\langle \exp -\frac{1}{\hbar} \sum_{p=1}^n S[\phi_p] \right\rangle \\ &= \hbar M \sum_{p=1}^n \int_0^{\lambda_{\text{th}}} d\tau \frac{1}{2} (\partial_\tau \phi_p)^2 - \frac{\hbar M^2 \sigma}{2} \sum_{p,q=1}^n \int_0^{\lambda_{\text{th}}} d\tau d\tau' \cos [\phi_p(\tau) - \phi_q(\tau')]. \end{aligned} \quad (3.93)$$

The corresponding Euler-Lagrange equation reads

$$\begin{aligned} 0 &= \partial_\tau^2 \phi_p - M\sigma \sum_{q=1}^n \int_0^{\lambda_{\text{th}}} d\tau' \sin[\phi_p(\tau) - \phi_q(\tau')] \quad \Rightarrow \\ 0 &= \partial_\tau^2 \phi_p - M\sigma \left[\sin \phi_p \cdot \sum_{q=1}^n \int_0^{\lambda_{\text{th}}} d\tau' \cos \phi_q - \cos \phi_p \cdot \sum_{q=1}^n \int_0^{\lambda_{\text{th}}} d\tau' \sin \phi_q \right] \end{aligned} \quad (3.94)$$

To solve this system of coupled partial differential equations, we follow the well-known sine-Gordon theory and make the one-step replica symmetry breaking ansatz:

$$\phi_p = \begin{cases} 2 \cdot \text{am}(\sqrt{w}\tau) + \pi & p \in \{1, \dots, k\} \\ 0 & p \in \{k+1, \dots, n\} \end{cases} \quad (3.95)$$

In contrast to the previous section 3.4.2, these solutions are exact. One should note, that in principle there is the freedom to add any constant to this ansatz, if this constant is the same for all replica solutions. This is so, because in the action only the difference between two

replica fields contributes. We fix this constant to be 0. With this choice, the integral over the sine vanishes for all q

$$\int_0^{\lambda_{\text{th}}} d\tau' \sin \phi_q = 0. \quad (3.96)$$

Thus the Euler-Lagrange equation reduces to

$$0 = \partial_\tau^2 \phi_p - M\sigma \left[\sin \phi_p \cdot \sum_{q=1}^n \int_0^{\lambda_{\text{th}}} d\tau' \cos \phi_q \right] \quad (3.97)$$

Moreover, our ansatz (3.95) yields

$$\int_0^{\lambda_{\text{th}}} d\tau' \cos \phi_q = \lambda_{\text{th}} - \frac{4}{\sqrt{w}} \quad \Rightarrow \quad \sum_{q=1}^n \int_0^{\lambda_{\text{th}}} d\tau' \cos \phi_q = n\lambda_{\text{th}} - \frac{4k}{\sqrt{w}}.$$

Plugging this result into (3.97), we obtain

$$0 = \partial_\tau^2 \phi_p - M\sigma \left[n\lambda_{\text{th}} - \frac{4k}{\sqrt{w}} \right] \sin \phi_p \quad (3.98)$$

We know from usual sine-Gordon theory, that our ansatz exactly fulfills

$$0 = \partial_\tau^2 \phi_p - w \cdot \sin \phi_p.$$

This gives us a self-consistence condition for the width of the kinks:

$$w = M\sigma \left[n\lambda_{\text{th}} - \frac{4k}{\sqrt{w}} \right]. \quad (3.99)$$

Before we embark on (3.99), we want to calculate the replica action for the ansatz ϕ_p .

$$\begin{aligned} \frac{S_{\text{rep}}[\{\phi_\gamma\}]}{\hbar M} &= \sum_{p=1}^n \int_0^{\lambda_{\text{th}}} d\tau \left[\frac{1}{2} (\partial_\tau \phi_p)^2 - \frac{M\sigma}{2} \cos \phi_p \cdot \sum_{q=1}^n \int_0^{\lambda_{\text{th}}} d\tau' \cos \phi_q \right] \\ &= \sum_{p=1}^n \int_0^{\lambda_{\text{th}}} d\tau \left[\frac{1}{2} (\partial_\tau \phi_p)^2 - \frac{w}{2} \cos \phi_p \right] = 6k \cdot \sqrt{w} - \frac{w}{2} n\lambda_{\text{th}}. \end{aligned} \quad (3.100)$$

The partition function is now given by

$$\langle Z^n \rangle = \prod_{\gamma=1}^n \left[\int \mathcal{D}\phi_\gamma \right] e^{-S_{\text{rep}}/\hbar} = \sum_{k=0}^n \binom{n}{k} e^{-6M\sqrt{w}k + \frac{Mw}{2}n\lambda_{\text{th}}} =: \sum_{k=0}^n \binom{n}{k} e^{\varepsilon(k)} \quad (3.101)$$

Equation (3.99) is a polynomial equation for $\omega := \sqrt{w}$ of third order. There are three solutions, we will as before take the real one. We have

$$0 = \omega^3 - M\sigma n\lambda_{\text{th}}\omega + 4M\sigma k =: \omega^2 - a\omega + b. \quad (3.102)$$

The real solution to this equation is given by

$$\omega = \frac{(12)^{\frac{1}{3}}a + (\sqrt{81b^2 - 12a^3} - 9b)^{\frac{2}{3}}}{(18\sqrt{81b^2 - 12a^3} - 2 \cdot 81b)^{\frac{1}{3}}}. \quad (3.103)$$

To simplify this expression, we follow our procedure from section 3.4.2. As (3.87) indicates, we are in truth only interested in the limit $n \rightarrow 0$. Hence, we will simplify (3.103) for the limiting case $a \ll b$. Of course, the width of the kink will thus become negative, but we shall not be bothered about this at the moment. Then we obtain

$$\omega = -\left(\sqrt[3]{b} + \frac{a}{3\sqrt[3]{b}}\right) + \mathcal{O}(a^2) \quad \Rightarrow \quad w = b^{\frac{2}{3}} + \frac{2}{3}a + \mathcal{O}(a^2). \quad (3.104)$$

Of course, this is not the whole story. We have to split off the replica symmetric solution with $k = 0$ because for this solution $a \ll b$ is always wrong! Replacing a and b by their original expressions, we get up to order $\mathcal{O}(n)$

$$w = \left[(4M\sigma k)^{\frac{2}{3}} + \frac{2}{3}M\sigma n\lambda_{\text{th}} \right] \mathbf{1}_{k \geq 1} + M\sigma n\lambda_{\text{th}} \cdot \mathbf{1}_{k=0} \quad (3.105)$$

$$-\sqrt{w} = \left[(4M\sigma k)^{\frac{1}{3}} + \frac{n\lambda_{\text{th}}}{12k} (4M\sigma k)^{\frac{2}{3}} \right] \cdot \mathbf{1}_{k \geq 1} - \sqrt{Mn\lambda_{\text{th}}\sigma} \cdot \mathbf{1}_{k=0} \quad (3.106)$$

For the exponent $\varepsilon(k)$ in (3.101) this yields

$$\begin{aligned} \varepsilon(k \geq 1) &= -6M\sqrt{wk} + \frac{Mw}{2}n\lambda_{\text{th}} \\ &= 6Mk \left[(4M\sigma k)^{\frac{1}{3}} + \frac{n\lambda_{\text{th}}}{12k} (4M\sigma k)^{\frac{2}{3}} \right] + \frac{M}{2}n\lambda_{\text{th}} \left[(4M\sigma k)^{\frac{2}{3}} + \frac{2}{3}M\sigma n\lambda_{\text{th}} \right] \\ &= 6 \cdot (4\sigma M^4)^{\frac{1}{3}} \cdot k^{\frac{4}{3}} + Mn\lambda_{\text{th}}(4M\sigma k)^{\frac{2}{3}} \end{aligned} \quad (3.107)$$

Before now starting to calculate the free energy, we should warn ourselves about what we are able to calculate. The replica method is a technique to calculate the averaged free energy but is not capable of making any statements about the partition function. In our one-instanton replica calculation we are only able to calculate

$$\tilde{F} = -\frac{1}{\beta} \ln(1 + Z_1). \quad (3.108)$$

The true disorder averaged free energy is, however (assuming that the instantons in many-instanton configurations are independent)

$$\langle F \rangle = -\frac{1}{\beta} \ln \left[1 + Z_1 + \frac{Z_1^2}{2} + \dots + \frac{Z_1^k}{k!} + \dots \right] = -\frac{Z_1}{\beta}. \quad (3.109)$$

Thus we have to extract Z_1 from (3.108), which yields

$$Z_1 = e^{-\beta\tilde{F}} - 1 \quad \Rightarrow \quad \langle F \rangle = \frac{1 - e^{-\beta\tilde{F}}}{\beta}. \quad (3.110)$$

For \tilde{F} the replica calculation now gives (keeping only the relevant terms which survive the limit $n \rightarrow 0$)

$$\tilde{F} = -\frac{1}{\beta} \lim_{n \rightarrow 0} \frac{1}{n} \sum_{k=1}^n \binom{n}{k} e^{\varepsilon(k)} = -\frac{1}{\beta} \lim_{n \rightarrow 0} \frac{1}{n} \sum_{k=1}^n \binom{n}{k} e^{6 \cdot (4\sigma M^4)^{\frac{1}{3}} \cdot k^{\frac{4}{3}}} \quad (3.111)$$

The combinatorial factor can be rewritten in a way such that the limit $n \rightarrow 0$ is feasible, as has been done before in [150]. With

$$\Gamma(-z) = \frac{\pi}{\Gamma(z+1) \cdot \sin(\pi z)}, \quad (3.112)$$

$$\sin(z - p\pi) = (-1)^p \cdot \sin z \quad (p \in \mathbb{Z}), \quad (3.113)$$

we obtain

$$\begin{aligned} \binom{n}{k} &= \frac{\Gamma(n+1)}{\Gamma(k+1)\Gamma(n-k+1)} = \frac{\Gamma(n+1)}{\Gamma(k+1)\Gamma(-(k-(n+1)))} \\ &= \frac{\Gamma(n+1)\Gamma(k-n) \sin[\pi(k-n-1)]}{\pi\Gamma(k+1)} = n \frac{(-1)^{k-1} \Gamma(k-n)}{k \Gamma(k)} \Gamma(n+1) \cdot \frac{\sin(\pi n)}{\pi n}, \end{aligned} \quad (3.114)$$

and conclude

$$\lim_{n \rightarrow 0} \frac{1}{n} \frac{\Gamma(n+1)}{\Gamma(k+1)\Gamma(n-k+1)} = \frac{(-1)^{k-1}}{k}. \quad (3.115)$$

Moreover we have to take care of the soft fluctuation mode which comes from the freedom to place the instanton anywhere between 0 and λ_{th} . The corresponding factor is now (the sign of \sqrt{w} does not matter!)

$$\lambda_{\text{th}} \frac{4}{\sqrt{2\pi}} w^{\frac{1}{4}} = \lambda_{\text{th}} \frac{4}{\sqrt{2\pi}} (4M\sigma k)^{\frac{1}{6}}. \quad (3.116)$$

Since $\binom{n}{k} = 0$ for $k > n$, we can safely extend the sum over k in Eq. (3.111) to infinity and thus, altogether we have

$$\begin{aligned} \tilde{F} &= -\frac{1}{\beta} \sum_{k=1}^{\infty} \frac{(-1)^{k-1}}{k} \left[\frac{\lambda_{\text{th}} 4}{\sqrt{2\pi}} \right]^k (4M\sigma k)^{\frac{k}{6}} e^{6 \cdot (4\sigma M^4)^{\frac{1}{3}} \cdot k^{\frac{4}{3}}} \\ &= -\frac{1}{\beta} \sum_{k=1}^{\infty} \frac{(-1)^{k-1}}{k} \left[\lambda_{\text{th}} \frac{4}{\sqrt{2\pi}} \right]^k \cdot \left\{ (4M\sigma k)^{\frac{1}{6}} \cdot e^{6M(4M\sigma k)^{\frac{1}{3}}} \right\}^k. \end{aligned} \quad (3.117)$$

I do not know how to sum up this divergent series. In [150] it was possible to rewrite the sum for a similar problem as an integral. One could do this for our case as well, however, the

integral does not look more friendly in any sense. In case everything in the curly brackets is equal to one (which is certainly not the case for every k), we can sum the series and get

$$\tilde{F} = -\frac{1}{\beta} \ln \left[1 + \frac{\lambda_{\text{th}}^4}{\sqrt{2\pi}} \right], \quad (3.118)$$

and thus

$$\langle F \rangle = \frac{1}{\beta} \left\{ 1 - \exp \left[-\beta \left(-\frac{1}{\beta} \right) \ln \left(1 + \frac{\lambda_{\text{th}}^4}{\sqrt{2\pi}} \right) \right] \right\} = \frac{1}{\beta} \frac{4\lambda_{\text{th}}}{\sqrt{2\pi}} = \hbar v \frac{4}{\sqrt{2\pi}}. \quad (3.119)$$

This shows, that at least there is hope to have a finite free energy even at zero temperature. At the moment it remains unclear, how the puzzle in connection with Eq. (3.117) can be resolved.

Appendix A

Appendices to chapter 1

A.1 Numerics

In this appendix, the details of our numerical methods shall be explained briefly. Numerically, we have solved the mean field equation of motion (1.11) for 20000 different disorder configurations using the well established classical Euler method. Before embarking on the details of the procedure in the two cases of dc and ac driving, respectively, we want to explain how the different realisations of the disorder forces are achieved.

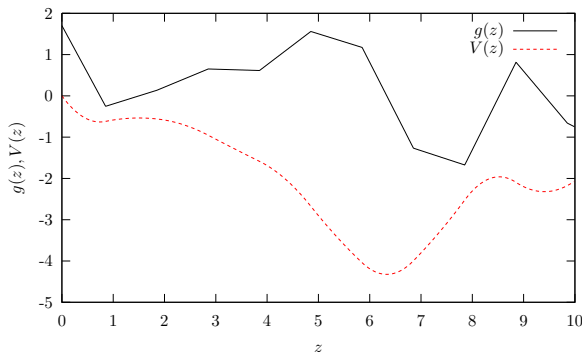


Fig. A.1: An example for a randomly generated disorder realisation with the method that leads to a statistics with a smooth correlator. Besides the force $g(z)$, also the disorder potential, determined from $g(z) = -V'(z)$ is visualised. The potential has a smooth shape.

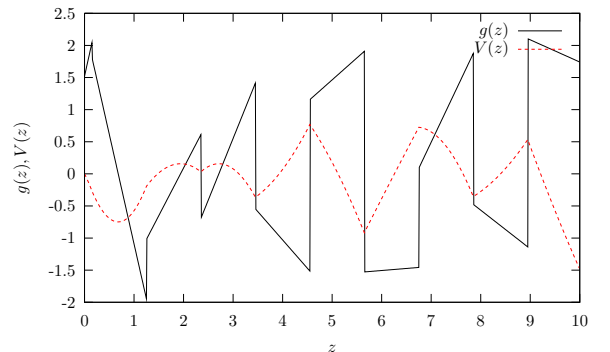


Fig. A.2: An example for a randomly generated disorder realisation with the method that leads to a statistics with a cusped correlator. Besides the force $g(z)$, also the disorder potential, determined from $g(z) = -V'(z)$ is visualised. It can be seen that most of the extrema of the potential reveal a cusp singularity.

The random force associated to the smooth disorder correlator is generated by concatenating straight lines at distance 1. The values of the disorder force at the concatenation points are randomly chosen out of a bounded interval $[-m; m]$. The bounds m for this interval are determined such that the correlator fulfills $\Delta(0) = 1$. We found $m \simeq 2.1$. Moreover, the position s of the concatenation point closest to the origin $z = 0$ has been determined randomly

out of the interval $[-\frac{1}{2}; \frac{1}{2}]$. This method has already been used earlier by A. Glatz [151]. A sample configuration is depicted in figure A.1.

To realise disorder forces with Gaussian statistics that are correlated with a cusp singularity at the origin, we have also used straight lines, the extension in z -direction being again 1. In contrast to the former case, these lines are now concatenated discontinuously. The values of $g(z)$ at both endpoints of a segment are determined randomly from a bounded interval $[-m; m]$. The size of this interval is again determined in such a way that the disorder correlator obeys $\Delta(0) = 1$ with the same result of $m \simeq 2.1$ as before. Also the position $s \in [-\frac{1}{2}; \frac{1}{2}]$ of the jump closest to $z = 0$ is created randomly. An example for such a configuration is shown in Fig. A.2. In App. A.2 we discuss the latter generation technique in more detail and also derive the force correlator.

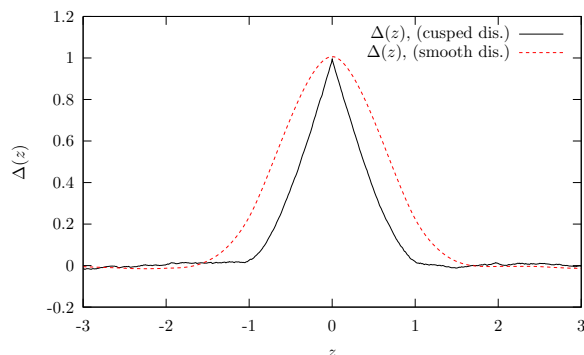


Fig. A.3: The numerically determined correlators for the disorder forces generated by the two different methods described in the text. Either disorder correlator decays on a length scale of order unity and obeys $\Delta(0) = 1$.

Moreover, we have verified numerically, that the assumed shapes for the disorder correlators are reflected by our two generation techniques. The result is shown in Fig. A.3. As required, one correlator is smooth and the other shows a cusp singularity at the origin, perfectly in agreement with the analytic result (cf. Eq. (A.8) below). In both cases, the correlations decay to zero on a length scale $\ell \simeq 1$.

To solve the equation of motion with a constant driving force for several values of Γ and h , we have chosen the initial condition $v(0) = 0$ and $z(0) = 0$. The time steps are chosen to be of size 2^{-10} and we have simulated the equation of motion for 2^{14} such time steps. To avoid that our results are spoiled by transience effects, we have only taken into account the values of v for the last 2^{10} time steps.

Our results that we have obtained for the ac driving case rely on the initial conditions $z(0) = 0$, $v(0) = h$ with $h(t) = h \cos \omega t$. Before making any measurements we have been waiting for at least 2 periods for transience effects to diminish. The values for $v(h = 0)$ and $v(h = h_p)$ are measured then over 3 periods with 2 datapoints per period.

In all cases where we have numerically determined important exponents, we have given error estimates. These include the statistical deviations.

A.2 Generation of disorder forces with a cusped correlator

In this appendix, we propose a generation technique for disorder forces with a cusp singularity in the correlator and prove, that the cusp is indeed present. The method described here has also been employed in our numerical analysis, cf. App. A.1.

Consider a function $g(z)$, that is constructed as follows. We decompose the z -axis in intervals $I_i = [z_i; z_{i+1}]$ of length 1. The starting point of each interval I_i is given by

$$z_i = i + s, \quad (\text{A.1})$$

where i is an integer (the label for the interval) and s is a random number, uniformly distributed in the interval $[-\frac{1}{2}; \frac{1}{2}]$. The function $g(z)$ shall now be given piecewise for each interval I_i as a straight line. This line is determined by the left boundary point (z_i, α_i) and the right boundary point (z_{i+1}, β_i) , where α_i and β_i are chosen randomly out of a bounded interval $[-m; m]$. The value of m will be determined further down in such a way, that $\Delta(0) = 1$.

In more mathematical terms, a specific realisation of the function $g(z)$ is specified by the random number $s \in [-\frac{1}{2}; \frac{1}{2}]$ and two stets of boundary values $\{\alpha_i\}$ and $\{\beta_i\}$. Using the indicator function $K(z; z_i, z_{i+1})$ for each interval I_i , defined by

$$K(z; z_i, z_{i+1}) = \begin{cases} 1 & z_i \leq z < z_{i+1} \\ 0 & \text{otherwise} \end{cases}, \quad (\text{A.2})$$

the function $g(z)$ is explicitly given by

$$g(z, [s; \{\alpha_i\}; \{\beta_i\}]) = \sum_i K(z; z_i, z_{i+1}) [(\beta_i - \alpha_i)(z - i - s) + \alpha_i]. \quad (\text{A.3})$$

Examples for typical configurations of $g(z)$ are depicted in the Figs. 1.3 and A.2. An il-

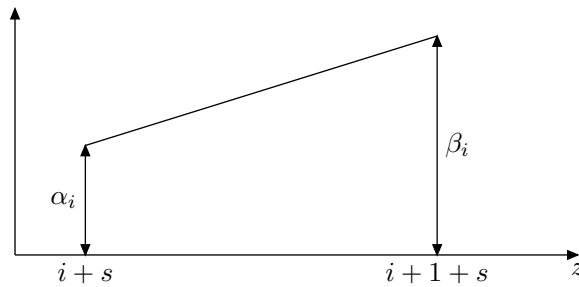


Fig. A.4: A segment of the disorder force with a cusp singularity in the correlator. The values α_i and β_i are chosen out of a bounded interval.

lustration for a single segment is sketched in Fig. A.4. In the following, we are going to show, that disorder forces $g(z)$ given by (A.3) fulfill our requirements $\langle g(z) \rangle = 0$ and $\langle g(z)g(z') \rangle = \Delta(z - z')$, where $\Delta(z - z')$ obeys $\Delta(0) = 1$, decays to zero over a length scale of

order 1 and shows a cusp singularity at the origin. Straightforwardly, we find

$$\langle g(z) \rangle = \int_{-\frac{1}{2}}^{\frac{1}{2}} ds \int_{-m}^m \frac{d\beta d\alpha}{4m^2} [(\beta - \alpha)(z - i - s) + \alpha] = 0. \quad (\text{A.4})$$

To calculate the second moment $\langle g(z)g(z') \rangle$, we have to distinguish two cases. If $|z - z'| \geq 1$, the points z and z' have to belong to two different intervals $z \in I_k$, $z' \in I_{k'}$, because their distance is then larger than the size of an interval and hence

$$\begin{aligned} g(z)g(z') &= \sum_{i,j} K(z; z_i, z_{i+1}) [(\beta_i - \alpha_i)(z - z_i) + \alpha_i] K(z'; z_j, z_{j+1}) [(\beta_j - \alpha_j)(z' - z_j) + \alpha_j] \\ &= [(\beta_k - \alpha_k)(z - k - s) + \alpha_k] [(\beta_{k'} - \alpha_{k'})(z' - k' - s) + \alpha_{k'}]. \end{aligned} \quad (\text{A.5})$$

This gives for the correlator

$$\begin{aligned} \langle g(z)g(z') \rangle &= \int_{-\frac{1}{2}}^{\frac{1}{2}} ds \int_{-m}^m \frac{d\beta_k d\beta_{k'} d\alpha_k d\alpha_{k'}}{16m^4} [(\beta_k - \alpha_k)(z - z_k) + \alpha_k] [(\beta_{k'} - \alpha_{k'})(z' - z_{k'}) + \alpha_{k'}] \\ &= 0. \end{aligned} \quad (\text{A.6})$$

On the other hand, in case $|z - z'| < 1$, those realisations which do not have a jump in between z and z' , i.e. for which z and z' belong to the same interval I_k , give a finite contribution. These correspond to values of s , for which

$$\zeta \equiv |z - z'| + \min(z, z') - i - s \quad (\text{A.7})$$

obeys $|z - z'| < \zeta < 1$. Instead of integrating over s , it is easier to integrate over ζ which gives us

$$\begin{aligned} \langle g(z)g(z') \rangle &= \int_{|z-z'|}^1 d\zeta \int_{-m}^m \frac{d\beta_k d\alpha_k}{4m^2} [(\beta_k - \alpha_k)\zeta + \alpha_k] [(\beta_k - \alpha_k)(\zeta - |z - z'|) + \alpha_k] \\ &= \frac{2m^2}{9} \left[1 - \frac{3}{2}|z - z'| + \frac{1}{2}|z - z'|^3 \right]. \end{aligned} \quad (\text{A.8})$$

As required, the correlator exhibits a cusp singularity at the origin and decays to 0 on a length scale $\ell = 1$. To fulfill $\Delta(0) = 1$, we have to take $m = 3/\sqrt{2} \simeq 2.1$, which is in agreement with our numerical technique, described in App. A.1.

A.3 Derivation of the potential energy balance

The equation of motion (1.11) can be considered to follow from a Hamiltonian

$$\partial_t z = -\frac{\delta H[z]}{\delta z}, \quad (\text{A.9})$$

with

$$H[z] = E[z] - h(t)z(t) \quad (\text{A.10})$$

$$E[z] = \frac{c}{2} (z(t) - \langle z(t) \rangle)^2 + V(z). \quad (\text{A.11})$$

Here, $E[z]$ denotes the total potential energy, $V(z)$ is the disorder potential related to $g(z)$ via $g(z) = -V'(z)$. The change of the potential energy in time thus follows as

$$\begin{aligned} \partial_t E[z] &= c(z - \langle z \rangle)(\partial_t z - v(t)) - g(z)\partial_t z \\ &= c(\langle z \rangle - z)v(t) - [c(\langle z \rangle - z) + g(z)]\partial_t z. \end{aligned} \quad (\text{A.12})$$

Using Eq. (1.11), we can replace the term in the square brackets and obtain

$$\partial_t E[z] = c(\langle z \rangle - z)v(t) + [h(t) - \partial_t z]\partial_t z. \quad (\text{A.13})$$

Taking the disorder average readily yields the result, stated in Eq. (1.74).

A.4 The functional integral approach

Apart from a perturbative expansion of the equation of motion (1.2), it is also possible to compute the disorder averaged correlation functions via a functional integral approach [152, 153]. Starting from (1.2)

$$\partial_t z_{\mathbf{x},t} = \Gamma \nabla_{\mathbf{x}}^2 z_{\mathbf{x},t} + h(t) + u \cdot g(\mathbf{x}, z_{\mathbf{x},t}) \equiv F[z_{\mathbf{x},t}] \quad (\text{A.14})$$

(with $z_{\mathbf{x},t}$ being a short-hand notation for $z(\mathbf{x}, t)$), we note that

$$\langle A[z_{\mathbf{x},t}] \rangle = \left\langle \int \mathcal{D}z_{\mathbf{x},t} A[z_{\mathbf{x},t}] \delta(\partial_t z_{\mathbf{x},t} - F[z_{\mathbf{x},t}]) \right\rangle \quad (\text{A.15})$$

for any functional $A[z_{\mathbf{x},t}]$. Writing

$$\delta(\partial_t z_{\mathbf{x},t} - F[z_{\mathbf{x},t}]) = \int \mathcal{D}\hat{z}_{\mathbf{x},t} \exp \left[i \int_{\mathbf{x},t} \hat{z}_{\mathbf{x},t} (\partial_t z_{\mathbf{x},t} - F[z_{\mathbf{x},t}]) \right] \quad (\text{A.16})$$

and using the usual cumulant expansion for Gaussian disorder, we find

$$\langle A[z_{\mathbf{x},t}] \rangle = \frac{1}{\mathcal{Z}} \int \mathcal{D}\hat{z}_{\mathbf{x},t} \mathcal{D}z_{\mathbf{x},t} A[z_{\mathbf{x},t}] e^{\mathcal{S}[\hat{z}, z]} \quad (\text{A.17})$$

$$\mathcal{Z} = \int \mathcal{D}\hat{z}_{\mathbf{x},t} \mathcal{D}z_{\mathbf{x},t} e^{\mathcal{S}[\hat{z}, z]} \quad (\text{A.18})$$

$$\mathcal{S}[\hat{z}, z] = \mathcal{S}_0[\hat{z}, z] + \mathcal{S}_h[\hat{z}, z] + \mathcal{S}_{\text{dis}}[\hat{z}, z]. \quad (\text{A.19})$$

The three contributions to the action for this functional integral formula read

$$\mathcal{S}_0[\hat{z}, z] = i \int_{\mathbf{x}, t} \hat{z}_{\mathbf{x}, t} [\partial_t - \Gamma \nabla_{\mathbf{x}}^2] z_{\mathbf{x}, t} \quad (\text{A.20})$$

$$\mathcal{S}_h[\hat{z}, z] = i \int_{\mathbf{x}, t} \hat{z}_{\mathbf{x}, t} h(t) \quad (\text{A.21})$$

$$\mathcal{S}_{\text{dis}}[\hat{z}, z] = -\frac{u^2}{2} \int_{\mathbf{x}, t, t'} \hat{z}_{\mathbf{x}, t} \hat{z}_{\mathbf{x}, t'} \Delta[z_{\mathbf{x}, t} - z_{\mathbf{x}, t'}]. \quad (\text{A.22})$$

Certainly, we can also compute correlation functions $A[z_{\mathbf{x}, t}, \hat{z}_{\mathbf{x}', t'}]$. For example, we re-obtain the propagator (1.80) by calculating the response function

$$i \langle z_{\mathbf{x}, t} \hat{z}_{\mathbf{x}', t'} \rangle_{\mathcal{S}_0} = G(\mathbf{x} - \mathbf{x}', t - t'). \quad (\text{A.23})$$

To set up a perturbative expansion in u , we decompose in the same way as in section 1.4.1 $z_{\mathbf{x}, t} = Z_t + \zeta_{\mathbf{x}, t}$ with $Z_t = (h/\omega) \sin \omega t$. Instead of $z_{\mathbf{x}, t}$ we have to consider the functional integral over $\zeta_{\mathbf{x}, t}$. Now,

$$\mathcal{S}[\hat{z}, \zeta] = \mathcal{S}_0[\hat{z}, \zeta] + \mathcal{S}_{\text{dis}}[\hat{z}, \zeta] \quad (\text{A.24})$$

$$\mathcal{S}_{\text{dis}}[\hat{z}, \zeta] = -\frac{u^2}{2} \int_{\mathbf{x}, t, t'} \hat{z}_{\mathbf{x}, t} \hat{z}_{\mathbf{x}, t'} \Delta[Z_t + \zeta_{\mathbf{x}, t} - Z_{t'} - \zeta_{\mathbf{x}, t'}]. \quad (\text{A.25})$$

To compute correlation functions perturbatively in powers of u requires to expand the normalisation \mathcal{Z} as well. A small reflection shows that the lowest order contribution coming from \mathcal{Z} is of order $\mathcal{O}(u^4)$. Thus, if we want to calculate the velocity to order $\mathcal{O}(u^2)$ we can ignore the u -dependence of \mathcal{Z} and write

$$\begin{aligned} v(t) &= h(t) + \partial_t \langle \zeta_{\mathbf{x}, t} \rangle \\ &= h(t) + \partial_t \langle \zeta_{\mathbf{x}, t} \mathcal{S}_{\text{dis}}[\hat{z}, \zeta] \rangle_{\mathcal{S}_0} + \mathcal{O}(u^4). \end{aligned} \quad (\text{A.26})$$

Of course, we may only retain $\mathcal{S}_{\text{dis}}[\hat{z}, \zeta]$ up to terms of order $\mathcal{O}(u^2)$, i.e.

$$\mathcal{S}_{\text{dis}}[\hat{z}, \zeta] = -\frac{u^2}{2} \int_{\mathbf{x}, t, t'} \hat{z}_{\mathbf{x}, t} \hat{z}_{\mathbf{x}, t'} [\Delta[Z_t - Z_{t'}] + \Delta'[Z_t - Z_{t'}](\zeta_{\mathbf{x}, t} - \zeta_{\mathbf{x}, t'})] + \mathcal{O}(u^4). \quad (\text{A.27})$$

Averages with respect to \mathcal{S}_0 are Gaussian, thus Wick's theorem applies and with (A.23) we get

$$\begin{aligned} v(t) &= h(t) - \frac{u^2}{2} \partial_t \int_{\mathbf{x}', t_1, t_2} \Delta'[Z_{t_1} - Z_{t_2}] \left\{ \langle \zeta_{\mathbf{x}, t} \hat{z}_{\mathbf{x}', t_1} \rangle_{\mathcal{S}_0} \langle \zeta_{\mathbf{x}, t_1} \hat{z}_{\mathbf{x}', t_2} \rangle_{\mathcal{S}_0} - \right. \\ &\quad \left. \langle \zeta_{\mathbf{x}, t} \hat{z}_{\mathbf{x}', t_2} \rangle_{\mathcal{S}_0} \langle \zeta_{\mathbf{x}, t_2} \hat{z}_{\mathbf{x}', t_1} \rangle_{\mathcal{S}_0} \right\} + \mathcal{O}(u^4). \end{aligned} \quad (\text{A.28})$$

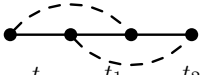
Using (A.23), we recover the result from equation (1.85)

$$\begin{aligned} v(t) &= h(t) - u^2 \partial_t \int_{\mathbf{x}', t_1, t_2} \Delta'[Z_{t_1} - Z_{t_2}] \{-iG(\mathbf{x} - \mathbf{x}', t - t_1)\} \{-iG(\mathbf{x} - \mathbf{x}', t_1 - t_2)\} + \mathcal{O}(u^4) \\ &= h(t) + u^2 \int_{t'} \Delta'[Z_t - Z_{t'}] G(0, t - t') + \mathcal{O}(u^4). \end{aligned} \quad (\text{A.29})$$

It is clear, that we can continue equation (A.26) to higher orders in u by taking into account higher orders in u of $\exp(\mathcal{S}_{\text{dis}})$ as well as higher order corrections from \mathcal{Z} . This way, it is possible to rearrive at the graphical expansion presented in section 1.4.1, albeit along a little more complicated route.

A.5 The regularity of all perturbative orders in case $D > 4$

Let us start with an example graph at which we demonstrate the steps, that are then generalised further down. We consider the following fourth order contribution to the correction of the disorder averaged velocity



$$= \int_0^t dt_1 \int_0^{t_1} dt_2 \int_0^{t_2} dt_3 \prod_{i=1}^3 \int d^D \mathbf{x}_i G(\mathbf{x} - \mathbf{x}_1, t - t_1) G(\mathbf{x}_1 - \mathbf{x}_2, t_1 - t_2) G(\mathbf{x}_2 - \mathbf{x}_3, t_2 - t_3) \times$$

$$\delta(\mathbf{x} - \mathbf{x}_2) \delta(\mathbf{x}_1 - \mathbf{x}_3) (-\Delta''[Z(t) - Z(t_2)]) \Delta'[Z(t_1) - Z(t_3)] \quad (\text{A.30})$$

$$= \int_0^t dt_1 \int_0^{t_1} dt_2 \int_0^{t_2} dt_3 (-\Delta''[Z - Z_2]) \Delta'[Z_1 - Z_3] \times$$

$$\int d^D \mathbf{x}' G(\mathbf{x} - \mathbf{x}', t - t_1) G(\mathbf{x}' - \mathbf{x}, t_1 - t_2) G(\mathbf{x} - \mathbf{x}', t_2 - t_3). \quad (\text{A.31})$$

Using

$$\int d^D \mathbf{x}' G(\mathbf{x} - \mathbf{x}', t - t_1) G(\mathbf{x}' - \mathbf{x}, t_1 - t_2) G(\mathbf{x} - \mathbf{x}', t_2 - t_3) =$$

$$\int \frac{d^D \mathbf{k}_1 d^D \mathbf{k}_2}{(2\pi)^{2D}} e^{-\Gamma [k_1^2(t-t_1) + (\mathbf{k}_1 + \mathbf{k}_2)^2(t_1-t_2) + k_2^2(t_2-t_3)]}, \quad (\text{A.32})$$

we can assign momenta to the branches of the tree



$$\bullet_{k_\alpha} \text{---} \bullet_{k_\beta} \text{---} \bullet_{k_\gamma}, \quad (\text{A.33})$$

and we can read off from (A.32), that

$$\mathbf{k}_\alpha = \mathbf{k}_1, \quad \mathbf{k}_\beta = \mathbf{k}_1 + \mathbf{k}_2, \quad \mathbf{k}_\gamma = \mathbf{k}_2. \quad (\text{A.34})$$

Obviously, \mathbf{k}_1 describes the momentum “flowing” from the root to vertex 2 and \mathbf{k}_2 is the momentum “flow” from vertex 1 to vertex 3. Estimating the disorder correlator derivatives in equation (A.31) by constants (that we can drop since they do not influence the asymptotics $t \rightarrow \infty$), all that has to be done is the integration of the right-hand side of (A.32) over the 3 time variables t_1 , t_2 and t_3 . We start with the outermost leaf, t_3 , and have

$$\int_0^{t_2} dt_3 e^{-\Gamma k_2^2(t_2-t_3)} = \frac{1}{\Gamma k_2^2} \left[1 - e^{-\Gamma k_2^2 t_2} \right] \leq \frac{1}{\Gamma k_2^2}. \quad (\text{A.35})$$

Proceeding in the same manner for the remaining time variables, we finally find

$$\left| \begin{array}{c} \text{---} \text{---} \text{---} \text{---} \\ \text{---} \text{---} \text{---} \end{array} \right| \leq \int \frac{d^D \mathbf{k}_1 d^D \mathbf{k}_2}{(2\pi)^{2D}} \frac{1}{\Gamma^3 k_1^2 (\mathbf{k}_1 + \mathbf{k}_2)^2 k_2^2}. \quad (\text{A.36})$$

This is certainly finite for $D > 4$.

Now, we turn to the general argument for all trees of general (even) order $2q$. Let \mathcal{T}_q denote the set of all rooted trees with q vertices, and $\mathcal{P}(T)$ all possible unordered pairings of vertices of $T \in \mathcal{T}_q$. Let moreover B_T be the set of all branches of the tree T . We want to agree that a branch $b = (b_1, b_2)$ has b_1 always closer to the root. Then, we have in general for every order

$$\langle v_{2q} \rangle = \sum_{T \in \mathcal{T}_{2q}} \sum_{P \in \mathcal{P}(T)} A_{T,P}. \quad (\text{A.37})$$

Here, $A_{T,P}$ is a single diagram, namely a tree T where all pairs $(p_1, p_2) \in P$ are connected by dashed lines for the Gaußian disorder average. The disorder correlators that enter $A_{T,P}$ can be estimated by constants $|\Delta^{(m)}[Z' - Z'']| \leq c_m \ell^{-m}$, that we drop in the following. They are finite and do not influence the behaviour of $A_{T,P}$ as $t \rightarrow \infty$. Denoting the root vertex by r , we estimate

$$|A_{T,P}| \leq \left(\prod_{b \in B_T} \int \frac{d^D \mathbf{k}_b}{(2\pi)^D} \int_0^{t_{b_1}} dt_{b_2} \int d^D \mathbf{x}_{b_2} \right) \left(\prod_{b \in B_T} e^{-\Gamma k_b^2 (t_{b_1} - t_{b_2}) + i \mathbf{k}_b (\mathbf{x}_{b_1} - \mathbf{x}_{b_2})} \right) \prod_{p \in P} \delta(\mathbf{x}_{p_1} - \mathbf{x}_{p_2}) \quad (\text{A.38})$$

$$\begin{aligned} &= \left(\prod_{b \in B_T} \int \frac{d^D \mathbf{k}_b}{(2\pi)^D} \int_0^{t_{b_1}} dt_{b_2} \right) \left(\prod_{\substack{p \in P \\ r \notin p}} \int d^D \mathbf{x}_{p_1} \right) \exp \left[-\Gamma \sum_{b \in B_T} k_b^2 (t_{b_1} - t_{b_2}) \right. \\ &\quad \left. + i \sum_{p \in P} \mathbf{x}_{p_1} \sum_{b \in B_T} \mathbf{k}_b (\delta_{b_1, p_1} + \delta_{b_1, p_2} - \delta_{b_2, p_1} - \delta_{b_2, p_2}) \right] \quad (\text{A.39}) \end{aligned}$$

The integration over the remaining \mathbf{x} -coordinates brings delta-functions for the momenta:

$$\begin{aligned} |A_{T,P}| &\leq \left(\prod_{b \in B_T} \int \frac{d^D \mathbf{k}_b}{(2\pi)^D} \int_0^{t_{b_1}} dt_{b_2} \right) \exp \left[-\Gamma \sum_{b \in B_T} k_b^2 (t_{b_1} - t_{b_2}) \right] \\ &\quad \prod_{\substack{p \in P \\ r \notin p}} (2\pi)^D \delta \left(\sum_{b \in B_T} \mathbf{k}_b (\delta_{b_1, p_1} + \delta_{b_1, p_2} - \delta_{b_2, p_1} - \delta_{b_2, p_2}) \right) \quad (\text{A.40}) \end{aligned}$$

The $q - 1$ delta-functions for the momenta mean, that the net out-flow (away from the root) of momentum from a vertex p_1 equals the net in-flow of momentum for the Gaußian partner vertex p_2 (i.e. $(p_1, p_2) \in P$). There is no delta-function ensuring this for the root and its partner vertex. However, this is not needed. The root itself has only out-flow of momentum

of the root and the outermost vertex. The momenta associated to the other two Gaussian pairs, \mathbf{k}_2 and \mathbf{k}_3 , occur only within exactly one bond. Thus, according to equation (A.41) the integration over \mathbf{k}_1 produces problems in $D \leq 6$, whereas integration over \mathbf{k}_2 and \mathbf{k}_3 is harmless in $D > 2$. One can now check, that the sum $4D_1^6 + 2D_2^6$ as well as the sum of $2D_3^6 + D_4^6$ is regular in $D > 4$. The factors that I have put count the incidence of each diagram in the expansion.

The mechanism of combining diagrams to improve the properties with respect to integration over some \mathbf{k}_i and make it worse for some other \mathbf{k}_j can already be demonstrated at graphs of order 4. If, from D_1^6 and D_2^6 the root and the upper vertex closest to the root are removed and the outermost leaf connected to the new root, we have the two diagrams of fourth order (cf. (1.94))

$$\begin{aligned}
 2D_1^4 &= 2 \cdot \text{Diagram 1} \\
 &= \int_{\mathbf{k}_1, \mathbf{k}_2} \int_0^t dt_1 e^{-\Gamma k_1^2(t-t_1)} \int_0^{t_1} dt_2 e^{-\Gamma k_2^2(t_1-t_2)} \Delta''[Z_1 - Z_2] \int_0^{t_1} dt_3 e^{-\Gamma k_1^2(t_1-t_3)} \Delta'[Z - Z_3]
 \end{aligned} \tag{A.44}$$

$$\begin{aligned}
 D_2^4 &= \text{Diagram 2} \\
 &= - \int_{\mathbf{k}_1, \mathbf{k}_2} \int_0^t dt_1 e^{-\Gamma k_1^2(t-t_1)} \int_0^{t_1} dt_2 e^{-\Gamma k_2^2(t_1-t_2)} \Delta''[Z_1 - Z_2] \int_0^{t_2} dt_3 e^{-\Gamma k_1^2(t_2-t_3)} \Delta'[Z - Z_3]
 \end{aligned} \tag{A.45}$$

$$= -2 \cdot \text{Diagram 3} + S \tag{A.46}$$

$$\begin{aligned}
 S &= \int_{\mathbf{k}_1, \mathbf{k}_2} \int_0^t dt_1 e^{-\Gamma k_1^2(t-t_1)} \int_0^{t_1} dt_2 e^{-\Gamma k_2^2(t_1-t_2)} \Delta'[Z - Z_2] \int_0^{t_2} d\tau e^{-\Gamma k_1^2(t_2-\tau)} \Delta''[Z_1 - Z(\tau)] \\
 &\quad - \int_{\mathbf{k}_1, \mathbf{k}_2} \int_0^t dt_1 e^{-\Gamma k_1^2(t-t_1)} \int_0^{t_1} dt_2 e^{-\Gamma k_2^2(t_1-t_2)} \Gamma k_1^2 \int_0^{t_2} dt_3 e^{-\Gamma k_1^2(t_2-t_3)} \Delta'[Z - Z_3] \times \\
 &\quad \int_0^{t_2} d\tau e^{-\Gamma k_1^2(t_2-\tau)} \Delta''[Z_1 - Z(\tau)]
 \end{aligned} \tag{A.47}$$

The modification of D_2^4 relies on integration by parts for the integral over t_2 . Upon inspection of the integrals, one sees, that the integral over \mathbf{k}_1 in the diagrams D_1^4 and D_2^4 is well-behaved for $t \rightarrow \infty$ in $D > 4$, while the integral over \mathbf{k}_2 requires only $D > 2$. The sum $S = 2D_1^4 + D_2^4$ on the other hand behaves vice versa. Of course, in expressions of order 4 not much is gained with that, but in higher orders this procedure can be used to understand, why the sum of all diagrams of a certain order $2q$ involves $q - 1$ integrals over momenta that are finite as $t \rightarrow \infty$

in $D > 4$ and one that works in $D > 2$. Note, that in equations (A.44-A.47) it is important to retain the disorder correlators, because cancellations have to be exact.

It is now easy to extend the calculations provided in (A.44-A.47) to see that $4D_1^6 + 2D_2^6$ (cf. equations (A.42) and (A.42)) is a regular expression in $D > 4$. The sum $4D_1^6 + 2D_2^6$ has the critical dimension for \mathbf{k}_1 , the momentum associated to the Gaussian pair made of the root and the outermost leaf, reduced so that it is regular in $D > 4$ at the price that now \mathbf{k}_3 also needs $D > 4$ instead of $D > 2$. For reasons of space, as the explicit expressions for the diagrams are rather huge, we do not provide the full calculation here.

The more general idea about the cancellation among trees goes as follows. Because too many details have to be ascertained which tends to result in a huge load of technicalities, we will merely sketch the procedure by mentioning all intermediate steps without proving the implicit claims. First of all, we note, that any tree T involves at least one distinguished momentum, we denote it by \mathbf{k}_T , the integration over which is regular in $D > 2$. In (A.44-A.47) we have seen that it is possible for any tree T_q of any given order q , that is regular in $D > 4$, to find partner trees T_q^1, \dots, T_q^m of the same order, all regular in $D > 4$, such that their sum is an expression in which the momentum associated to the root has the property of \mathbf{k}_T . Thus, we will without loss of generality assume that for any tree that is regular in $D > 4$, \mathbf{k}_T is the momentum flowing out of the root. All our arguments in the following will also hold for trees for which this is not the case, if we repeat it for all partner trees and take the sum.

Let, for some tree T the integration over some momentum \mathbf{k}_p associated to a Gaussian pair p be problematic in $D > 2N_0 + 2$. This can happen if along the line from p_1 to p_2 there are N_0 vertices which form the root of independent subtrees $\{S_i\}$ or if the momentum flow along the route from p_1 to p_2 is interrupted by N_0 independent (w.r.t. the disorder average) inner subtrees $\{S_i\}$ and continues at the Gaussian partner of the root of those subtrees. The first case corresponds to the diagram D_1^6 given by (A.42) and the second scenario is exemplified by D_4^6 which is depicted in (A.43) (both for $N_0 = 2$). Of course, also a mixture of both events, N_0 in total, has the same effect, as is illustrated by D_2^6 and D_3^6 . If, as a kind of induction hypothesis, we assume that all independent subtrees S_1, \dots, S_{N_0} are regular in $D > 4$, we can describe the scheme how to find all trees that have to be added to T to yield an expression that is regular in $D > 4$. Let us consider first $N_0 = 2$. Let s_1 be the root of S_1 and s'_1 be its Gaussian partner vertex in S_1 . As mentioned above, the integration over the momentum \mathbf{k}_s , associated to (s_1, s'_1) , is regular in $D > 2$. Without loss of generality, we assume that in T , s_1 is a vertex on the non-interrupted path from p_1 to p_2 . Then there is another tree T' , for which the flow of \mathbf{k}_p along the connection between p_1 and p_2 is interrupted by the connection between s_1 and s'_1 . The sum of T and T' is then regular in $D > 4$. The integral over \mathbf{k}_p in the sum $T + T'$ has decreased its critical dimension by 2 at the cost, that now the integration over \mathbf{k}_s needs $D > 4$ to be bounded for large t .

So far, this is the idea, how the cancellation among trees works in $D > 4$ to give a regular expression. For a thorough proof, we would have to give evidence for each single intermediate step. After all, the practical benefit of such a detailed proof is little and no further insight can be expected. Thus, although a rigorous proof has not been established, a consistent picture of the behaviour of the perturbation expansion has emerged. In $D > 4$ all perturbative orders are regular, and in $D \leq 4$ our somewhat crude estimate of the disorder correlator derivatives by constants gives bad results.

A.6 Analysis of the bush graphs

To analyse the term

$$T_1 = \int_0^t dt_1 dt_2 \Delta[Z(t_1) - Z(t_2)] \int \frac{d^D \mathbf{k}}{(2\pi)^D} e^{-\Gamma k^2(2t-t_1-t_2)} \quad (\text{A.48})$$

from equation (1.97), we start with the decomposition of the function $\Delta[Z(t_1) - Z(t_2)]$ in a double Fourier series in t_1 and t_2 , respectively. Recall, that $Z(t) = (h/\omega) \sin \omega t$.

$$\Delta[Z(t_1) - Z(t_2)] = \int_q \hat{\Delta}(q) \sum_{m,n} J_m(qh/\omega) J_n(-qh/\omega) e^{i\omega(mt_1+nt_2)}. \quad (\text{A.49})$$

Here, $\hat{\Delta}$ is the Fourier transform of Δ and J_m is the Bessel function of the first kind. For symmetry reasons, only terms with an even value of $m+n$ contribute. This gives

$$T_1 = \int_q \hat{\Delta}(q) \left[L_{0,0}(q, t) + \sum_{m \neq 0} L_{2m,0}(q, t) + \sum_{m,n \neq 0} L_{m,n}(q, t) \right], \quad (\text{A.50})$$

where we have introduced

$$\begin{aligned} L_{m,n}(q, t) &= J_m\left(\frac{qh}{\omega}\right) J_n\left(-\frac{qh}{\omega}\right) \int_0^t dt_1 dt_2 e^{i\omega(mt_1+nt_2)} \int \frac{d^D \mathbf{k}}{(2\pi)^D} e^{-\Gamma k^2(2t-t_2-t_2)} \\ &= J_m\left(\frac{qh}{\omega}\right) J_n\left(-\frac{qh}{\omega}\right) \int \frac{d^D \mathbf{k}}{(2\pi)^D} \frac{[e^{im\omega t} - e^{-\Gamma k^2 t}]}{\Gamma k^2 + im\omega} \frac{[e^{in\omega t} - e^{-\Gamma k^2 t}]}{\Gamma k^2 + in\omega}. \end{aligned} \quad (\text{A.51})$$

The behaviour for $t \rightarrow \infty$ is dominated by the leading term $L_{0,0}(q, t)$, which is given by

$$L_{0,0}(q, t) = J_0^2\left(\frac{qh}{\omega}\right) \frac{S_D}{\Gamma^2(2\pi)^D} \int_0^\Lambda dk k^{D-5} [1 - e^{-\Gamma k^2 t}]^2 = J_0^2\left(\frac{qh}{\omega}\right) \frac{t^{\frac{4-D}{2}}}{\Gamma^{\frac{D}{2}}} A_D(t/\vartheta). \quad (\text{A.52})$$

The function $A_D(x)$ has already been introduced in equation (1.102). For the sub-leading terms we obtain

$$L_{2m,0} = J_0\left(\frac{qh}{\omega}\right) J_{2m}\left(\frac{qh}{\omega}\right) \int \frac{d^D \mathbf{k}}{(2\pi)^D} \frac{[1 - e^{-\Gamma k^2 t}]}{\Gamma k^2} \frac{[e^{i2m\omega t} - e^{-\Gamma k^2 t}]}{\Gamma k^2 + i2m\omega}. \quad (\text{A.53})$$

Thus,

$$\sum_{m \neq 0} L_{2m,0}(q, t) = \sum_{m=1}^{\infty} J_0\left(\frac{qh}{\omega}\right) J_{2m}\left(\frac{qh}{\omega}\right) \frac{t^{\frac{2-D}{2}}}{\omega \Gamma^{\frac{D}{2}}} \alpha_D^m(t/\vartheta, \omega t). \quad (\text{A.54})$$

Here, the function $\alpha_D^m(x, y)$ is given by

$$\alpha_D^m(x, y) = \frac{2S_D}{(2\pi)^D} \int_0^{\sqrt{x}} dp p^{D-3} \left[1 - e^{-p^2} \right] \frac{\frac{p}{y} \cos 2my + 2m \sin 2my - \frac{p}{y} e^{-p^2}}{(p^2/y^2) + 4m^2}, \quad (\text{A.55})$$

which, for $x \rightarrow \infty$ behaves in the same way, as $a_D(x)$ (cf. (1.89)), independent of $m \neq 0$.

The last term in (A.50) does not require further consideration. For $m, n \neq 0$, the function $L_{m,n}$ remains finite as $t \rightarrow \infty$. There is no infrared problem with the k -integral in equation (A.51) any more. Recalling the two time scales τ and ϑ , that we have encountered before (cf. (1.100) and (1.101)) we thus have

$$T_1 = \frac{\ell^2}{u^2} \left[\left(\frac{t}{\tau} \right)^{\frac{4-D}{2}} \kappa_D \left(\frac{t}{\vartheta} \right) + \left(\frac{t}{\tau} \right)^{\frac{4-D}{4}} \frac{u\Lambda^{\frac{D}{2}}}{\omega\ell} k_D \left(\frac{t}{\vartheta}, \omega t \right) + \frac{u^2\Lambda^D}{\omega^2\ell^2} P_D \left(\frac{t}{\vartheta}, \omega t \right) \right]. \quad (\text{A.56})$$

Hereby, we have introduced

$$\kappa_D \left(\frac{t}{\vartheta} \right) = A_D(t/\vartheta) \int_q \hat{\Delta}(q) J_0^2 \left(\frac{qh}{\omega} \right) \quad (\text{A.57})$$

$$k_D \left(\frac{t}{\vartheta}, \omega t \right) = \left(\frac{\vartheta}{t} \right)^{\frac{D}{4}} \sum_{m=1}^{\infty} \alpha_D^m \left(\frac{t}{\vartheta}, \omega t \right) \int_q \hat{\Delta}(q) J_0 \left(\frac{qh}{\omega} \right) J_{2m} \left(\frac{qh}{\omega} \right) \quad (\text{A.58})$$

$$P_D \left(\frac{t}{\vartheta}, \omega t \right) = \frac{\omega^2}{\Lambda^D} \sum_{m,n \neq 0} \int_q \hat{\Delta}(q) L_{m,n}(q, t). \quad (\text{A.59})$$

The second factor in (1.97)

$$T_2 = \int_0^t dt' \Delta^{(2p-1)}[Z(t) - Z(t')] \int \frac{d^D \mathbf{k}}{(2\pi)^D} e^{-\Gamma k^2(t-t')} \quad (\text{A.60})$$

can be treated in the same way, like the second order graph in section 1.4.1, by splitting off the Fourier-0-mode

$$\Delta^{(2p-1)}[Z(t) - Z(t')] = \frac{F_0^{[2p-1]}(\omega t) + p(t, t')}{\ell^{2p-1}}. \quad (\text{A.61})$$

Following the calculations in section 1.4.1, with $F_0(\omega t)$ replaced by $F_0^{[2p-1]}(\omega t)$, we arrive at

$$T_2 = \frac{\omega\ell}{u^2\ell^{2(p-1)}} \left[\frac{u\Lambda^{\frac{D}{2}}}{\omega\ell} \left(\frac{t}{\tau} \right)^{\frac{4-D}{4}} f_D \left(\frac{t}{\vartheta}, \omega t \right) + \frac{u^2\Lambda^D}{\omega^2\ell^2} p_D \left(\frac{t}{\vartheta}, \omega t \right) \right], \quad (\text{A.62})$$

where

$$f_D \left(\frac{t}{\vartheta}, \omega t \right) = \left(\frac{\vartheta}{t} \right)^{\frac{D}{4}} a_D(t/\vartheta) F_0^{[2p-1]}(\omega t) \quad (\text{A.63})$$

$$p_D \left(\frac{t}{\vartheta}, \omega t \right) = \frac{S_D}{(2\pi)^D} \int_0^{\sqrt{t/\vartheta}} dp p^{D-1} e^{-p^2} \int_0^t dt' \frac{p(t, t-t')}{[\Gamma t']^D}. \quad (\text{A.64})$$

The integral over p in p_D is certainly convergent for any D in the limit $t \rightarrow \infty$, and the integral over t' converges for any $D > 0$, since $p(t, t - t')$ is a bounded oscillation around zero (without zero Fourier mode) in t' .

A.7 The width of ac-driven interfaces

Apart from the velocity of the mean position of an interface in a random potential, there is another interesting quantity that deserves investigation: the mean square deviation of a given realisation from the mean. More precisely, we refer to the quantity

$$w = \langle (\langle z \rangle - z)^2 \rangle. \quad (\text{A.65})$$

In the first order of the perturbation expansion, w reads

$$w = \langle (\langle Z + u\zeta_1 \rangle - Z - u\zeta_1)^2 \rangle = u^2 \langle \zeta_1^2 \rangle + \mathcal{O}(u^4). \quad (\text{A.66})$$

In the case of infinitely extended interfaces, this quantity measures thus the typical width of the interface.

So, for infinitely extended domain walls, the typical width to first order in perturbation theory is given by (cf. (1.83))

$$\langle \zeta_1^2 \rangle(\mathbf{x}, t) = \int_0^t dt_1 dt_2 \Delta[Z(t_1) - Z(t_2)] \int \frac{d^D \mathbf{k}}{(2\pi)^D} e^{-\Gamma k^2(2t-t_1-t_2)}. \quad (\text{A.67})$$

Comparing this to T_1 , given by equation (1.98), we find $\langle \zeta_1^2 \rangle = T_1$. Using equation (1.99), we thus have for the asymptotics $t \rightarrow \infty$

$$u^2 \langle \zeta_1^2 \rangle \sim \ell^2 \left[\frac{t}{\tau} \right]^{\frac{4-D}{2}} A_D(t/\vartheta) \quad (\text{A.68})$$

The function A_D , given by (1.102), remains bounded for $D < 4$ and grows logarithmically in its argument in case $D = 4$. Thus, the growth of the perturbative estimate of w in time is given by the prefactor $t^{\frac{4-D}{2}}$ and $\ln t$ for $D < 4$ and $D = 4$, respectively.

So, in contrast to the first order perturbative result for the interface's velocity, which remains finite as $t \rightarrow \infty$ for $D > 2$, the width of the interface indicates the correct critical dimension $D = 4$ already to first order.

Another paradox that can be illustrated in terms of the interface width concerns the fact, that the unbounded growth results from the small- \mathbf{k} contributions to the integrals. Hence, at first sight the problem seems to be fixed, if the integral is cut off at small wavevectors $k \leq 1/L$, where L is the linear dimension of the domain wall. On the other hand, it is expected, that essentially the spatial average behaves like a single particle (a $D = 0$ -dimensional interface) and thus, we should have $\langle \zeta_1^2 \rangle(t) \sim t^2$. Indeed, writing

$$\zeta_1(\mathbf{x}, t) = \int d^D \mathbf{x}' dt' G(\mathbf{x} - \mathbf{x}', t - t') \cdot g\left(\mathbf{x}', \frac{h}{\omega} \sin \omega t'\right), \quad (\text{A.69})$$

(cf. (1.83)) and estimating the residual disorder force for one period

$$\left\langle \left[\frac{1}{T} \int_t^{t+T} dt' \frac{1}{L^D} \int d^D \mathbf{x}' g \left(\mathbf{x}', \frac{h}{\omega} \sin \omega t' \right) \right]^2 \right\rangle = \frac{\delta^2}{L^D}, \quad (\text{A.70})$$

one obtains

$$\zeta_1(\mathbf{x}, t) \sim \int d^D \mathbf{x}' dt' \frac{\delta}{L^D} \cdot G(\mathbf{x} - \mathbf{x}', t - t') = \frac{\delta}{L^{D/2}} t. \quad (\text{A.71})$$

The point is, that naïvely extrapolating (A.67) to finite interfaces by just introducing an infrared cutoff neglects the boundary conditions, which have an important impact on the behaviour of the solution. Taking care of appropriate boundary conditions for finite interfaces is not so easy, but doable. We are going to present the calculation tersely, following [154]. Demanding, that $\nabla \zeta_1(\mathbf{b}, t) = 0$ for any point \mathbf{b} of the boundary, i.e. taking the Neumann conditions such that the interface is free at the boundary, we can give the solution as an expansion in the eigenfunctions $v_{\mathbf{k}}$ of the Laplacian. The eigenfunctions $v_{\mathbf{k}}$ are taken to satisfy the same Neumann conditions and shall be suitably normalised. Their corresponding eigenvalue is denoted by $\lambda_{\mathbf{k}}$. The solution then takes the form

$$\zeta_1(\mathbf{x}, t) = \sum_{\mathbf{k}=0}^{\infty} v_{\mathbf{k}}(\mathbf{x}) \int_0^t dt' e^{-\lambda_{\mathbf{k}}(t-t')} b_{\mathbf{k}}(h, \omega, t') \quad (\text{A.72})$$

$$b_{\mathbf{k}}(h, \omega, t) = \int d^D \mathbf{y} g \left(\mathbf{y}, \frac{h}{\omega} \sin \omega t \right) v_{\mathbf{k}}(\mathbf{y}). \quad (\text{A.73})$$

To calculate the time integral, we expand the disorder in a Fourier series

$$g(\mathbf{y}, \frac{h}{\omega} \sin \omega t) = \sum_n g_n(\mathbf{y}) \cdot e^{in\omega t} \quad (\text{A.74})$$

$$\int_0^t dt' e^{-\lambda_{\mathbf{k}}(t-t') + in\omega t'} = \frac{e^{-in\omega t} - e^{-\lambda_{\mathbf{k}} t}}{\lambda_{\mathbf{k}} - in\omega t}. \quad (\text{A.75})$$

Obviously, the contribution from $\mathbf{k} = 0$ is special, since $\lambda_0 = 0$. The associated eigenfunction is just constant $v_0(\mathbf{x}) = L^{-D/2}$. Splitting off the Fourier-0-mode, we finally get

$$\begin{aligned} \zeta_1(\mathbf{x}, t) &= \frac{t}{L^{D/2}} \int d^D \mathbf{y} g_0(\mathbf{y}) + \frac{1}{L^{D/2}} \sum_{n \neq 0} \frac{1 - e^{-in\omega t}}{in\omega t} \int d^D \mathbf{y} g_n(\mathbf{y}) \\ &\quad + \sum_{\mathbf{k}=1}^{\infty} v_{\mathbf{k}}(\mathbf{x}) \int_0^t dt' e^{-\lambda_{\mathbf{k}}(t-t')} b_{\mathbf{k}}(h, \omega, t'), \end{aligned} \quad (\text{A.76})$$

in agreement with what we expected from the simple argument before (cf. (A.71)).

Finally, as we have promised in a footnote in section 1.4.1, we briefly consider the self-consistent perturbative expansion $z(\mathbf{x}, t) = \langle z(t) \rangle + \xi(\mathbf{x}, t)$. In this decomposition, we have exactly $w = \langle \xi^2 \rangle$. However, there is no longer a definite expansion parameter, but what has to be done is mere power-counting in ξ . Plugging the decomposition into the equation of motion, we obtain the following set of equations

$$\partial_t \langle z(t) \rangle = h \cos \omega t + u \langle g(z) \rangle \quad (\text{A.77})$$

$$(\partial_t - \Gamma \nabla^2) \xi = u [g(z) - \langle g(z) \rangle]. \quad (\text{A.78})$$

Expanding the disorder in a Taylor series and using $\langle g(\langle z \rangle) \rangle = 0$ yields

$$(\partial_t - \Gamma \nabla^2) \xi = u g(\langle z \rangle) + \mathcal{O}(\xi). \quad (\text{A.79})$$

Thus, we finally arrive at the lowest order result

$$\langle \xi^2 \rangle(t) = \int_0^t dt_1 dt_2 \Delta[\langle z(t_1) \rangle - \langle z(t_2) \rangle] \int \frac{d^D \mathbf{k}}{(2\pi)^D} e^{-\Gamma k^2(2t-t_1-t_2)} + \mathcal{O}(\xi). \quad (\text{A.80})$$

Though the trajectory of $\langle z(t) \rangle$ is unknown, our simple argument from section 1.4.2 predicts that, in a perturbative estimate, the width of the interface grows unboundedly in time for $D \leq 4$.

A.8 Regularity of the mean-field perturbation expansion

In section 1.5.2 we have analysed, how the unbounded contributions, contained in the two diagrams that involve a curly line, mutually cancel in the second non-vanishing perturbative order. In this appendix, we are going to explain how this cancellation process generalises to all orders in perturbation theory. As before, for simplicity, we work with the diagrams for the disorder-averaged velocity, that arise by just removing the curly lines from the root of the diagrams for $\langle \zeta \rangle$ (cf. equation (1.121)). In a velocity diagram contributing to the n -th order (recall, that only for even n the corrections are non-zero), any curly line connects two trees of order p and q (both even) with the restriction $p + q = n$. Both trees appear in the expansion of lower orders, namely p and q , respectively. In the following, we sketch an inductive proof for the claim that the unbounded terms originating from trees with curly internal lines cancel among each other.

Let us assume, that for order n we have achieved to ensure regularity. For every unbounded tree T , there is thus a set T^1, \dots, T^a of, let us call them *cancelling trees*, such that $T + T^1 + \dots + T^a$ is a regular, bounded expression in time. As a starting point for the induction, take $n = 4$, where the validity of the claim has been verified in section 1.5.2. It is now the task to validate the regularity for order $n + 2$. First of all, we consider the process of attaching the root of a regular tree S (with no internal curly line) of order s by a curly line to a vertex v of another regular tree R of order $r = n + 2 - s$ to obtain a new irregular tree A of order $n + 2$. The vertex v must be connected to another vertex $w \in R$ by a dashed line, to carry out the Gaussian disorder average. Without loss of generality, we assume that v is connected to w by

a path that first makes a step towards the root. The rules for the diagrammatic expansion ensure, that there is a maximal regular subtree $T \subset R$, which contains v and w .

Using partial integration, it is possible to move the vertex to which S is connected (via the curly line) to a neighbouring vertex in T . Thus, it is possible to move the connection vertex along the unique way (in T) from v to w . We are going to show, that once w is reached, we have obtained the cancelling tree which is unique. Diagrammatically, the process of moving the connection vertex from v to w reads:

Here, the blank circle represents S , the lightgrey circle stands for the subtree R_1 of R , to which v connects and the darkgrey shaded circle denotes trees which run out of v (summarised in the following as R_2). Certainly, in general there may be dashed lines between the dark and the lightgrey circle, which we have omitted as they are not relevant for the forthcoming discussion. The dotted line just serves as a joker - it is not important to specify how many lines go out of v . The last term D collects the left-over terms from the partial integration. Note, that, if it takes several steps to go from v to w , the intermediate expressions (in the partial integration) are not in accordance with our diagrammatic rules, because the order of derivative of the disorder correlators does not appear correctly (it remains the same but the graph has changed). Keeping this small peculiarity in mind, it is nevertheless instructive to think in diagrammatic terms.

To illustrate the procedure, we take a look at the first step:

The order of the derivative (i.e. the number of outgoing lines) of w and v are denoted by μ and ν , respectively. The time, at which the whole diagram is to be evaluated, is t , the time corresponding to the vertex to which v is connected is given by T_1 , t_1 is thus the time associated to v and so on. The time of w is τ . Thus, we see, that if w is not the vertex to which v is directly connected (then $T_1 \neq \tau$ in general), the first expression after partial integration cannot be a valid diagram: v has lost one order of derivative ($\nu - 1$ lines go out instead of ν), but the derivative of the correlator Δ has not changed. A valid diagram however reappears, when the connection of S has reached w . Then, v has lost an outgoing line, but w received one more and we indeed have achieved a cancelling tree: the factor $(-1)^\nu$ remains,

the true diagram, however, has $(-1)^{\nu-1}$. The signs are different, thus the two trees cancel. The left-over term from the partial integration is again regular. This can be seen because all time integrals carry an exponential damping term. It is clear, that this is generally true for every partial integration step.

To go one step further, we assume now S to be irregular. Essentially, the same procedure works, but there are more cancelling trees: one has take all cancelling trees $\{S^i\}$ for S into account (which exist by induction hypothesis), thus S is replaced by $\sum S^i$ and thence the left-over terms are again regular.

A possible irregularity of R can be accounted for in the same way. It is, however, important to explain why this is possible, i.e. what are v and w in the cancelling trees for R . In the case of irregular S the problem was easy, since all trees have a unique root. As we have seen already, the procedure of creating cancelling trees does not change the structure of regular subtrees. Thence, all cancelling trees for R contain T . This makes clear, which v and w have to be chosen in the cancelling trees: they are well-defined in T and T is a well-defined subtree of the cancelling trees. Thus, repeating the whole procedure described above for all cancelling trees of R yields the complete set of cancelling trees for A in the most general setting.

Appendix B

Appendices to chapter 2

B.1 Interface Hamiltonian for the ϕ^4 model

For illustrational purposes, we derive the interface Hamiltonian for the simple ϕ^4 -model. The Hamiltonian reads

$$H = \int d^3\mathbf{r} [D(\nabla\phi)^2 + A\phi^2 + B\phi^4]. \quad (\text{B.1})$$

Here, as in the main text, A is taken temperature dependent as usual for the phenomenological Landau theory, $A = A_0(T - T_c)$ with $A_0 > 0$. The Hamiltonian (B.1) immediately leads to the associated Euler-Lagrange equation

$$D\Delta\phi = A\phi + 2B\phi^3, \quad (\text{B.2})$$

which for $T < T_c$ admits the two stable homogeneous solutions

$$\phi_0 \equiv \pm\sqrt{\frac{-A}{2B}}. \quad (\text{B.3})$$

Moreover, there is a domain wall solution, interpolating between the two degenerate ground states, given by

$$\phi_{\text{dw}}(\mathbf{r}) = \phi_0 \tanh\left(\frac{x}{b}\right) \quad (\text{B.4})$$

with $b = \sqrt{-2D/A}$. Here, we have implicitly selected the x -direction to be perpendicular to the wall. The aim is now to establish an interface Hamiltonian to measure the energy cost of a structured interface configuration with respect to a flat one. Let $\xi(\mathbf{r}_\perp)$ be the x -coordinate of the center of the domain wall as a function of $\mathbf{r}_\perp = (y, z)$. Then

$$\begin{aligned} H[\phi_{\text{dw}}(x - \xi)] - H[\phi_{\text{dw}}(x)] &= \int d^3\mathbf{r} D \phi_{\text{dw}}'^2(x - \xi) (\nabla_\perp \xi)^2 \\ &= \frac{4D}{3b} \int d^2\mathbf{r}_\perp (\nabla_\perp \xi)^2. \end{aligned} \quad (\text{B.5})$$

The result in (B.5) gives the first nontrivial order in $\nabla_{\perp}\xi$ of an expansion of the exact result

$$H[\phi_{\text{dw}}(x - \xi)] \propto \int d^2\mathbf{r}_{\perp} \sqrt{1 + [\nabla_{\perp}\xi(\mathbf{r})]^2}, \quad (\text{B.6})$$

which can be derived by taking into account thermal fluctuations around the mean-field solution ϕ_{dw} [155].

B.2 The harmonic approximation

In this appendix, the derivation of the harmonic approximation for the wall configuration shall be presented. For the polarisation, we assume a configuration given by

$$P(\mathbf{r}) = f(x - \xi(\mathbf{r}_{\perp})), \quad (\text{B.7})$$

where \mathbf{r}_{\perp} is a 2d vector $\mathbf{r}_{\perp} = (y, z)$. Then, by a shift of the integration variable x , we easily find

$$P_{\mathbf{k}} = \int d^3\mathbf{r} f(x - \xi(\mathbf{r}_{\perp})) e^{ik_x x + i\mathbf{k}_{\perp}\mathbf{r}_{\perp}} = f_{k_x} \int d^2\mathbf{r}_{\perp} e^{ik_x \xi(\mathbf{r}_{\perp}) + i\mathbf{k}_{\perp}\mathbf{r}_{\perp}}. \quad (\text{B.8})$$

This immediately gives

$$P_{\mathbf{k}} P_{-\mathbf{k}} = f_{k_x} f_{-k_x} \int d^2\mathbf{r}_{\perp 1} d^2\mathbf{r}_{\perp 2} e^{ik_x [\xi(\mathbf{r}_{\perp 1}) - \xi(\mathbf{r}_{\perp 2})] + i\mathbf{k}_{\perp}(\mathbf{r}_{\perp 1} - \mathbf{r}_{\perp 2})}, \quad (\text{B.9})$$

which we can expand in the difference $\xi(\mathbf{r}_{\perp 1}) - \xi(\mathbf{r}_{\perp 2})$. Up to second order, we obtain

$$P_{\mathbf{k}} P_{-\mathbf{k}} \simeq |f_{k_x}|^2 \int d^2\mathbf{r}_{\perp 1} d^2\mathbf{r}_{\perp 2} \left\{ 1 + ik_x [\xi(\mathbf{r}_{\perp 1}) - \xi(\mathbf{r}_{\perp 2})] - \frac{k_x^2}{2} [\xi(\mathbf{r}_{\perp 1})^2 + \xi(\mathbf{r}_{\perp 2})^2 - 2\xi(\mathbf{r}_{\perp 1})\xi(\mathbf{r}_{\perp 2})] \right\} e^{i\mathbf{k}_{\perp}(\mathbf{r}_{\perp 1} - \mathbf{r}_{\perp 2})}. \quad (\text{B.10})$$

The term independent of ξ is proportional to the extension of the whole system in y - and z -direction, but it does not influence the interfacial energy measured relative to a flat wall. The first order term vanishes for symmetry reasons. Thus, we end up with

$$P_{\mathbf{k}} P_{-\mathbf{k}} \simeq f_{k_x} f_{-k_x} k_x^2 \left[\xi_{\mathbf{k}_{\perp}} \xi_{-\mathbf{k}_{\perp}} - \delta(\mathbf{k}_{\perp}) \int_{\mathbf{k}'} \xi_{\mathbf{k}} \xi_{-\mathbf{k}} \right]. \quad (\text{B.11})$$

The special choice $f(x) = \text{sign}(x)$ with $f_{k_x} = 2i/k_x$ finally yields

$$P_{\mathbf{k}} P_{-\mathbf{k}} \simeq 4 \left[\xi_{\mathbf{k}_{\perp}} \xi_{-\mathbf{k}_{\perp}} - \delta(\mathbf{k}_{\perp}) \int_{\mathbf{k}'} \xi_{\mathbf{k}} \xi_{-\mathbf{k}} \right]. \quad (\text{B.12})$$

This approximation has already been used earlier in [72] to determine the influence of dipolar interactions on the domain wall stiffness.

B.3 Derivation of H_{ee}

As we have agreed to restrict ourselves to the case when there is no modulation in z -direction, equation (B.9) readily gives us

$$P_{\mathbf{k}}P_{-\mathbf{k}} = \frac{4P_0^2}{k_x^2} \int dy_1 dy_2 e^{ik_x \Delta_\xi + ik_y \Delta_y}, \quad (\text{B.13})$$

with $\Delta_\xi = \xi(y_1) - \xi(y_2)$ and $\Delta_y = y_1 - y_2$. We now have to calculate the integral

$$I \equiv \int_{\mathbf{k}}' \frac{P_{\mathbf{k}}P_{-\mathbf{k}}}{P_0^2} \frac{k_x^2 k_y^2}{k^4} = 4 \int_{\mathbf{k}}' \int dy_1 dy_2 e^{ik_x \Delta_\xi + ik_y \Delta_y} \frac{k_y^2}{k^4}. \quad (\text{B.14})$$

To circumvent the problems with the non-analyticity of the integrand at $\mathbf{k} = 0$ (which is excluded from the integration), we employ a trick and write

$$I = 4I_1 + 4I_2 \quad (\text{B.15})$$

$$I_1 = \int_{\mathbf{k}}' \int dy_1 dy_2 \left[e^{ik_x \Delta_\xi} - 1 \right] e^{ik_y \Delta_y} \frac{k_y^2}{k^4} \quad (\text{B.16})$$

$$I_2 = \int_{\mathbf{k}}' \int dy_1 dy_2 e^{ik_y \Delta_y} \frac{k_y^2}{k^4}. \quad (\text{B.17})$$

Since the integration over y_1 and y_2 in I_2 leaves a $\delta(k_y)$, we have $I_2 = 0$. For $k_x \neq 0$ this is because of the k_y^2 in the numerator and $k_x = 0$ is excluded from the integral. Hence $I = 4I_1$. This way we have removed potential singularities of the integral before exchanging the order of integration over y_1 , y_2 and \mathbf{k} . Now,

$$\begin{aligned} I &= 4 \int_{\mathbf{k}}' \int dy_1 dy_2 e^{ik_x \Delta_\xi + ik_y \Delta_y} \frac{k_y^2}{k^4} = \int dy_1 dy_2 \int \frac{dk_x}{2\pi} \left[\frac{1}{|k_x|} - |\Delta_y| \right] e^{-|k_x \Delta_y|} \left[e^{ik_x \Delta_\xi} - 1 \right] \\ &= \frac{1}{\pi} \int dy_1 dy_2 \left[\frac{g^2}{1+g^2} - \frac{1}{2} \ln(1+g^2) \right], \end{aligned} \quad (\text{B.18})$$

with $g = \Delta_\xi / \Delta_y$ (cf. equation (2.63)).

Bibliography

- [1] D. S. Fisher, Phys. Rev. Lett. **56**, 1964 (1986).
- [2] D. Belitz and T. R. Kirkpatrick, Rev. Mod. Phys. **66**, 261 (1994).
- [3] K. Efetov and A. Larkin, Sov. Phys. JETP **45**, 1236 (1977).
- [4] Y. Imry and S. K. Ma, Phys. Rev. Lett. **35**, 1399 (1975).
- [5] C. L. Kane and M. P. A. Fisher, Phys. Rev. Lett. **68**, 1220 (1992).
- [6] T. Giamarchi, *Quantum Physics on One Dimension* (Clarendon Press, Oxford, 2003).
- [7] D. S. Fisher, Phys. Rep. **301**, 113 (1998).
- [8] M. Kardar, Phys. Rep. **301**, 85 (1998).
- [9] T. Nattermann, J. Phys. C **18**, 6661 (1985).
- [10] M. A. Rubio, C. A. Edwards, A. Dougherty, and J. P. Gollub, Phys. Rev. Lett. **63**, 1685 (1989).
- [11] N. Martys, M. Cieplak, and M. O. Robbins, Phys. Rev. Lett. **66**, 1058 (1991).
- [12] G. Blatter, M. V. Feigel'man, V. B. Geshkenbein, A. I. Larkin, and V. M. Vinokur, Rev. Mod. Phys. **66**, 1125 (1994).
- [13] T. Giamarchi and P. Le Doussal, Phys. Rev. Lett. **72**, 1530 (1994).
- [14] T. Nattermann and S. Scheidl, Adv. Phys. **49**, 607 (2000).
- [15] L. B. Ioffe and V. M. Vinokur, J. Phys. C **20**, 6149 (1987).
- [16] G. Grüner, Rev. Mod. Phys. **60**, 1129 (1988).
- [17] S. Brazovskii and T. Nattermann, Adv. Phys. **53**, 177 (2004).
- [18] T. Nattermann, S. Stepanow, L. H. Tang, and H. Leschhorn, J. Phys. II France **2**, 1483 (1992).
- [19] O. Narayan and D. S. Fisher, Phys. Rev. B **48**, 7030 (1993).

- [20] H. Leschhorn, T. Nattermann, S. Stepanow, and L. H. Tang, *Ann. Phys. (Leipzig)* **509**, 1 (1997).
- [21] A. A. Fedorenko and S. Stepanow, *Phys. Rev. E* **67**, 057104 (2003).
- [22] O. Narayan and D. S. Fisher, *Phys. Rev. B* **46**, 11520 (1992).
- [23] D. Ertas and M. Kardar, *Phys. Rev. E* **49**, R2532 (1994).
- [24] P. Chauve, P. Le Doussal, and K. J. Wiese, *Phys. Rev. Lett.* **86**, 1785 (2001).
- [25] P. Le Doussal, K. J. Wiese, and P. Chauve, *Phys. Rev. B* **66**, 174201 (2002).
- [26] P. Le Doussal, K. J. Wiese, and P. Chauve, *Phys. Rev. E* **69**, 026112 (2004).
- [27] A. A. Middleton, *Phys. Rev. B* **45**, 9465 (1992).
- [28] P. Chauve, T. Giamarchi, and P. Le Doussal, *Phys. Rev. B* **62**, 6241 (2000).
- [29] P. J. Metaxas, J. P. Jamet, A. Mougin, M. Cormier, J. Ferré, V. Baltz, B. Rodmacq, B. Dieny, and R. L. Stamps, *Phys. Rev. Lett.* **99**, 217208 (2007).
- [30] S. Bustingorry, A. B. Kolton, and T. Giamarchi, *EPL* **81**, 26005 (2008).
- [31] S. Lemerle, J. Ferré, C. Chappert, V. Mathet, T. Giamarchi, and P. Le Doussal, *Phys. Rev. Lett.* **80**, 849 (1998).
- [32] A. B. Kolton, A. Rosso, T. Giamarchi, and W. Krauth, *Phys. Rev. B* **79**, 184207 (2009).
- [33] W. Kleemann, J. Rhensius, O. Petravic, J. Ferré, J. P. Jamet, and H. Bernas, *Phys. Rev. Lett.* **99**, 097203 (2007), and references therein.
- [34] W. Kleemann, *Annu. Rev. Mater. Res.* **37**, 415 (2007).
- [35] I. F. Lyuksyutov, T. Nattermann, and V. Pokrovsky, *Phys. Rev. B* **59**, 4260 (1999).
- [36] T. Nattermann, V. Pokrovsky, and V. M. Vinokur, *Phys. Rev. Lett.* **87**, 197005 (2001).
- [37] A. A. Fedorenko, V. Mueller, and S. Stepanow, *Phys. Rev. B* **70**, 224104 (2004).
- [38] A. Glatz, T. Nattermann, and V. Pokrovsky, *Phys. Rev. Lett.* **90**, 047201 (2003).
- [39] D. P. Daroca, G. S. Lozano, G. Pasquini, and V. Bekeris, *Phys. Rev. B* **81**, 184520 (2010).
- [40] W. Jeżewski, W. Kuczyński, and J. Hoffmann, *Phys. Rev. B* **77**, 094101 (2008).
- [41] F. Schütze, *Phys. Rev. E* **81**, 051128 (2010), [arXiv:0906.1917].
- [42] F. Schütze and T. Nattermann, in preparation (2010).
- [43] M. V. Feĭgel'man, *Sov. Phys. JETP* **58**, 1076 (1983).

- [44] R. Bruinsma and G. Aeppli, Phys. Rev. Lett. **52**, 1547 (1984).
- [45] J. Koplik and H. Levine, Phys. Rev. B **32**, 280 (1985).
- [46] T. Nattermann, Y. Shapir, and I. Vilfan, Phys. Rev. B **42**, 8577 (1990).
- [47] D. S. Fisher, Phys. Rev. B **31**, 1396 (1985).
- [48] D. S. Fisher, Phys. Rev. Lett. **50**, 1486 (1983).
- [49] H. Leschhorn, J. Phys. A **25**, L555 (1992).
- [50] J. Vannimenus and B. Derrida, J. Stat. Phys. **105**, 1 (2001).
- [51] C. M. Bender and S. A. Orszag, *Advanced mathematical methods for scientists and engineers* (McGraw-Hill, New York, 1978).
- [52] J. Z. Imbrie, Phys. Rev. Lett. **53**, 1747 (1984).
- [53] J. Z. Imbrie, Comm. Math. Phys. **98**, 145 (1985).
- [54] J. Villain, J. Phys. A **21**, L1099 (1988).
- [55] A. I. Larkin, Sov. Phys. JETP **31**, 784 (1970).
- [56] J. Villain and B. Séméria, J. Physique Lett. **44**, 889 (1983).
- [57] A. Engel, J. Physique Lett. **46**, 409 (1985).
- [58] G. Schehr and P. Le Doussal, Europhys. Lett. **71**, 290 (2005).
- [59] A. B. Kolton, G. Schehr, and P. Le Doussal, Phys. Rev. Lett. **103**, 160602 (2009).
- [60] I. S. Gradshteyn and I. M. Ryzhik, *Table of Integrals, Series, and Products* (Academic Press, San Diego, London, 2000), sixth ed.
- [61] M. E. Lines and A. M. Glass, *Principles and Applications of Ferroelectrics and Related Materials* (Clarendon Press, Oxford, 1996).
- [62] M. Dawber, K. M. Rabe, and J. F. Scott, Rev. Mod. Phys. **77**, 1083 (2005).
- [63] J. F. Scott and C. A. Paz de Araujo, Science **246**, 1400 (1989).
- [64] J. F. Scott, *Ferroelectric Memories* (Springer, Berlin, 2000).
- [65] R. Waser and A. Rüdiger, Nat. Mater. **3**, 81 (2004).
- [66] P. Muralt, J. Micromech. Microeng. **10**, 136 (2000).
- [67] C. Caliondi, I. Fratoddi, and M. V. Russo, Appl. Phys. Lett. **80**, 4849 (2002).
- [68] R. Ott and R. Wördenweber, Appl. Phys. Lett. **80**, 2150 (2002).

- [69] T. Tybell, P. Paruch, T. Giamarchi, and J. M. Triscone, *Phys. Rev. Lett.* **89**, 097601 (2002).
- [70] P. Paruch, T. Giamarchi, and J. M. Triscone, *Phys. Rev. Lett.* **94**, 197601 (2005).
- [71] P. Paruch and J. M. Triscone, *Appl. Phys. Lett.* **88**, 162907 (2006).
- [72] T. Nattermann, *J. Phys. C* **16**, 4125 (1983).
- [73] F. P. Jona and G. Shirane, *Ferroelectric Crystals* (Pergamon Press, Oxford, 1962).
- [74] P. C. Kwok and P. B. Miller, *Phys. Rev.* **151**, 387 (1966).
- [75] A. F. Devonshire, *Adv. Phys.* **3**, 85 (1954).
- [76] V. G. Vaks, *Zh. Eksp. Teor. Fiz.* **54**, 910 (1968), (engl. translation *Sov. Phys. JETP* **27**, 486).
- [77] A. P. Levanyuk and A. A. Sobyenin, *ZhEFT Pis. Red.* **11**, 540 (1970), (engl. translation *JETP Lett.* **11**, 371).
- [78] J. Villain, *Solid State Comm.* **8**, 295 (1970).
- [79] A. Amin *et al.*, *Ferroelectrics* **65**, 107 (1985).
- [80] M. J. Haun *et al.*, *Ferroelectrics* **99**, 13 (1989).
- [81] M. J. Haun *et al.*, *Ferroelectrics* **99**, 27 (1989).
- [82] B. Jaffe, W. J. Cook, and H. Jaffe, *Piezoelectric Ceramics* (Academic Press, London, 1971), page 136.
- [83] L. D. Landau and E. M. Lifshitz, *Theory of Elasticity*, vol. 7 (Pergamon Press, Oxford, 1977).
- [84] D. J. Bergman and B. I. Halperin, *Phys. Rev. B* **13**, 2145 (1976).
- [85] H. Wagner and J. Swift, *Z. Physik* **239**, 182 (1970).
- [86] S. Nambu and D. A. Sagala, *Phys. Rev. B* **50**, 5838 (1994).
- [87] A. Dyan, F. Enguehard, S. Lallich, H. Piombini, and G. Duchateau, *JOSA B* **25**, 1087 (2008).
- [88] H. Navirian, H. Enquist, R. Nüske, A. Jurgilaitis, C. v. Korff Schmising, P. Sondhauss, and J. Larsson, *Phys. Rev. B* **81**, 024113 (2010).
- [89] R. R. Levitskii and B. M. Lisnii, *phys. stat. sol. (b)* **241**, 1350 (2004).
- [90] R. A. Cowley, *Phys. Rev. B* **13**, 4877 (1976).
- [91] J. Fousek and V. Janovec, *J. Appl. Phys.* **40**, 135 (1968).

- [92] J. Sapriel, Phys. Rev. B **12**, 5128 (1975).
- [93] T. Mitsui and J. Furuichi, Phys. Rev. **90**, 193 (1953).
- [94] J. Bornarel and J. Lajzerowicz, J. Appl. Phys. **39**, 4339 (1968).
- [95] J. Bornarel, J. Appl. Phys. **43**, 845 (1972).
- [96] J. Bornarel and J. Lajzerowicz, Ferroelectrics **4**, 177 (1972).
- [97] S. Kh. Aknazarov, L. G. Shabe'lnikov, and V. Sh. Shekhtman, Fiz. Tverd. Tela **17**, 30 (1975), (engl. translation Sov. Phys. Solid State, **17**, 16).
- [98] J. Bornarel, Ferroelectrics **9**, 197 (1975).
- [99] J. Bornarel, Ferroelectrics **71**, 255 (1987).
- [100] J. Bornarel, Ferroelectrics **172**, 53 (1995).
- [101] I. Rychetský and O. Hudák, Ferroelectrics **191**, 79 (1997).
- [102] T. Nattermann, J. Phys. A **21**, L645 (1988).
- [103] P. W. Anderson, Phys. Rev. **109**, 1492 (1958).
- [104] E. Abrahams, P. W. Anderson, D. C. Licciardello, and T. V. Ramakrishnan, Phys. Rev. Lett. **42**, 673 (1979).
- [105] A. M. Finkel'stein, Z. Physik B **56**, 189 (1984).
- [106] T. Stöferle, H. Moritz, C. Schori, M. Köhl, and T. Esslinger, Phys. Rev. Lett. **92**, 130403 (2004).
- [107] M. Tzolov, B. Chang, A. Yin, D. Straus, J. M. Xu, and G. Brown, Phys. Rev. Lett. **92**, 075505 (2004).
- [108] J. Cumings and A. Zettl, Phys. Rev. Lett. **93**, 086801 (2004).
- [109] A. N. Aleshin, J. Y. Lee, S. W. Chu, S. W. Lee, B. Kim, S. J. Ahn, and Y. W. Park, Phys. Rev. B **69**, 214203 (2004).
- [110] W. Kang, H. L. Stormer, L. N. Pfeiffer, K. W. Baldwin, and K. W. West, Nature (London) **403**, 59 (2000).
- [111] O. M. Auslaender, A. Yacoby, R. de Picciotto, K. W. Baldwin, L. N. Pfeiffer, and K. W. West, Science **295**, 825 (2002).
- [112] F. D. M. Haldane, J. Phys. C **14**, 2585 (1981).
- [113] J. Voit, Rep. Prog. Phys. **58**, 977 (1995).

-
- [114] B. I. Shklovskii, *Fiz. Tekh. Poluprovodn. (S.-Petersburg)* **6**, 2335 (1972), (engl. translation *Sov. Phys. Semicond.* **6**, 1964 (1973)).
- [115] T. Nattermann, T. Giamarchi, and P. Le Doussal, *Phys. Rev. Lett.* **91**, 056603 (2003).
- [116] N. F. Mott, *Metal-Insulator Transitions* (Taylor and Francis, London, 1990).
- [117] J. Sólyom, *Adv. Phys.* **28**, 209 (1979).
- [118] S. K. Ma, *Phys. Rev. B* **26**, 5097 (1982).
- [119] H. Pang, S. Liang, and J. F. Annett, *Phys. Rev. Lett.* **71**, 4377 (1993).
- [120] E. Orignac, T. Giamarchi, and P. Le Doussal, *Phys. Rev. Lett.* **83**, 2378 (1999).
- [121] T. Giamarchi, P. Le Doussal, and E. Orignac, *Phys. Rev. B* **64**, 245119 (2001).
- [122] Y. Suzumura and M. Isobe, *J. Phys. Soc. Jpn.* **73**, 3092 (2004).
- [123] T. Nattermann, A. Petković, Z. Ristivojevic, and F. Schütze, *Phys. Rev. Lett.* **99**, 186402 (2007).
- [124] L. S. Schulman, *Techniques and Applications of Path Integration* (Wiley, New York, 1981).
- [125] J. Langer, *Ann. Phys. (NY)* **54**, 258 (1969).
- [126] C. M. Newman and L. S. Schulman, *J. Stat. Phys.* **23**, 131 (1979).
- [127] W. Zwerger, *J. Phys. A* **18**, 2079 (1985).
- [128] S. Malinin, T. Nattermann, and B. Rosenow, *Phys. Rev. B* **70**, 235120 (2004).
- [129] J. von Delft and H. Schoeller, *Ann. Phys. (Leipzig)* **7**, 225 (1998).
- [130] D. Sénéchal (1999), arXiv:cond-mat/9908262.
- [131] F. D. M. Haldane, *Phys. Rev. Lett.* **47**, 1840 (1981).
- [132] R. P. Feynman and A. R. Hibbs, *Quantum Mechanics and Path Integrals* (Mc Graw-Hill, New York, 1965).
- [133] O. Bratelli and D. Robinson, *Operator Algebras and Quantum Statistical Mechanics* (Springer, Berlin, 1996).
- [134] I. M. Lifshits, S. A. Gredeskul, and L. A. Pastur, *Introduction to the theory of disordered systems* (John Wiley & Sons, New York, 1988), sec. 1.3.
- [135] P. Nozieres, *Solids far from Equilibrium* (Cambridge University Press, Cambridge, 1992).
- [136] W. Kohn, *Phys. Rev.* **133**, A171 (1964).

- [137] A. Rivero (2002), arXiv:quant-ph/0209072.
- [138] N. F. Mott, *Philos. Mag.* **17**, 1259 (1968).
- [139] M. V. Feĭgel'man and V. M. Vinokur, *Phys. Lett. A* **87**, 53 (1981).
- [140] M. M. Fogler, *Phys. Rev. Lett.* **88**, 186402 (2002).
- [141] B. Rosenow and T. Nattermann, *Rhys. Rev. B* **73**, 085103 (2006).
- [142] S. Fujimoto and N. Kawakami, *Rhys. Rev. B* **54**, R11018 (1996).
- [143] I. F. Herbut, *Rhys. Rev. B* **57**, 13729 (1998).
- [144] U. Schultz, J. Villain, E. Brezin, and H. Orland, *J. Stat. Phys.* **51**, 1 (1988).
- [145] B. I. Shklovskii and A. L. Éfros, *Zh: Eksp. Teor. Fiz.* **81**, 406 (1981), (engl. translation *Sov. Phys. JETP* **54**, 218).
- [146] M. P. A. Fisher, P. B. Weichman, G. Grinstein, and D. S. Fisher, *Phys. Rev. B* **40**, 546 (1989).
- [147] T. Emig and T. Nattermann, *Phys. Rev. Lett.* **81**, 1469 (1998).
- [148] J.-P. Bouchaud and A. Georges, *Phys. Rev. Lett.* **68**, 3908 (1992).
- [149] K. Hida and U. Eckern, *Phys. Rev. B* **30**, 4096 (1984).
- [150] V. Dotsenko, *J. Phys. A* **32**, 2949 (1999).
- [151] A. Glatz, Ph.D. thesis, Universität zu Köln (2004).
- [152] P. C. Martin, E. Siggia, and H. Rose, *Phys. Rev. A* **8**, 423 (1973).
- [153] C. De Dominicis, *Phys. Rev. B* **18**, 4913 (1978).
- [154] W. I. Smirnow, *Lehrgang der höheren Mathematik*, vol. IV (VEB Deutscher Verlag der Wissenschaften, Berlin, 1961), Kapitel IV.3.249.
- [155] H. W. Diehl, D. M. Kroll, and H. Wagner, *Z. Physik B* **36**, 329 (1980).

Danksagungen

- Mein besonderer Dank gilt Herrn Prof. Dr. Thomas Nattermann für die Betreuung der Arbeit, sowie zahlreiche Diskussionen und Ideen. Für sein Verständnis und sein Entgegenkommen während meiner langen Krankheit bin ich ihm ebenfalls sehr dankbar.
- Für viele Diskussionen, sowohl über Physik als auch anderes, unterhaltsame Mittagspausen und die gemeinsamen Freizeitunternehmungen danke ich Dr. Aleksandra Petković und Dr. Zoran Ristivojevic. Auch für die angenehme Atmosphäre in unserem Arbeitszimmer bin ich beiden dankbar.
- Herrn Dr. Gianmaria Falco und Herrn Dr. Andrey A Fedorenko gilt mein Dank für viele Diskussionen, Hilfestellungen und Ideen, wie auch für die angeregten Gespräche während der Mittags- und Kaffeepausen.
- Herrn Dr. Leiming Chen und Herrn Dr. Christophe Deroulers danke ich ebenfalls für Diskussionen.
- Für Ratschläge und Diskussionen hinsichtlich vieler numerischer Fragestellungen möchte ich Herrn Dr. Andreas Glatz meinen Dank aussprechen.
- Schließlich danke ich meiner Familie, die mir sowohl während meines Studiums als auch in der Promotionszeit immer zur Seite stand. Gleichmaßen danke ich meinen Freunden Alexander Hertsch, Julia Orthey, Julia Schütz und Volker Künzel, die darauf geachtet haben, daß ich auch in besonders arbeitsamen Phasen das Leben nicht vergesse. Jan Fuhrmann, Kay-Uwe Giering und Nadine Große danke ich für fachliche Gespräche in lockerer Atmosphäre.

Abstract

The present thesis addresses three different topics that are all in direct connection to the statistical physics of disordered systems. Each topic is assigned an own chapter.

The first chapter, which is the main part of this work, is devoted to driven interfaces in random media, neglecting the influence of thermal fluctuations. The main focus is on the case of an ac driving. Interfaces, driven by a constant force, have been a subject of theoretical studies for quite a while. For the problem without thermal noise it has been known since as early as the eighties, that interfaces are pinned due to the presence of disorder and do not move unless the external force exceeds some threshold. The transition from a pinned to a moving interface, called depinning transition, exhibits many similarities to second order phase transitions in equilibrium systems, where the velocity plays the role of an order parameter. As a function of the distance to the threshold, the velocity obeys a power law.

Our investigations start with the associated mean field theory. At the beginning we consider the case of a constant driving force and discuss the critical behaviour close to the depinning transition. For this purpose, we generalise the reasoning by Daniel S. Fisher, who addressed the closely related problem of charge density waves. Subsequently, we examine the velocity hysteresis curve for small frequencies by use of analytical and numerical methods. It turns out that all observables under consideration exhibit scaling behaviour on approaching the adiabatic case.

Next, we analyse perturbation theory for ac-driven interfaces. The basic idea consists in a Taylor expansion of the disorder force, which resolves the complicated non-linear structure of the equation of motion. Because in the limit of high frequencies the motion of an interface segment is restricted to a small range, we can expect that the approximation of the disorder by a Taylor polynomial is justified. Nevertheless, for interface dimensionalities $D \leq 4$ it turns out, that perturbation theory yields an unbounded growth in time. This phenomenon is discussed and traced back to transience effects that fade away on a disorder dependent time scale. Moreover, we argue that the perturbative expansion is regular in case $D > 4$. Especially for the mean field problem this is shown by an inductive proof. Using the first non-vanishing perturbative correction, we study the decay of the Fourier coefficients for the mean field solution with increasing harmonic order.

The second part of this thesis is concerned with the influence of electroelastic coupling on the behaviour of domain walls in ferroelectrics.

For the case of electrostrictive coupling in the high temperature phase we find, that merely the interface tension coefficients are changed in an anisotropic fashion. However, this kind of

electroelastic coupling does not yield a long range interaction.

On the contrary, a piezo effect in the paraphase does entail a long range term. After deriving the interface hamiltonian in the harmonic approximation, we determine the roughness of domain walls due to random field disorder using an Imry-Ma type argument. On large length scales, domain walls turn out to be flat. If, for simplicity, we assume a homogeneous configuration along the ferroelectric axis, which effectively reduces the problem to two dimensions, our considerations can be extended beyond the harmonic approximation. We are thus able to explain the appearance of needle shaped domain wall deformations that have been observed experimentally.

In the last chapter, we consider one-dimensional electronic systems, so-called Luttinger liquids, for which also quantum effects are important.

The subject of the first part is the competition of two phases of one-dimensional disordered fermionic systems, namely the Mott and the Anderson insulator. In previous works, the existence of an intermediate Mott glass phase has been postulated, which should be incompressible and at the same time exhibit a gap in the optical conductivity. Since, however, as is demonstrated in this work, both, the compressibility as well as a finite optical conductivity depend on a vanishing mass of charged excitations, a Mott glass phase can be excluded for systems with solely short range interaction. Combining informations about the renormalisation group flow and the energy of topological excitations, as well as using simple scaling arguments, we construct the phase diagram.

In the second part we study the utility of the replica trick in order to reproduce and possibly extend results on the quantum creep and the linear conductivity at finite temperatures for Luttinger liquids with relevant disorder, that have been achieved in previous works. We provide approximate solutions to the Euler-Lagrange equations for the replica action. The replica limit $n \rightarrow 0$ turns out to be problematic. At the example of a toy model we illustrate a method for the replica limit and demonstrate the emergent difficulties.

Zusammenfassung

Die vorliegende Dissertation befaßt sich mit drei Problemfeldern, die in unmittelbarem Bezug zur statistischen Physik ungeordneter Systeme stehen. Jedem Themengebiet ist ein eigenes Kapitel zugeordnet.

Das erste Kapitel, der Hauptteil dieser Arbeit, widmet sich getriebenen Grenzflächen in ungeordneten Medien, wobei der Einfluß thermischer Fluktuationen unberücksichtigt bleibt. Der Schwerpunkt liegt auf dem Fall eines Wechselfeldantriebs. Grenzflächen, getrieben durch eine konstante Kraft, sind schon seit längerer Zeit Gegenstand theoretischer Studien. So ist für das Problem ohne thermische Fluktuationen schon seit den achtziger Jahren bekannt, daß Grenzflächen durch die Gegenwart von Unordnung verankert sind und sich erst dann bewegen, wenn die Kraft, der sie ausgesetzt sind, einen bestimmten Schwellwert überschreitet. Der Übergang von der Situation einer verankerten Grenzfläche zu einer bewegten, im folgenden Depinningübergang genannt, weist viele Ähnlichkeiten mit Gleichgewichtsphasenübergängen zweiter Ordnung auf, wobei der Geschwindigkeit die Rolle eines Ordnungsparameters zukommt. So gehorcht die Geschwindigkeit als Funktion der Differenz zwischen der treibenden Kraft und dem Schwellwert einem Potenzgesetz.

Die Untersuchungen beginnen mit der zugehörigen Molekularfeldtheorie. Anfangs wird auf eine zeitlich konstante Antriebskraft eingegangen, und das kritische Verhalten in der Nähe des Depinningübergangs diskutiert. Dabei werden die Argumente von Daniel S. Fisher, die sich auf das verwandte Problem von Ladungsdichtewellen beziehen, hinsichtlich der vorliegenden Fragestellung verallgemeinert. Im Anschluß wird die Geschwindigkeitshysteresekurve für kleine Frequenzen sowohl analytisch als auch numerisch untersucht. Es stellt sich heraus, daß alle untersuchten Größen Skalenverhalten bei Annäherung an den adiabatischen Fall aufzeigen.

Den Betrachtungen zum Verhalten der Molekularfeldtheorie bei niedrigen Frequenzen folgt die Analyse der Störungstheorie wechselfeldgetriebener Grenzflächen. Die grundsätzliche Idee besteht darin, das Unordnungskraftfeld durch eine Taylorentwicklung zu nähern und damit die komplizierte nichtlineare Struktur der Bewegungsgleichung aufzulösen. Da sich im Grenzfall hoher Frequenzen ein Grenzflächenabschnitt nur innerhalb eines kleinen Bereiches bewegt, kann man erwarten, daß die Näherung durch ein Taylorpolynom gerechtfertigt ist. Dennoch wird für Grenzflächendimensionen $D \leq 4$ gefunden, daß die störungstheoretischen Resultate ein unbeschränktes Wachstum in der Zeit liefern. Dieses Verhalten der Störungstheorie wird diskutiert und auf Anfangsvorgänge zurückgeführt, die auf einer unordnungsabhängigen Zeitskala abklingen. Desweiteren wird dargelegt, daß die Störungsreihe im Falle $D > 4$ regulär ist. Insbesondere für das Molekularfeldproblem wird dies durch einen Induktionsbeweis gezeigt.

Mithilfe des störungstheoretischen Resultats erster nichtverschwindender Ordnung kann der Zerfall der Fourierkoeffizienten für die Molekularfeldlösung mit steigender harmonischer Ordnung studiert werden.

Der zweite Abschnitt befaßt sich mit dem Einfluß elektroelastischer Kopplung auf das Verhalten von Domänenwänden in Ferroelektrika.

Im Fall elektrostriktiver Kopplung in der Hochtemperaturphase zeigt sich, daß lediglich die Grenzflächenspannungskoeffizienten anisotrop verändert werden. Eine langreichweitige Wechselwirkung wird durch die elektroelastische Kopplung nicht hervorgerufen.

Im Gegensatz dazu führt ein Piezoeffekt in der Paraphase durchaus zu langreichweitiger Wechselwirkung. Aus der Grenzflächen-Hamiltonfunktion in harmonischer Näherung wird die Rauigkeit von Domänenwänden in Gegenwart von Zufallsfeldunordnung durch ein Imry-Ma Argument ermittelt. Es stellt sich heraus, daß Domänenwände auf großen Skalen flach sind. Unter der vereinfachenden Annahme homogener Beschaffenheit des Systems entlang der ferroelektrischen Achse, womit das Problem effektiv von drei auf zwei Dimensionen reduziert wird, gelingt die Ausdehnung der Betrachtungen über die harmonische Näherung hinaus. Damit kann man das Auftreten nadelförmiger Domänenwanddeformationen, wie sie in experimentellen Studien beobachtet worden sind, erklären.

Im letzten Kapitel werden eindimensionale elektronische Systeme, sogenannte Luttingerflüssigkeiten, betrachtet, in denen auch Quanteneffekte eine große Rolle spielen.

Gegenstand des ersten Teils ist das Gegenspiel zweier Phasen eindimensionaler ungeordneter Fermisysteme, dem Mott- und dem Andersonisolator. In vorherigen Arbeiten wurde die Existenz einer intermediären Mott-Glas-Phase postuliert, die einerseits inkompressibel sei, andererseits aber keine Frequenzlücke in der optischen Leitfähigkeit aufweise. Da sich jedoch, wie in der vorliegenden Arbeit dargelegt, sowohl die Kompressibilität als auch die endliche optische Leitfähigkeit auf die Masselosigkeit topologischer Anregungen des elektronischen Versetzungsfeldes zurückführen lassen, kann in Systemen mit ausschließlich kurzreichweitigen Wechselwirkungen die Existenz einer intermediären Mott-Glas-Phase ausgeschlossen werden. Das Phasendiagramm wird durch Zusammenführung der Informationen über den Renormierungsgruppenfluß und die Energie geladener Anregungen, sowie aus einfachen Skalenargumenten konstruiert.

Im zweiten Teil wird untersucht, inwieweit die Replikamethode zur Behandlung der Unordnung zweckmäßig ist, um frühere Ergebnisse zum Quantenkriechverhalten und der linearen Leitfähigkeit bei endlichen Temperaturen, die für Luttingerflüssigkeiten mit relevanter Unordnung und Dissipation erzielt worden sind, zu reproduzieren und gegebenenfalls zu erweitern. Es werden genäherte Instantonlösungen der Euler-Lagrange-Gleichungen für die Replikawirkung angegeben. Als problematisch erweist sich der Replikalimes $n \rightarrow 0$. Anhand eines Spielzeugmodells wird eine Herangehensweise zur Durchführung des Replikalimes vorgestellt und dargelegt, welche Schwierigkeiten dabei auftreten.

Erklärung

Ich versichere, daß ich die von mir vorgelegte Dissertation selbständig angefertigt, die benutzten Quellen und Hilfsmittel vollständig angegeben und die Stellen der Arbeit - einschließlich Tabellen, Karten und Abbildungen -, die anderen Werken im Wortlaut oder dem Sinn nach entnommen sind, in jedem Einzelfall als Entlehnung kenntlich gemacht habe; daß diese Dissertation noch keiner anderen Fakultät oder Universität zur Prüfung vorgelegen hat; daß sie - abgesehen von unten angegebenen Teilpublikationen - noch nicht veröffentlicht worden ist sowie, daß ich eine solche Veröffentlichung vor Abschluß des Promotionsverfahrens nicht vornehmen werde. Die Bestimmungen der Promotionsordnung sind mir bekannt. Die von mir vorgelegte Dissertation ist von Prof. Dr. Thomas Nattermann betreut worden.

Köln, den 27. Oktober 2010

Friedmar Schütze

Teilpublikationen

1. “*Absence of the Mott Glass Phase in 1D Disordered Fermionic Systems*”, T. Nattermann, A. Petković, Z. Ristivojevic, and F. Schütze, *Phys. Rev. Lett.* **99**, 186402 (2007).
2. “*Perturbation theory for ac-driven interfaces in random media*”, Friedmar Schütze, *Phys. Rev. E* **81**, 051128 (2010).
3. “*Mean field theory for driven domain walls in disordered environments*”, F. Schütze and T. Nattermann, submitted to *Phys. Rev. B*.

Lebenslauf

Persönliche Angaben

Geburtsdatum 9. Februar 1981
Nationalität Deutsch
Familienstand Ledig
Anschrift Kronstädter Str. 31
50858 Köln

Ausbildung

1987 – 1991 Grundschulbesuch
1991 – 1999 König-Albert-Gymnasium, Leipzig
Abschluß: Abitur
1999 – 2000 Zivildienst an der Kaiserswerther Diakonie in Düsseldorf
2000 – 2002 Grundstudium Physik (Universität Leipzig)
Abschluß: Vordiplom
2002 – 2003 Hauptstudium Physik (University of Edinburgh)
2003 – 2005 Stipendiat der Studienstiftung des deutschen Volkes
2003 – 2006 Hauptstudium Physik (Universität Leipzig)
Abschluß: Diplom
Diplomthema: “Konstruktive Aspekte fermionischer Modelle der Quantenfeldtheorie”. Betreuer: Prof. Dr. Manfred Salmhofer.
seit Mai 2006 Promotionsstudium am Institut für Theoretische Physik der Universität zu Köln, Betreuer: Prof. Dr. Thomas Nattermann.

Beschäftigungsverhältnisse

seit Mai 2006 wissenschaftlicher Mitarbeiter am Institut für Theoretische Physik der Universität zu Köln